Dynamics of Li_3 in the vicinity of the Jahn-Teller conical intersection

Elham Nour Ghassemi

A thesis submitted to the faculty of
Stockholm University
in partial fulfillment of the requirements for the degree of

Master of Science

Åsa Larson, Jonas Larson, Chair

Department of Physics and Astronomy

Stockholm University

June 2011

ABSTRACT

Dynamics of Li_3 in the vicinity of the Jahn-Teller conical intersection

Elham Nour Ghassemi
Department of Physics and Astronomy
Master of Science

The Li_3 system is a well known triangular system that exhibit a Jahn-Teller conical intersection between the lowest two electronic states. Furthermore, the ground state of Li_3 is bound, which makes it possible to follow the dynamics in the vicinity of the conical intersection. The adiabatic potential energy surfaces of Li_3 are computed using the Multi-Reference Configuration Interaction method. The quantum chemistry model is tested by comparing computed potential energy curves of the excited states of Li_2 with other theoretical as well as experimental determined curves. The adiabatic potentials of Li_3 are fitted to a Jahn-Teller Hamiltonian and the molecular dynamics is explored with wave packet propagation using the Multi-Configuration Time-Dependent Hartree method. All three internal degrees of freedom are included in our wave packets simulation. Attempts to describe the dynamics using a molecular gauge theory will be performed. Linear Jahn-Teller models are considered in terms of a generalized gauge theory. Rather than regarding the non-adiabatic coupling terms as constituting an effective gauge field, we instead construct a field, possessing the appropriate gauge properties, acting upon the momentum wave-functions. The idea is that, with generalized gauge theories, the dynamics can be qualitatively understood in terms non-Abelian gauge arguments.

Keywords: Born-Oppenheimer approximation, Schrödinger equation, Molecular dynamics, non-adiabatic coupling term, Adiabatic to Diabatic representation, the Jahn-Teller effect, Conical Intersection, Pseudorotation, the Berry phase, Vector potential, Gauge field, Wavepacket propagation

ACKNOWLEDGMENTS

I would like to express my deepest gratitude to my supervisor, Åsa Larsron, for never ending supports and excellent guidance. Her full energy and great pedagogical skills and cool attitude have inspired me enormously and encouraged me to go ahead in my studies during the past year. I am also greatly indebted to my co-supervisor, Jonas Larson, for his support and numerous interesting discussions. He had put much effort to assist me to finish this diploma thesis. During the writing of this thesis, they have also given me many instructive suggestions and every time when I asked them questions, they always answered patiently.

My warmest thanks go to professor Mats Larsson for accepting me as a member in the Molecular Physics group. I am grateful to professor Nils Elander for his helpful scientific advices. I would also like to acknowledge to past and present members of Molecular Physics group for both science related issues and nice coffee breaks. Especially, I would like to thank Michael Stenrup for his scientific helps and being such a unforgettalbe friend.

During the last year I had a great chance to attend in the 20th international symposium on the Jahn-Teller effect, first I would like to thank Åsa to give me this opportunity. Secondly, I would like to thank professor Horst Köppel from Heidelberg University to his warm advice during the symposium. Also I am grateful to professor Wolfgang E. Ernst from Graz University of Technology to his friendly advice for fitting processes and sending me his recent articles.

I would also like to take a chance to thank all my friends for all their warm supports.

Mamma, baba thank you for your unconditional supports. I would also like to thank my brother, Behnam, for his warm supports.

My special thanks and a big hug to my life friend, Afshin, thank you for your patient and helping me to endure homesick.

Contents

Chapter 1

Introduction

1.1 Introduction

To describe phenomena in our environment such as an apple falling from a tree, the laws of classical physics are good approximations. But, on the atomic scales the classical physics has to be replaced with quantum physics. To Study properties of molecular systems as many particle systems, fundamental concepts of quantum physics has to be applied. Molecular systems involve fast and slow degrees of freedom, these would be electronic and nuclear variables respectively. Such a systems can be analyzed by means of the *Born-Oppenheimer approximation* [1] which makes it possible to investigate dynamics of nuclei on the single potential energy surface by separating the fast electronic motions from the slow nuclear motions and neglecting the non-adiabatic coupling between two potential energy surfaces. However, there are some situations where a strong coupling between the electronic potential energy surfaces are encountered via vibrational motion usually termed *vibronic* or *non-adiabatic* coupling which makes the Born-Oppenheimer approximation to break down.

The coupling between adiabatic potential energy surfaces manifests itself in terms of derivative operators with respect to nuclear coordinates. Calculation of these non-adiabatic coupling elements for several potential energy surfaces and many nuclear degrees of freedom is rather cumbersome. Often it is more convenient to employ new electronic basis functions, the so-called *diabatic* basis where the non-adiabatic couplings vanish or at least make them very small. Transformation from *adiabatic to diabatic representations* [2] by means of an unitary transformation matrix removes the non-adiabatic coupling elements in the exchange

of the off-diagonal elements for the potential matrix.

The non-adiabatic coupling effects usually become more important when adiabatic potential energy surfaces are very close energetically or degenerate along a region in nuclear configuration space. In such cases the non-adiabatic coupling terms may become infinity. One specific case is characterized by the fact that the non-adiabatic coupling terms are singular at an isolated point which is called a *conical intersection*. In these special cases, studying of the nuclear dynamics needs to consider more than one adiabatic potential energy surface.

In molecular systems with three or more atoms, degeneracy occurs in highly symmetrical nuclear configurations. According to the well-known *Janh-Teller effect* [3], which is a most fascinating phenomena in the quantum physics and chemistry, any nonlinear molecule with a highly symmetric geometry is unstable in orbitally degenerate electronic states and tend to distort into more stable nondegenerate state with lower symmetry. The simplest case is the $E \otimes e$ Jahn-Teller effect with a conical intersection involving the two-fold degenerate electronic states E with a two-fold degenerate nuclear vibration modes e.

The two lowest adiabatic potential energy surfaces of most alkali trimers exhibit a conical intersection of the $E \otimes e$ Jahn-Teller type for the high symmetry D_{3h} configuration and distorts when the local symmetry is lowered from D_{3h} to C_{2v}. The most common shape of the potential energy surface is similar to a Mexican hat when the diabatic Jahn-Teller model Hamiltonian involves only the linear vibronic coupling term. Including as well the quadratic vibration coupling term, the potential energy surface becomes altering with three equivalent minima separated with three saddle points. In particular, a sufficiently strong quadratic coupling changes the potential energy surface drastically in the Jahn-Teller systems.

In the vicinity of the conical intersection another fascinating phenomena arise by tunneling from one potential well to another in the adiabatic potential energy surface, the so-called *pseudorotational* motion. Adiabatic electronic wavefunctions change sign when the system encircles a closed loop around the point of degeneracy. In order to obtain single valued total wavefunction of the system, the nuclear part must exhibit such a sign change leading to a half-integer quantization of the so-called pseudorotational motion around the conical intersection. It has been shown that this sign change is a special case of the well-known an adiabatic *geometric or Berry phase* [4] which can be related to any quantum system that undergoes cyclic evolution in some parameter space. In the molecular system, the geometric phase reduces to a sign change of the electronic wavefunction. Choosing the single valued

electronic wavefunction is at the expense of taking into account a derivative term in the nuclear Schrödinger equation. This term behaves as a vector potential and systems where the gauge vector potential is abelian or non-abelian have been investigated [5]. Recognizing the derivative coupling terms as quantities which transform like appropriate gauge fields under unitary transformation of electronic basis functions, leads to looking for a gauge theoretical formulation for the nuclear motions [6].

1.2 Problem statement

In this master thesis, we will study the Li_3 trimer which is the simplest three atomic alkali trimers due to few number of electrons. Only three internal degrees of freedom have to be considered for the nuclear motions. The two lowest potential energy surfaces for Li_3 exhibit a conical intersection at D_{3h} symmetry [7, 8]. Furthermore its ground state is bound and this makes it possible to follow the dynamics of the system in the vicinity of the conical intersection. The adiabatic potential energy surfaces are here directly computed by means of quantum chemistry methods. The quality of these *ab initio* calculations is investigated by computing the potential energy curves for the Li_2 diatomic molecule. For a better description of the symmetry of the system and the Jahn-Teller effect we exploit the normal mode coordinates for the nuclear degrees of freedom. To investigate nuclear dynamics, a transformation from the adiabatic to diabatic representations is carried out using an unitary transformation matrix. The transformation matrix is given by the Jahn-Teller parameters obtained by optimizing the eigen values of the diabatic Jahn-Teller Hamiltonian to the computed adiabatic potential. Different orders of the $E \otimes e$ Jahn-Teller model are investigated.We use the computed adiabatic potential energy surfaces and transform them to the diabatic representation. By using this approach we can set up the diabatic potential energy matrix further away from the conical intersection where the Jahn-Teller Hamiltoniam is no longer valid. Using the diabatic Jahn-Teller Hamiltonian, dynamics of the system is explored using time-dependent wavepacket propagations. The wavepacket propagation is performed using the Multi-Configuration Time-Dependent Hartree (MCTDH) method [9] including two coupled electronic states and three nuclear degrees of freedom.

1.3 Report structure

This work is organized as following. In chapter two we present the Schrödinger equation for general molecular systems. The standard quantum chemistry methods for solving the electronic part of the problem and finding the adiabatic potential energy surfaces for a molecular system are introduced. In chapter three the adiabatic and diabatic representations of electronic states are discussed and it is shown how one can transform from one representation to the other. Chapter four is devoted to the description of normal mode coordinates of the X_3 molecular systems by exploiting molecular group theory. In chapter five, the model of the Jahn-Teller Hamiltonian is introduced and the $E \otimes e$ Jahn-Teller effect is particularly discussed. In this chapter, we also discuss the gauge theory for molecular systems and the corresponding gauge field of the linear $E \otimes e$ Jahn-Teller system. The results with perspectives for future work are given in the final chapter.

Chapter 2

Adiabatic molecular dynamics

2.1 Molecular Schrödinger equation

"*For calculating molecular properties, quantum chemistry seems to be the obvious tool to use. Calculation that does not use the Schrödinger equation are acceptable only to the extent that they reproduce the result of high level quantum mechanical calculation [10].*"

A number of experimental observations have shown that the motion of microscopic particles cannot be correctly described within the framework of classical or Newtonian mechanics. Since the development of quantum mechanics in the 1920s, this tool has become essential in understanding phenomena at the microscopic scale. Meanwhile, the quantum chemistry gives us the possibility to describe the fundamental behaviour of chemical systems by applying quantum mechanics theory.

To study a molecule as a microscopic system, we start from solving the time-independent molecular Schrödinger equation

$$H\Psi(r,R) = E\Psi(r,R), \tag{2.1}$$

where the Hamiltonian H for the system describes the atomic nuclei and the electrons and it is composed of the kinetic and potential energies. $\Psi(r,R)$ is the wavefunction for the stationary state with energy E. r and R are used to denote the set of electronic and nuclear coordinates respectively. The non-relativistic Hamiltonian of a molecular system in atomic

units[1] for N electrons and N_a nuclei is given by

$$H = -\sum_{A=1}^{N_a} \frac{1}{2M_A}\nabla_A^2 - \sum_{i=1}^{N} \frac{1}{2}\nabla_i^2 - \sum_{i=1}^{N}\sum_{A=1}^{N_a} \frac{Z_A}{r_{iA}} + \sum_{i=1}^{N}\sum_{i<j}^{N} \frac{1}{r_{ij}} + \sum_{A=1}^{N_a}\sum_{A<B}^{N_a} \frac{Z_A Z_B}{R_{AB}}, \tag{2.2}$$

where $r_{iA} = |r_i - R_A|$ is the distance between the electron i and the nucleus A, $r_{ij} = |r_i - r_j|$ denotes the distance between the electrons i and j. The distance between the nucleus A and the nucleus B is $R_{AB} = |R_A - R_B|$. M_A is the mass for the nucleus A and Z_A is its atomic number. For convenience we rewrite it as

$$H = T_N + T_e + V_{e-N}(r, R) + V_{e-e}(r) + V_{N-N}(R). \tag{2.3}$$

Here T_N and T_e are the kinetic energy for nuclei and electrons respectively. V_{e-N} is the electron- nuclear attraction; V_{e-e} is the repulsion energy between electrons and V_{N-N} is the repulsion energy between nuclei.

2.2 The Born-Oppenheimer Approximation

It is well-known that the Schrödinger equation for the hydrogen atom composed of one nucleus (proton) and one electron can be solved analytically. Whereas a molecular system is a many-body problem, to solve the Schrödinger equation approximations must be applied. As a result of the great difference in masses between electrons and nuclei, one can separate the motions of the electrons from the motions of the nuclei. It means that electrons move much faster than the nuclei. Assuming the nuclei to be fixed, we can omit the nuclear kinetic energy term from the Hamiltonian (2.3) and obtain the Schrödinger equation for the electronic motion

$$H_{el}\psi(r; R) = U(R)\psi(r; R). \tag{2.4}$$

Here the electronic Hamiltonian is

$$H_{el} = T_e + V_{e-N}(r, R) + V_{e-e}(r). \tag{2.5}$$

[1] Atomic units are introduced when the charge of an electron $e = 1$, the mass of the electron $m = 1$ and $\hbar = \frac{h}{2\pi} = 1$. Then the derived atomic units of the length and energy will be

- 1 bohr$= 1\ a_0 = 1\ \frac{\hbar}{me^2} = 0.529$ Å
- 1 Hartree $= 1\frac{e^2}{a_0} = 4.3598 \times 10^{-18}$ J $= 627.51\ \frac{\text{kcal}}{\text{mol}} = 27.212$ eV

The wavefunction and the potential energy depend parametrically on the nuclear configuration, R. The repulsion between the nuclei is considered to be constant. It adds to the eigenvalues of the electronic Hamiltonian operator. Then it has no effect on the operator eigenfunctions or other properties. This term shifts only the eigenvalue by some constant.

In the adiabatic approximation the nuclear configuration will change slowly and the motions of the electrons will immediately adjust to the new nuclear configuration and remain in the same electronic eigenstate. When R is changing to R', the electronic wavefunction changes from $\psi(r;R)$ to $\psi(r;R')$ and the potential energy changes from $U(R)$ to $U(R')$. Solving the electronic Schrödinger equation for different nuclear configurations allows us to construct the potential energy curve for a diatomic molecule or in general a potential energy surface for a polyatomic molecule.

When the electronic Schrödinger equation (2.4) is solved, an infinite number of eigenfunctions, $\psi_i(r;R)$, are obtained with energies $U_i(R)$, where $i = 1, 2, 3, \cdots$. These eigenfunctions form a complete set of states and to go beyond the adiabatic approximation the full molecular wavefunction can be expanded in the adiabatic electronic wavefunctions

$$\Psi(r,R) = \sum_i \psi_i(r;R)\chi_i(R), \tag{2.6}$$

where the expansion coefficients $\chi_i(R)$ are functions of nuclear coordinates. Inserting wavefunction (2.6) into the total Schrödinger equation (2.1), and multiplying from the left with $\psi_j^*(r;R)$ and integrating over the electronic coordinates yields

$$\sum_i \langle \psi_j(r;R) \mid [T_N + H_{el}]\chi_i(R) \mid \psi_i(r;R)\rangle = \sum_i \langle \psi_j(r;R) \mid E\chi_i(R) \mid \psi_i(r;R)\rangle. \tag{2.7}$$

Here, the Dirac bracket notation implies integration over all electron coordinates. The right hand side can be written as

$$RHS = E\sum_i \chi_i(R)\langle \psi_j(r;R) \mid \psi_i(r;R)\rangle = E\sum_i \chi_i(R)\delta_{ij} = E\chi_j(R). \tag{2.8}$$

Since the integration is over r, $\chi_i(R)$ has been brought out of the bracket and by using the orthonormality properties of the electronic states the sum is eliminated.

For the left hand side we have

$$LHS = \sum_i \left\{ \langle \psi_j(r;R) \mid T_N\chi_i(R) \mid \psi_i(r;R)\rangle + \langle \psi_j(r;R) \mid H_{el}\chi_i(R) \mid \psi_i(r;R)\rangle \right\}. \tag{2.9}$$

We should notice that the nuclear kinetic energy operator contains derivatives with respect to the nuclear coordinates R, and it acts on the both factors in the product $\psi_i(r;R)\chi_i(R)$, so the first term of $\{\}$ in the LHS will be

$$\langle\psi_j(r;R) \mid T_N\{\chi_i(R) \mid \psi_i(r;R)\rangle\} = \\ \{T_N\chi_i\}\langle\psi_j(r;R) \mid \psi_i(r;R)\rangle + \chi_i(R)\{\langle\psi_j(r;R) \mid T_N \mid \psi_i(r;R)\rangle\}. \tag{2.10}$$

Since we use adiabatic eigenfunctions that by definition diagonalize the electronic Hamiltonian, the second term of $\{\}$ in the LHS becomes

$$\langle\psi_j(r;R) \mid H_{el} \mid \psi_i(r;R)\rangle = U_i(R)\delta_{ij}. \tag{2.11}$$

By substituting equations (2.10) and (2.11) into equation (2.9) and once again using the orthonormality of the electronic states, the sum is eliminated and we finally obtain

$$[T_N + U_j(R)]\chi_j(R) + \sum_i \{\langle\psi_j(r;R) \mid T_N \mid \psi_i(r;R)\rangle\}\chi_i(R) = E\chi_j(R). \tag{2.12}$$

In 1927, Born and Oppenheimer [1] showed that the coupling term $\langle\psi_j \mid T_N \mid \psi_i\rangle$ is usually small compared to $U_j(R)$ and the interaction between different electronic states can be neglected. Thus we obtain the uncoupled Schrödinger equation for the nuclear motion

$$[T_N + U_j(R)]\chi_j(R) = E\chi_j(R). \tag{2.13}$$

Here, the eigenvalue E is the total energy of the molecule within the Born-Oppenheimer approximation including a set of vibrational and rotational levels for the nuclear motion. The Born-Oppenheimer approximation is well justified as long as the involved adiabatic potential energy surfaces are well separated in energy compared to the energy scale of the nuclear motion. It is now clear that in many important cases this approximation breaks down for example when there are energetically close-lying electronic states or large kinetic energies of the nuclear motion. This causes a vibronic mixing of different electronic states[2] and this will be discussed further in chapter 3. In the following section, only the electronic Schrödinger equation will be considered.

[2]The coupling between electronic and nuclear motions is termed vibronic coupling.

2.3 Electronic Schrödinger equation

We have seen that within the Born-Oppenheimer approximation the electronic motions can be separated from nuclear motions and one can solve the electronic Schrödinger equation (2.4) independently at fixed nuclear configurations. For molecular systems contain more than one electron, the electronic Schrödinger equation is still a many-body problem and approximations have to be applied. We will now discuss different quantum chemistry methods used to solve the electronic Schrödinger equation.

2.3.1 Hartree-Fock approximation

The essence of the Hatree-Fock approximation [11] is to replace the many-electron problem with the one electron problem where the electron-electron repulsion is considered as an averaged field experienced by one electron due to the presence of all the other electrons. We start from the electronic Hamiltonian (2.5) which depends on all the electronic coordinates and introduce the Hamiltonian for the individual electron with index i that depends only on r_i

$$h(i) = -\frac{1}{2}\nabla_i^2 - \sum_{A=1}^{M} \frac{Z_A}{|r_{iA}|}. \tag{2.14}$$

We also introduce the two electron Hamiltonian that depends on r_i and r_j

$$g(i,j) = \frac{1}{|r_{ij}|}. \tag{2.15}$$

Then the electronic Hamiltonian (2.5) can be rewritten as

$$H_{el} = \sum_{i}^{N} h(i) + \frac{1}{2}\sum_{i,j\neq i}^{N} g(i,j). \tag{2.16}$$

In a simpler system containing no interacting electrons, the electronic Schrödinger equation can be solved by the separating variable method and a set of orthonormal eigenfunctions, $\{\phi_j\}$, can be obtained via

$$h(i)\phi_j(r_i) = \varepsilon_i \phi_j(r_i), \tag{2.17}$$

where $\phi_j(r_i)$ is called spin-orbital and describes the one electron wavefunction. It consists of a spatial part $\varphi_j(r)$ (molecular orbital) and a spin part. The spin up and the spin down

states are denoted by α and β, respectively

$$\phi_j(r) = \begin{cases} \varphi_j(r)\alpha \\ \\ \varphi_j(r)\beta \end{cases} \tag{2.18}$$

The simplest form used for describing molecular orbitals is by applying the linear combination of atomic orbitals (LCAO) approximation

$$\varphi_i(r) = \sum_j c_{ij}\zeta_j(r). \tag{2.19}$$

In this expression, the c_{ij} are the coefficients or weights of the atomic orbital ζ_j for the molecular orbitals φ_i.

The simplest wavefunction for the N-particle system in the independent particle approximation will be:

$$\psi(r_1, r_2, \ldots, r_N) = \phi_i(r_1)\phi_j(r_2)\ldots\phi_k(r_N), \tag{2.20}$$

which is termed a Hartree product and it is an uncorrelated wavefunction. The chosen spin-orbitals are orthogonal.

For an N-electron (fermion) system this wavefunction, $\psi(r_1, r_2, \ldots, r_N)$, must be antisymmetric with respect to the exchange of the coordinates of any two electrons to satisfy the so-called "*Pauli principle*" or the *antisymmetric principle* [12]

$$\begin{aligned} P_{ij}\psi(r_1, \ldots, r_i, \ldots, r_j, \ldots, r_N) &= \psi(r_1, \ldots, r_j, \ldots, r_i, \ldots, r_N) \\ &= -\psi(r_1, \ldots, r_i, \ldots, r_j, \ldots, r_N). \end{aligned}$$

The simplest antisymmetric arrangement of these spin-orbitals is given by a determinant called the *Slater determinant* to describe the wavefunction for the N electron system:

$$\psi = \frac{1}{\sqrt{N!}} \begin{vmatrix} \phi_1(r_1) & \phi_2(r_1) & \ldots \phi_N(r_1) \\ \phi_1(r_2) & \phi_2(r_2) & \ldots \phi_N(r_2) \\ \vdots & & \\ \phi_1(r_N) & \phi_2(r_N) & \ldots \phi_N(r_N) \end{vmatrix}. \tag{2.21}$$

The single Slater determinant can be used to describe the ground state of the N-electron system. The best wavefunction is determined by the variational principle. According to this

principle, the energy expectation value of a trial wavefunction $\tilde{\psi}$ is larger than the energy of the true ground state.

$$E[\tilde{\psi}] = \frac{\langle\tilde{\psi}|H_{el}|\tilde{\psi}\rangle}{\langle\tilde{\psi}|\tilde{\psi}\rangle} \geq E_0. \tag{2.22}$$

Since the energy $E[\tilde{\psi}]$ depends on the whole function $\tilde{\psi}$, it is a functional of $\tilde{\psi}$. By minimizing E with respect to the choice of spin-orbitals (atomic orbital coefficients) one can derive the Hartree-Fock equation and determine the optimal molecule orbitals. The expectation value of the electronic Hamiltonian (2.16) is given by

$$\begin{aligned} E_{HF} &= \sum_{i}^{N}\langle\phi_i|h(i)|\phi_i\rangle + \frac{1}{2}\sum_{i,j\neq i}^{N}\{\langle\phi_i\phi_j|g(i,j)|\phi_i\phi_j\rangle - \langle\phi_i\phi_j|g(i,j)|\phi_j\phi_i\rangle\}, \\ &\equiv \sum_{i}^{N} h_{ii} + \frac{1}{2}\sum_{ij}^{N}\{J_{ij} - K_{ij}\}. \end{aligned} \tag{2.23}$$

Here h_{ii} is the one electron integral and J_{ij} is called the Coulomb integral that describes the Coulomb interaction between the electron in the orbital i and the electron in the orbital j. K_{ij} is called the exchange integral which describes interaction between the electrons with parallel spin. There is no classical interpretation for the exchange energy. This term arises because of the antisymmetric nature of the wavefunction in the Slater determinant. It is convenient to express the energy in terms of operators and the one electron operator called the Fock operator can then be defined as:

$$\mathbf{F} = \mathbf{h} + \sum_{j}(\mathbf{J}_j - \mathbf{K}_j). \tag{2.24}$$

The canonical form of the Hartree-Fock equation is [3]

$$\mathbf{F}\phi_i = \epsilon_i\phi_i. \tag{2.25}$$

The Fock operator depends on its eigenfunctions, ϕ_i, i.e. the solution of the Hartree-Fock equation. The specific Fock orbital can only be determined when all other MOs are known.

[3] Using "Lagrange multipliers" to derive the Hartree-Fock equation one finds $\mathbf{F}\phi_i = \sum_j^N \epsilon_{ij}\phi_j$ which is not a standard eigenvalue form for the Hartree-Fock equation. So by exploiting the unitary transformation of the MO among themselves it is possible to obtain the new set of MO $\{\phi_i'\}$ from the old set $\{\phi_i\}$ and then diagonalize ϵ . This new set of MOs is called canonical MOs. They form a basis for an irreducible representation of the point group of the molecule. We drop the primes and find the Hartree-Fock equation (2.25) [13].

This problem can be solved by using an iterative method. The set of functions that are solutions to the Hartee-Fock eigenvalue equation are called the self consistent field orbitals. The procedure of solving this equation will be continued until a self-consistent solution is reached. This procedure is called the self-consistent field (SCF) method [13].

In the HF/SCF approximation, the electronic energy is variational and by choosing a better basis set the total energy will be lower. By using a larger and larger basis set one can obtain the best possible energy and this total energy approaches the Hartree-Fock limit. The Hartree-Fock energy will always be above the exact energy. Within the Hartree-Fock approximation, by assuming a single determinant form for the wavefunction, the motions of the electrons with opposite spin are not correlated. To go beyond the Hartree-Fock approximation it is crucial to include this correlation energy by more advanced methods [See the next subsection].

For an N electron system containing an even number of electrons, each spatial orbital is occupied by two electrons with different spin functions and the molecule is called a *closed-shell* system. If the spatial orbitals are restricted to be identical for α and β spin functions, the wavefunction is a Restricted Hartree-Fock (RHF) wavefunction and contains $N/2$ spin orbitals with an α spin function and $N/2$ spin orbitals with a β spin function and the obtained determinant wavefunction is describing a pure singlet state. A molecule with odd number of electrons where one of the restricted spatial orbitals contains a single electron is referred to as *open-shell* system and the wavefunction will be the Restricted Open-shell Hartee-Fock (ROHF) wavefunction. But if there is no restriction on the form of spatial orbitals, we deal with an Unrestricted Hartree-Fock (UHF) wavefunction. For RHF there is another problem known as the Restricted Hartree-Fock dissociation problem that will cause the dissociation energy computed using the RHF method to be too high. This problem is another witness that leads to a poor description of the electronic structure by the Hartree-Fock approximation.

2.3.2 Beyond Hartree-Fock approximation

We have seen that by applying the Hartree-Fock approximation to solve the electronic Schrödinger equation one can determine the ground state energy and wavefunction for the many electron system. But there is a difference between the exact solution of the non relativistic Schrödinger equation and the solution given by the Hartree-Fock approximation.

The difference between these two energies is called the correlation energy

$$E_{corr} = E_{exact} - E_{HF}. \tag{2.26}$$

Electron correlation in general describes how individual electrons interact with each other. The correlation between electrons having the same spin is called Fermi correlation and it prevents to find two electrons with parallel spins in one and the same spatial orbital [14]. The Fermi correlation is the simplest form of correlation and it is already taken into account at the Hartree-Fock level of theory. On the other hand the correlation between two electrons with opposite spins due to their Coulomb repulsion is described, by Coulomb correlation. The Coulomb correlation is larger than the Fermi correlation. Since the 1960s [15], the correlation between the electrons has been divided into the dynamical correlation (the instantaneous correlation in the motion of the electrons) and the static (near-degeneracy) correlation, based on partitioning of MOs into internal and external sets. The static correlation is a long-rang effect and sends electrons to individual atoms as the molecule dissociates. It is an effect of the near-degeneracy and the fact that several configurations might be equally important for the description of an electronic state. The dynamical correlation energy is a short-rang effect and it is a reduction in the repulsion energy due to a decreased probability to find two electrons close to each other [16].

In quantum chemistry, more advanced methods are developed to improve on the Hartree-Fock method by including a better description of the correlation. There are main methods for treating the electron correlation such as Configuration Interaction (CI), Many Body Perturbation Theory (MBPT), Coupled Cluster (CC) and Density functional theory (DFT)[4]. The simplest and most straightforward method is the configuration interaction method that here will be discussed.

2.3.3 The CI method

From the RHF calculation for a system with N electrons one can obtain M basis functions or spatial MOs, where $N/2$ are occupied and $M - N/2$ are virtual or unoccupied. One can

[4]We should recall here that for calculating properties of a chemical system there are two main groups of methods in quantum chemistry, wavefunction based methods, where a direct but approximate solution of the Schrödinger equation is considered and density functional theory based methods, where the energy is a functional of the electron density.

construct the Slater determinant by these occupied MOs, then there are N spin-orbitals (multiply each spatial MO with the spin functions α and β). A whole series of determinants can be generated from the Hartree-Fock determinant by replacing occupied MOs with the virtual ones. So we can have determinants describing singly, doubly, triply ... excited configurations. Thus, we can use the occupied and virtual molecular orbitals obtained in the Hartree-Fock calculation to construct these new determinants. We can write the exact wave function for any state of the system as linear combination of these determinants

$$|\Phi_{CI}\rangle = c_0|\psi_0\rangle + \sum_{ra} c_a^r|\psi_a^r\rangle + \sum_{\substack{a<b\\r<s}} c_{ab}^{rs}|\psi_{ab}^{rs}\rangle + \sum_{\substack{a<b<c\\r<s<t}} c_{abc}^{rst}|\psi_{abc}^{rst}\rangle + ..., \tag{2.27}$$

where $r, s, t, \cdots$ denote the occupied MOs and $a, b, c, \cdots$ refer to the unoccupied MOs. For instance we have $|\ \psi_0\rangle$ as the reference determinant [5]

$$|\ \psi_0\rangle = |\ \phi_1\bar{\phi}_1\phi_2\bar{\phi}_2\cdots\phi_r\bar{\phi}_r\cdots\phi_N\bar{\phi}_N\ |,$$

so singles (singly excited determinants) by replacing $\bar{\phi}_r$ with $\bar{\phi}_a$ will be:

$$|\ \psi_a^r\rangle = |\ \phi_1\bar{\phi}_1\phi_2\bar{\phi}_2\cdots\phi_r\bar{\phi}_a\cdots\phi_N\bar{\phi}_N\ |\ .$$

Doubly excited determinants will be

$$|\ \psi_{ab}^{rs}\rangle = |\ \phi_1\bar{\phi}_1\phi_2\bar{\phi}_2\cdots\phi_r\bar{\phi}_a\cdots\phi_s\bar{\phi}_b\cdots\phi_N\bar{\phi}_N\ |,$$

and higher excited determinants are defined in a similar way. By using the linear variational method we can determine the CI coefficients. This is conceptually the simplest method that includes the electron correlation and also excited states can be computed. However, the method is impractical for large molecules, since a larger basis set gives rise to more virtual MOs, then more excited determinants can be constructed i.e. the size of the CI-matrix will grow very fast with the number of basis functions included. Due to the long CPU time for the CI calculations, they are constrained for small systems and many CI calculations include only single or double excitations (CISD).

By taking the appropriate linear combination of the determinants one can find the function which fulfills the spin and spatial symmetry constrains called Configuration State Function (CSF). It is eigenfunction of the square of the spin operator, S^2, called spin adopted

[5] Here, we use the notation $\phi_i = \varphi_i\alpha$ and $\bar{\phi}_i = \varphi_i\beta$ for the spin orbitals. Furthermore, we introduce a short notation for a normalized Slater determinant (2.21).

configuration, and also is eigenfunction of the square of the angular momentum operator, J^2, called symmetry adopted configuration. There is no mixing of the wavefunctions with different spins. We can eliminate most of the determinants from the trial wavefunctions which do not have the same number of α and β spin orbitals, consequently we obtain a much shorter CI expansion.

2.3.4 The Multi-Configuration Self-Consistent Field (MCSCF) method

The Hartree-Fock orbitals in general are not the best choice of orbitals to use in a truncated CI expansion. The Multi-Configuration Self Consistent Field (MCSCF) method makes it possible to construct wavefunctions by taking linear combination of configuration state functions into account

$$\mid \Phi_{MCSCF}\rangle = \sum_I c_I \mid \psi_I\rangle, \tag{2.28}$$

where $\mid \psi_I\rangle$ are configuration state functions. This method gives a qualitatively correct description of the electronic structure in a molecular system. In the MCSCF method, both the MOs and the wavefunction coefficients are optimized simultaneously using the variational principle. In any chemical process where the number of electrons changes, correlation effects must be taken into account. One of the most important correlation effects is the so called near degeneracy effect (static correlation). Several electronic configurations are close in energy so the configuration mixing occurs in near-degenerate systems. Thus, the MCSCF wave-function estimates near-degeneracy effects that are essential to calculate the correct dissociation energy of a molecule.

By increasing the number of configurations in the MCSCF wave-functions, the energy will be lowered. The MCSCF optimization is an iterative scheme like the SCF procedure. By increasing the number of included configurations, the number of iterations required to reach convergence will be increased. Selecting the necessary configurations is the major problem of the MCSCF method. One of the most popular methods to determine what configurations to be included in the wavefunction is the Complete Active Space Self-Consistent Field (CASSCF) method [17]. Here the selection of configurations is done by partitioning the MOs into the active and the inactive spaces. The inactive MOs are classified into the core orbitals that always hold two electrons so they are always doubly occupied, and the virtual orbitals that hold zero electrons and they are always empty. The active MOs will be some of the

highest occupied and some of the lowest unoccupied MOs from a RHF calculation [14]. All possible configurations are included in the MSCSF calculation generated in the active space by promoting electrons from one MO to another. [See Fig.(2.1)]

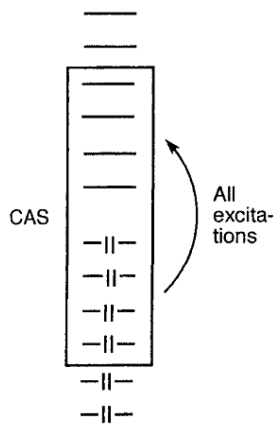

Figure 2.1 Complete active space

The excited states of a molecule play important roles in the various phenomena. The MCSCF method is a good method to compute excited states. However, important problems are encountered in practice during the MCSCF computation for the excited states. These kinds of calculations do not always converge and, even when they do, the interpretation of the obtained state is unclear, namely the active or inactive space is not well chosen [18]. In quantum chemistry this problem is called root flipping. If there are two states of the same symmetry that energetically are very close, the MCSCF algorithm may oscillate between these states and never converge. To avoid this problem during the computation for the excited states it is usually best to optimize the average energy for all states under consideration [19]. This is called a state-averaged MCSCF calculation.

2.3.5 The Multi-reference configuration interaction (MRCI) method

In the CI method we have seen that the Hartree-Fock configuration is selected as a single reference determinant. However, an MCSCF wavefunction may also be chosen as the reference. The CISD wavefunction has been shown to yield results of high quantitative accuracy for a molecular system where the Hartree-Fock single determinant is a good reference wavefunction. But in many case, in particular in open-shell systems, for excited states or in

case of degeneracies on near degeneracies, the Hartree-Fock wavefunction is not suitable as a reference wavefunction. In the MCSCF method the qualitative problems with the single configuration Hartree-Fock approximation can be corrected by adding a few other configurations. The simplest idea to extend the CISD wavefunction is to construct a reference wavefunction from some configurations that are known to be important for the description of the relevant electronic states. Out of these reference configurations single and double excitations into virtual orbitals can then be added. Often in the MRCI calculations, the reference configurations are constrained by defining an active space (similar to what is done in CASSCF method [see figure 2.1] with active orbitals and electrons). Reference configurations are constructed by all excitations of the active electrons among the active orbitals. In general, the wavefunction can be written in form of

$$\mid \Phi_{MRCI}\rangle = \sum_{I} \mid \Phi_{SD}(I)\rangle = \sum_{I} \mid \psi(I)\rangle + \sum_{S}\sum_{a} c_a^S \mid \psi_S^a\rangle + \sum_{D}\sum_{ab} c_{ab}^D \mid \psi_D^{ab}\rangle, \qquad (2.29)$$

where a, b denote external orbitals and S and D denote internal $N-1$ and $N-2$ electron hole states, respectively. Moreover, $\mid \psi(I)\rangle$ are the reference wavefunctions, $\mid \psi_S^a\rangle$ is the singly external (virtual) configuration, and $\mid \psi_D^{ab}\rangle$ is the doubly external configuration [20, 21]. This is the Multi-Reference Configuration Interaction (MRCI) wavefunction. Despite all the improvement to describe electron correlation, the MRCI method has been limited by the fact that the size of the configuration expansion and computational effort rapidly increase with the number of reference configurations [14]. The dynamical correlation effects are described by configurations with one or more electrons in the virtual MOs, i.e. excitation of the active electrons into the external (virtual) molecular orbitals of the MCSCF wavefunction account for the dynamical correlation energy. The most obvious approach to dynamical correlation is the MRCI calculation using the MCSCF as the reference wavefunction [22].

2.3.6 Basis set

We have mentioned before that the molecular orbitals can be created by linear combinations of a set of functions called atomic orbitals. The basis sets typically model atomic orbitals centered on the atoms. When the minimum number of the basis functions is used to describe the orbitals in each atom we have the minimal basis sets. For an atom such as Li with an electron configuration of $(1s)^2(2s)^1$, we have $1s$, $2s$ atomic orbitals.

In quantum chemistry calculations approximate atomic orbitals are used with different forms. One type of basis functions is the Slater type function (STO) which is similar to the hydrogen wavefunction

$$\phi = Nr^n e^{-\zeta r} Y_{l,m}(\theta, \phi),$$

where ζ controls the width of the orbital and N is the normalization constant. Another type of normalized basis functions is the Gaussian type function (GTO)

$$\phi = N' r^n e^{-\alpha r^2} Y_{l,m}(\theta, \phi),$$

where α is the Gaussian orbital exponent [13]. The important difference between these two types of basis functions occur when $r \to 0$ and at large values of r. At $r = 0$ the STO has finite slope but the slope of the GTO is zero. At larger r the GTO decays more rapidly than the STO. So the STO has more correct short-range and long range behaviors than the GTO. The STO function describes the molecular orbitals more correctly and we need fewer STO functions than GTO functions for comparable results. Using the GTO basis functions makes the calculation of the two electron integrals in the Hartree-Fock equation much easier and faster in the SCF process. Because the product of the two Gaussian functions with two different centers will be a Gaussian function on a third center, the integrals can be computed analytically.

A larger basis set can give a more accurate result. For better description, the number of basis functions per atom can be increased by multiplying a minimal basis set and obtain the double, triple, quadruple zeta, $\cdots$ basis sets. For the Li atom it will be $1s$, $1s'$, $2s$, $2s'$ atomic orbitals. When only the valance orbitals are duplicated one can get the Split Valence basis sets. For the Li atom this will be $1s$, $2s$, $2s'$ atomic orbitals [23].

Furthermore, the basis sets can be improved by adding polarization functions, which include higher angular momentum functions $(d, f, g, \cdots)$. Polarization functions are essential to reduce the error in the correlation energy.

For some systems, especially anions and Rydberg systems where the electron distribution is more extended, we need to add basis functions with small exponent in order to describe the diffuse electron distribution and provide more accurate description of excited states. Although there are procedures to reach the complete basis set limit by enlarging the basis set, this approach is slowly convergent.

Most recently, the correlation-consistent polarized valence double (D)-, triple (T)-, quadruple (Q)-, quintuple (5)-, and sextuple (6)-, ζ basis set which are developed by Dunning and coworkers [24] [25], have been employed [26]. These are arranged in two series, in particular $(cc-PVXZ, X = D, T, Q, 5, 6)$ and aug-$(cc-PVXZ, X = D, T, Q, 5, 6)$. The prefix aug-(for 'augmented') denotes the addition of diffuse basis functions, i.e. Gaussian functions with small exponential parameters times spherical harmonics [27]. The coefficients and exponents of the basis functions are optimized using calculations on atoms.

The accuracy of the electronic structure depends not only on which level of theory should be chosen, but also on the quality of the finite set of basis functions used to expand the orbitals.

Chapter 3

Non-Adiabatic molecular dynamics

3.1 Non-adiabatic coupled Schrödinger equation

In the previous chapter we have seen that the Born-Oppenheimer approximation is very useful for solving the Schrödinger equation for a molecular system. It is a good approximation to simplify many calculations as long as the nuclear motion is considered to be restrained to one potential energy surface. To go beyond the Born-Oppenheimer approximation the total wavefunction can be expanded in the adiabatic electronic functions [See the equation (2.6)]. The eigenstates of the electronic Hamiltonian and the corresponding eigenvalues will parametrically depend on the nuclear coordinates.

The Hamiltonian (2.3) can be rewritten as

$$H = -\frac{1}{2M}\nabla_R^2 + H_{el}, \tag{3.1}$$

where M is a measure of nuclear mass in units of the electronic mass. H_{el} is the electronic Hamiltonian for fixed nuclear configuration and it is including the nuclear repulsion also to obtain a compact form. For convenience all the nuclear reduced masses have the same value M since we use scaled nuclear coordinates [28]. We consider the equation (2.12) and rewrite it as

$$-\frac{1}{2M}\left(\nabla_R^2\chi_j(R) + 2\sum_i T_{ji}^{(1)}(R)\cdot\nabla_R\chi_i(R) + \sum_i T_{ji}^{(2)}(R)\chi_i(R)\right) + U_j(R)\chi_j(R) = E\chi_j(R), \tag{3.2}$$

A set of coupled differential equations is obtained for the nuclear motion. In matrix form, they can be written as

$$\left(-\frac{1}{2M}\nabla_R^2\mathbf{1} - \frac{1}{M}\mathbf{T^{(1)}}\cdot\nabla_R - \frac{1}{2M}\mathbf{T^{(2)}} + \mathbf{U}\right)\chi(R) = E\mathbf{1}\chi(R), \tag{3.3}$$

or

$$\left(-\frac{1}{2M}\nabla_R^2\mathbf{1} - \mathbf{\Lambda} + \mathbf{U}\right)\chi(R) = E\mathbf{1}\chi(R),$$

where ∇_R denotes the gradient operator in nuclear coordinate space, $\mathbf{1}$ denotes the unit matrix, $\chi(R)$ is a column vector containing the nuclear wavefunctions $\chi_j(R)$. The vector valued matrix (tensor) $\mathbf{T^{(1)}}$ and the matrix $\mathbf{T^{(2)}}$ both have off-diagonal elements, which are the non-adiabatic couplings between different electronic states, together denoted by $\mathbf{\Lambda}$. Here, $\mathbf{T}^{(1)}$ is the first derivative non-adiabatic coupling (vector) matrix with the elements

$$T_{ji}^{(1)}(R) = \langle\psi_j(r;R)|\nabla_R\psi_i(r;R)\rangle, \tag{3.4}$$

and $\mathbf{T}^{(2)}$ is the second derivative non-adiabatic (scalar) matrix with the elements [29]

$$T_{ji}^{(2)}(R) = \langle\psi_j(r;R)|\nabla_R^2\psi_i(r;R)\rangle. \tag{3.5}$$

By definition the potential energy matrix

$$U_{ij}(R) = \langle\psi_i(r;R)|H_{el}|\psi_j(r;R)\rangle, \tag{3.6}$$

is diagonal at each R and contains the adiabatic potential surfaces.

If the adiabatic electronic wavefunctions are assumed to be real, $\mathbf{T^{(1)}}$ is antisymmetric, i.e.

$$T_{ij}^{(1)}(R) = -T_{ji}^{(1)}(R). \tag{3.7}$$

The coupled Schrödinger equation (3.3) includes the complete, infinite set of adiabatic electronic states. The Born-Oppenheimer approximation is achieved by the assumption that the non-adiabatic couplings $\mathbf{\Lambda}$ can be neglected. The nuclei will then remain on a single potential energy surface, i.e. no population transfer between surfaces occurs. However, there are many cases where the non-adiabatic couplings $\mathbf{\Lambda}$ are not negligible and it often turns out that they vary rapidly with R and thereby may cause problems in the numerical calculations.

We will now take a closer look at the first derivative non-adiabatic coupling terms and discuss the relation between these couplings and the adiabatic potential energy surfaces. We

can rewrite the first derivative non-adiabatic coupling terms by considering the electronic Schrödinger equation as following:

$$\nabla_R\{(H_{el}\psi_i(r;R))\} = \nabla_R\{U_i(R)\psi_i(r;R)\}$$
$$\{\nabla_R H_{el}\}\psi_i(r;R) + H_{el}\{\nabla_R\psi_i(r;R)\} = \{\nabla_R U_i(R)\}\psi_i(r;R) + U_i(R)\{\nabla_R\psi_i(r;R)\} \quad (3.8)$$

Multiplying from the left with ψ_j^* and integrating over the electronic coordinates, r, leads to:

$$\langle\psi_j(r;R)|\nabla_R H_{el}|\psi_i(r;R)\rangle + U_j(R)\langle\psi_j(r;R)|\nabla_R\psi_i(r;R)\rangle = \langle\psi_j(r;R)|\nabla_R U_i(R)|\psi_i(r;R)\rangle + U_i(R)\langle\psi_j(r;R)|\nabla_R\psi_i(r;R)\rangle \quad (3.9)$$

If $i = j$ we obtain

$$\langle\psi_i(r;R)|\nabla_R H_{el}|\psi_i(r;R)\rangle = \nabla_R U_i(R), \quad (3.10)$$

otherwise we have

$$T_{ji}^{(1)}(R) = \langle\psi_j(r;R)|\nabla_R\psi_i(r;R)\rangle = \frac{\langle\psi_j(r;R)|\nabla_R H_{el}|\psi_i(r;R)\rangle}{U_i(R) - U_j(R)}. \quad (3.11)$$

These are the diagonal and non-diagonal 'Hellmann-Feynman' theorems. According to the non-diagonal Hellmann-Feynman theorem, the non-adiabatic coupling depends inversely on the energy gap between the adiabatic surfaces. If the energy separation between two electronic states becomes small, the coupling element becomes large and the nuclear motions on different energy surfaces are coupled. In a diatomic molecular system, the adiabatic potential energy curves for states of the same electronic symmetry can not cross. This is called the non crossing rule which was first recognized by Hund in 1927 [30] and demonstrated by Von Neumann and Wigner in 1929 [31]. When two adiabatic curves come close in energy, they will repel each other and an avoided crossing will appear. In some situations it will be convenient to define curves which do cross and this will be discussed further bellow. [See figure 3.1] For polyatomic molecular systems, it might be possible that two energy surfaces cross each other even when they have same symmetry. This is called a conical intersection[1].

[1] In the degeneracy of two electronic states, non-adiabatic couplings are strong, which was first pointed out by Teller [32] in 1937, who extended the work of Zener [33] in 1932 on non-adiabatic transition probabilities. In polyatomic molecules where we expect an avoided crossing, there are the possible existence of point in the configuration space where the adiabatic electronic states are degenerate. The name of conical intersection comes from the local shape of the two potential energy surfaces around the degeneracy point in contrast to the avoided crossing appearing in diatomic molecules.

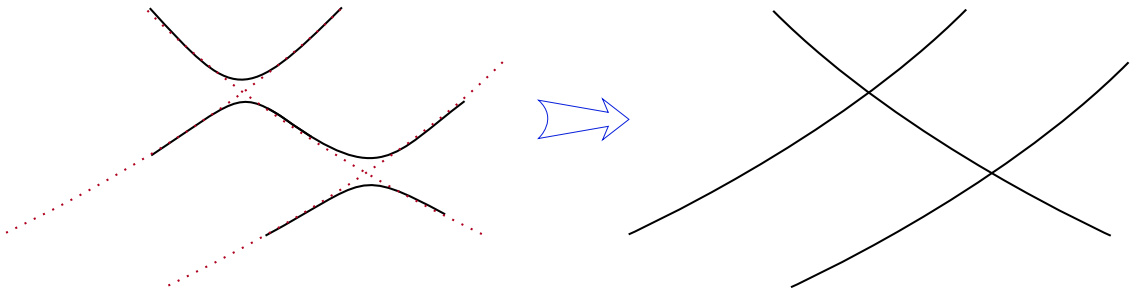

Figure 3.1 Schematical representation of adiabatic potential energy curves shows how the potentials approach each other but never cross [left hand side]. Diabatic potential curves in a region of avoided crossing [right hand side].

At the degeneracy points where the electronic wavefunctions change rapidly as a function of the nuclear coordinates, the derivative couplings can diverge and singularity may exist. Then the adiabatic approximation is expected to break down. The nuclear motion on lower and upper adiabatic potential energy surfaces is then strongly coupled. Consequently, the vibrational energy levels on the adiabatic energy surface have no longer any physical meaning. The approximation (2.6) becomes meaningless as well [34]. These singularities of the non-adiabatic coupling terms complicate the solution of the equation (3.3). It is therefore preferable to transform the electronic Schrödinger equation by using basis functions for the electronic states where some or all of the nonadiabatic coupling terms disappear.

3.2 Adiabatic to diabatic transfromation

In the adiabatic representation, the coupling terms involve derivative operators. For the aim of canceling these non-adiabatic couplings, diabatic electronic states are introduced which are obtained from an unitary transformation, first introduced by Hellmann and Syrkin [35] in 1935 and later generalized by Smith [36] and Baer [2]. All types of adiabatic to diabatic transformations, called *diabatizations*, are based on smoothness of either wavefunctions or the expectation values of physical properties. In 1975, Baer [2] showed how to transform the adiabatic states to a diabatic representation. The '*adiabatic to diabatic transformation*' (ADT) matrix can be obtained by solving a line integral equation containing the non-adiabatic coupling elements. It is assumed that the total wavefunction (2.6) can be represented in a finite set of N adiabatic basis functions. Then a sub-space of dimension M $(M < N)$ is considered

with the following feature [37]

$$T_{ij}^{(1)} \cong 0 \quad \text{for} \quad i \leq M, \quad j > M. \tag{3.12}$$

If we consider the derivative of $T_{ij}^{(1)}$, we have

$$\nabla_R T_{ij}^{(1)} = \langle \nabla_R \psi_i(r;R) \mid \nabla_R \psi_j(r;R) \rangle + \langle \psi_i(r;R) \mid \nabla_R^2 \psi_j(r;R) \rangle. \tag{3.13}$$

Here, we need to evaluate the first term of the right hand side of this expression and by using the completeness relation, we obtain

$$\langle \nabla_R \psi_i(r;R) \mid \nabla_R \psi_j(r;R) \rangle = \langle \nabla_R \psi_i(r;R) \mid \left(\sum_{k=1}^{M} \mid \psi_k(r;R) \rangle \langle \psi_k(r;R) \mid \right) \mid \nabla_R \psi_j(r;R) \rangle$$

$$= \sum_{k=1}^{M} \langle \nabla_R \psi_i(r;R) \mid \psi_k(r;R) \rangle \langle \psi_k(r;R) \mid \nabla_R \psi_j(r;R) \rangle = \sum_{k=1}^{M} T_{ki}^{(1)} T_{kj}^{(1)},$$

or finally we have

$$\langle \nabla_R \psi_i(r;R) \mid \nabla_R \psi_j(r;R) \rangle = -\sum_{k=1}^{M} T_{ik}^{(1)} T_{kj}^{(1)}. \tag{3.14}$$

Substituting equation (3.14) into equation (3.13) yields

$$T_{ij}^{(2)} = \sum_{k=1}^{M} T_{ik}^{(1)} T_{kj}^{(1)} + \nabla_R T_{ij}^{(1)}. \tag{3.15}$$

Thus, the same applies to $T_{ij}^{(2)}$, i.e.

$$T_{ij}^{(2)} = \langle \psi_i(r;R) \mid \nabla_R^2 \psi_j(r;R) \rangle = 0 \quad \text{for} \quad i \leq M, \quad j > M. \tag{3.16}$$

For $i,\ j \leq M$, a new set of M electronic basis functions can be defined by the following transformation in terms of an orthogonal transformation matrix $A_{ij}(R)$ as

$$\tilde{\psi}_i(r;R) = \sum_{j=1}^{M} \psi_j(r;R) A_{ij}^{\dagger}(R). \tag{3.17}$$

Here, $A_{ij}^{\dagger}$ is the complex conjugate of A_{ij}. Since the total wavefunction has to be unchanged we shall introduce a different set of nuclear wavefunctions according to

$$\tilde{\chi}_i(R) = \sum_{j=1}^{M} \chi_j(R) A_{ij}^{\dagger}(R). \tag{3.18}$$

Such that total wavefunction will take the form

$$\Psi(r;R) = \sum_{i}^{M} \tilde{\psi}_i(r;R)\tilde{\chi}_i(R). \tag{3.19}$$

The R dependent transformation matrix A should be capable to make the basis $\tilde{\psi}_i$ strictly diabatic, i.e. [28]

$$\tilde{T}^{(1)}_{ij}(R) = \langle \tilde{\psi}_i(R) \mid \nabla_R \tilde{\psi}_j(R) \rangle = 0. \tag{3.20}$$

From the equation (3.17) we have

$$\nabla_R \tilde{\psi}_i(r;R) = \sum_{j=1}^{M} [\{\nabla_R \psi_j(r;R)\} A^{\dagger}_{ij} + \psi_j(r;R)\{\nabla_R A^{\dagger}_{ij}\}], \tag{3.21}$$

so

$$\tilde{T}^{(1)}_{ij} = \sum_{j=1}^{M} A^{\dagger}_{ij} \langle \psi_i(r;R) \mid \nabla_R \psi_j(r;R) \rangle A_{ij} + A^{\dagger}_{ij} \nabla_R A_{ij}, \tag{3.22}$$

or in the matrix form

$$\tilde{\mathbf{T}}^{(1)} \equiv \mathbf{T}^{(1)d} = \mathbf{A}^{\dagger}[\mathbf{T}^{(1)} + \nabla_R \mathbf{1}]\mathbf{A}. \tag{3.23}$$

In the same way, we can obtain

$$\nabla^2_R \tilde{\psi}_i(r;R) = \sum_{j=1}^{M} [\{\nabla^2_R \psi_j(r;R)\} A^{\dagger}_{ij} + 2\nabla_R \psi_j(r;R) \cdot \nabla_R A^{\dagger}_{ij} + \psi_j(r;R)\nabla^2_R A^{\dagger}_{ij}], \tag{3.24}$$

or in matrix form

$$\tilde{\mathbf{T}}^{(2)} \equiv \mathbf{T}^{(2)d} = \quad \mathbf{A}^{\dagger} \left\{ \mathbf{T}^{(2)} + 2\mathbf{T}^{(1)} \cdot \nabla_R + \nabla^2_R \mathbf{1} \right\} \mathbf{A}. \tag{3.25}$$

Substitution of eqution (3.23) and (3.25) into equation (3.3) yields [38]:

$$\left(-\frac{1}{2M} \nabla^2_R \mathbf{1} - \frac{1}{M} \mathbf{T}^{(1)d} \cdot \nabla_R - \frac{1}{2M} \mathbf{T}^{(2)d} + \mathbf{U}^d \right) \tilde{\chi}(R) = E\mathbf{1}\tilde{\chi}(R), \tag{3.26}$$

where

$$\mathbf{U}^d = \mathbf{A}^{\dagger}\mathbf{U}\mathbf{A}. \tag{3.27}$$

To satisfy the condition (3.20), matrix $\mathbf{A}$ must be a solution of equation

$$(\mathbf{T}^{(1)} + \nabla_R \mathbf{1})\mathbf{A} = 0. \tag{3.28}$$

Also $\mathbf{T}^{(2)d}$ can be shown to vanish according to equation (3.15), by substituting $\mathbf{T}^{(2)} = (\mathbf{T}^{(1)})^2 + \nabla_R \mathbf{T}^{(1)}$ in the equation (3.25) [39]. The coupled equations finally take the form

$$\left(-\frac{1}{2M}\nabla_R^2 \mathbf{1} + \mathbf{U}^d\right)\tilde{\chi}(R) = E\mathbf{1}\tilde{\chi}(R). \tag{3.29}$$

In the diabatic framework, the nonadiabatic couplings transform into off-diagonal elements of the potential matrix $\mathbf{U}^d$ and as a consequence its diagonal elements may cross each other.

The integral representation of the equation (3.28) along a line is suggested as a convenient way to treat the first-order differential equation [40]

$$\mathbf{A}(R, R_0) = \mathbf{A}(R_0) - \int_{R_0}^{R} d\mathbf{R}' \cdot \mathbf{T}^{(1)}\mathbf{A}(R', R_0), \tag{3.30}$$

where the integral is performed along a path Γ, and R and R_0 are two points defined on Γ. The matrix $\mathbf{A}(R_0)$ is the boundary condition and dot denotes a scaler product between the vector matrix $\mathbf{T}^{(1)}$ and the differential path element $d\mathbf{R}$. By employing the propagation technique, the more straightforward integration of equation (3.28) leads to following representation of $\mathbf{A}$ [37]

$$\mathbf{A}(R) = \exp\left(-\int_{R_0}^{R} d\mathbf{R}' \cdot \mathbf{T}^{(1)}\right)\mathbf{A}(R_0). \tag{3.31}$$

The solution of the equation (3.31) is well defined when $\mathbf{T}^{(1)}$ has a non-zero component[2] along Γ. For different paths, there are different results for a given point R. As long as $\mathbf{A}$ is uniquely defined at each point, the same holds for $\mathbf{U}^d$. Necessary condition for having a uniquely defined diabatic potential matrix has been proved by Baer for a closed path [See ref. [37,41]]. A diagonal matrix $\mathbf{S}$ is defined which contains diagonal complex numbers whose norm is 1

$$\mathbf{A}(R = 2\pi) = \mathbf{S}\mathbf{A}(R = 0). \tag{3.32}$$

For a closed path, equation (3.32) becomes similar to equation (3.31), hence the $\mathbf{S}$ matrix can be derived as

$$\mathbf{S} = \exp(\oint_{\Gamma} d\mathbf{R}' \cdot \mathbf{T}^{(1)}). \tag{3.33}$$

A unitary matrix $\mathbf{G}$ is introduced to diagonalize $\mathbf{T}^{(1)}$. The diagonal matrix $i\mathbf{t}(R)$ contains the eigenvalues of $\mathbf{T}^{(1)}(R)$ as calculated at a point R on Γ. Since all $\mathbf{T}^{(1)}$ matrices are

[2]The scaler product $\mathbf{T}^{(1)} \cdot d\mathbf{R}' = \mathbf{T}_R^{(1)} dR'$, where $\mathbf{T}_R^{(1)}$ is the component of $\mathbf{T}^{(1)}$ along Γ, is scaler matrix.

antisymmetric, they have imaginary or zero eigenvalues $it_m(R)$. For a uniquely defined matrix $\mathbf{T}^{(1)}$ at each point we have[3]

$$\mathbf{S} = \mathbf{G}(R_0) \exp\left(-i \oint_\Gamma d\mathbf{R}' \cdot \mathbf{t}(R)\right) \mathbf{G}^\dagger(R_0). \tag{3.34}$$

Consequently, in the diabatic representation the electronic wavefunctions used to expand the total wavefunction are not the eigenfunctions of the electronic Hamiltonian, but they are chosen to eliminate the derivative coupling terms. However, the truncated sum over the diabatic states causes the derivative coupling to not completely vanish and the strict diabatic condition is not fulfilled. The derivative coupling becomes negligible small. Furthermore, in the adiabatic representation the coupling term is a vector containing the operator ∇_R, whereas in the diabatic representation it becomes a scaler and hence it is easier to use numerically.

3.3 Two states systems

The two state system has been discussed by Baer *et al.* [37]. In the two state system, we have two coupled adiabatic potential surfaces. First we obtain the ADT matrix then we use this matrix to transform from adiabatic to diabatic representations. The non-adiabatic coupling matrix in this case is given by [37]

$$\mathbf{T} = \begin{pmatrix} 0 & t(R) \\ -t(R) & 0 \end{pmatrix}. \tag{3.35}$$

The matrix $\mathbf{G}$ diagonalizing $\mathbf{T}$ has the form

$$\mathbf{G} = \frac{1}{\sqrt{2}} \begin{pmatrix} 1 & 1 \\ i & -i \end{pmatrix}. \tag{3.36}$$

The corresponding eigenvalues of $\mathbf{T}$ are $\pm it(R)$. By using equation (3.34), the matrix $\mathbf{S}$ can be derived

$$\mathbf{S} = \frac{1}{2} \begin{pmatrix} 1 & 1 \\ i & -i \end{pmatrix} \begin{pmatrix} exp[-i\gamma(R)] & 0 \\ 0 & exp[i\gamma(R)] \end{pmatrix} \begin{pmatrix} 1 & -i \\ 1 & i \end{pmatrix}, \tag{3.37}$$

[3] $\mathbf{G}^\dagger$ is complex conjugate

$$\mathbf{S} = \begin{pmatrix} \cos[\gamma(R)] & -\sin[\gamma(R)] \\ \\ \sin[\gamma(R)] & \cos[\gamma(R)] \end{pmatrix}.$$

Here, $\gamma(R)$ is defined as the adiabatic to diabatic transformation angle:

$$\gamma(R) = \oint_{\Gamma} dR' \cdot \mathbf{t}(R). \tag{3.38}$$

Consequently, the ADT matrix elements, $\mathbf{S} \equiv \mathbf{A}$, is known when the transformation angle is determined. Then, it is possible to transform the adiabatic basis functions, $\psi_i(r;R)$, to diabatic basis functions, $\tilde{\psi}_i(r;R)$, via the equation (3.17), i.e.

$$\begin{pmatrix} |\tilde{\psi}_1(r;R)\rangle \\ |\tilde{\psi}_2(r;R)\rangle \end{pmatrix} = \mathbf{S} \begin{pmatrix} |\psi_1(r;R)\rangle \\ |\psi_2(r;R)\rangle \end{pmatrix}. \tag{3.39}$$

According to equation (3.29) the 2×2 diabatic potential energy matrices has the following form:

$$\mathbf{U}^d = \begin{pmatrix} U^d_{11} & U^d_{12} \\ \\ U^d_{21} & U^d_{22} \end{pmatrix}. \tag{3.40}$$

Here, U^d_{11} and U^d_{22} are assumed to be diabatic potential surfaces which cross each other at a configuration R_0 and U^d_{12} is the matrix element of the electronic Hamiltonian of the system between two diabatic wavefunctions. The electronic Hamiltonian is diagonalized and the eigenvalues and eigenfunctions are obtained

$$U^a_{1,2} = \frac{[U^d_{11} + U^d_{22}]}{2} \pm \frac{1}{2}\sqrt{\left[U^d_{11} - U^d_{22}\right]^2 + 4{U^d_{12}}^2}, \tag{3.41}$$

where

$$\gamma(R) = \frac{1}{2}\arctan\frac{2U^d_{12}}{U^d_{11} - U^d_{22}}.$$

The eigenvalues are degenerate if $U^d_{11} = U^d_{22}$ and $U^d_{12} = 0$. These are two sufficient conditions for existence of a conical intersection. In order to satisfy these conditions, at least two degrees of freedom for nuclear coordinates are required, i.e. for a system with N_a degrees of freedom, the two conditions are satisfied in an $N_a - 2$ subspace which has been argued by Teller in 1937 [32] as well as by Herzberg and Longuet-Higgins in 1963 [42].

Naqvi and Bayer Brown in 1972 [43] objected that for a molecule with N_a degrees of freedom it can be shown that there are $N_a + 1$ conditions that must be fulfilled to obtain a crossing. Hence the non-crossing rule applies to polyatomic molecules as well as diatomic molecules. They proposed an alternative pairs of conditions for a crossing to occur at R_0, i.e.

$$U_1^a(R_0) = U_2^a(R_0)$$

and

$$F_{12} = \sum_{i=1}^{N_a} \langle \psi_1 \mid \frac{\partial H_{el}}{\partial R_i} \mid \psi_2 \rangle = 0.$$

These two conditions should be simultaneously satisfied [43,44]. This argue has been refused by Longuet-Higgins [45], when there are always enough independent internuclear coordinates for polyatomic molecules (See chapter 4) which satisfy both conditions at once, so that the noncrossing rule no longer applies. Longuet-Higgins has shown that if the sign of an electronic wavefunction changes when passing around a closed path in configuration space then there must be a point within the loop where states are degenerate. Figure 3.2-(a) shows a double cone with a vertex at the origin which often referred as conical intersection, and 3.2-(b) illustrates $N_a - 2$ dimensional intersection space consisting of an infinite number of conical intersection points. If we move in 2-dimensional branching space away from the apex of the cone, the degeneracy is lifted, but moving from the apex of the cone along the remaining $N_a - 2$ dimensional intersection space does not lift degeneracy.

These relations (3.41) are useful when the matrix $\mathbf{U^d}$ is known. In the next chapter we shall discuss about the Hamiltonian model and find $\mathbf{U^d}$.

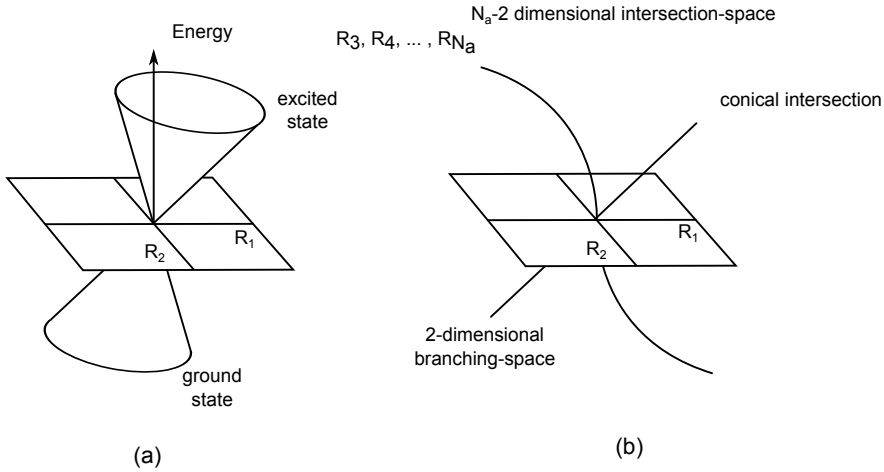

Figure 3.2 (a) One double-cone with the same vertex (conical intersection), (b) $N_a - 2$ dimensional intersection space

Chapter 4

Symmetry and normal mode coordinates

In this chapter we will first discuss symmetry that is an important concept used when describing physical systems. In molecular physics, symmetry simplifies the explanation of molecular structures. In the history of molecular physics, symmetry and group theoretical methods were employed very early by Wigner [31] to prove the non-crossing rule for adiabatic potential energy curves of a diatomic molecule. We shall here discuss molecular symmetries and also introduce the normal mode coordinates used for describing nuclear motion of a molecule. These coordinates simplify the description of nuclear motions of polyatomic molecules by exploiting the underlying symmetry of the systems.

4.1 Symmetry properties and point group

Molecular symmetry describes the classification of molecules according to the symmetry of the equilibrium structure. One framework to study of the molecular symmetry is by using group theory. There are in general five types of symmetry elements that can describe the symmetry of a molecule:

1. *Symmetry axis or n fold rotational axis*, C_n,
2. *Plane of symmetry or mirror plane*, σ,
3. *Center of symmetry or inversion center*, i,
4. *N-fold rotation-reflection axis of symmetry*, S_n,

5. *Identity*, E.

These five symmetry elements are associated with different symmetry operations, transforming the atoms in the molecule into final positions that are indistinguishable from the initial positions. For every symmetry transformation acting on a molecule there is a corresponding operator P_R.

The structure of a molecule is symmetric under certain symmetry elements and these elements form a mathematical group and one point, i.e. the center of mass, is fixed under all symmetry operations. This group is called the point group. Every molecule with a given nuclear configuration belongs to a particular point group. The table 4.1 contains a list of some important point groups.

Furthermore, for each point group, a character table summarizes information on symmetry operations and the irreducible representation[1] which we will discuss further below. The rows of the character table shows the irreducible representations and the columns correspond to classes of group elements. In chemistry, the character tables are used to classify the molecules according to their symmetries. Table 4.2 shows character tables for common point groups that are used in diatomic and planar triatomic systems. In this work we use the abelian point group D_{2h} to describe the diatomic molecules X_2, and C_{2v} and C_s to describe the planar molecules X_3. We also exploit the non-abelian[2] point group D_{3h} for description of high symmetry triatomic planar molecule.

A common representation of a group is the matrix representation and the symbol Γ will be used to denote a general representation. A particular matrix belonging to the jth representation will be identified by $\Gamma^{(j)}(R)$ where R denote the group elements or symmetry operators. The character of a representation matrix $\Gamma^{(j)}(R)$ is the sum of diagonal elements (trace)

$$\chi^{(j)}(R) = \sum_{\alpha} \Gamma^{(j)}_{\alpha\alpha}(R). \tag{4.1}$$

Assume we have a general representation of Γ. If there is a matrix M where the transformation $M\Gamma(R)M^{-1}$ forms a matrix consisting of blocks along the main diagonal and the

[1] An irreducible representation of a group is a group representation that has no nontrivial invariant subspaces.

[2] In the non-abelian point group, there are at least two operation elements which are not commutative, i.e. $P_{R_1}P_{R_2} \neq P_{R_2}P_{R_1}$. That is, the order in which the two operations are applied is important.

point group	*irreducible representation*	*degeneracy*
K_n (spherical) for atoms	$s\ p\ d\ f\ \cdots$	1 3 5 7
$D_{\infty h}$, for homonuclear diatomic molecule	$\sigma_g\ \sigma_u\ \pi_u\ \pi_g\ \delta_g\ \cdots$	1 1 2 2 2 $\cdots$
$C_{\infty v}$, for heteronuclear diatomic molecule	$\sigma\ \pi\ \delta\ \pi\ \cdots$	1 2 2 2 $\cdots$
C_{2v}, planar molecule with two symmetry planes	$a_1\ b_1\ b_2\ a_2$	1 1 1 1
C_s, planar molecule with one symmetry plane	$a^{'}\ a^{''}$	1 1
D_{3h}, planar molecule with three symmetry planes	$a_1'\ a_2'\ e'\ \cdots$	1 1 2 $\cdots$

Table 4.1 The different point groups and their degeneracy and irreducible representation.

dimension of the blocks is smaller than the dimension of Γ, we have a reducible representation. An irreducible representation is one whose matrix cannot be reduced [46], for example:

$$\Gamma^{(6)}(R) = \left(\begin{array}{cc|cc|c|c} \mathrm{a} & \mathrm{b} & 0 & 0 & 0 & 0 \\ \mathrm{c} & \mathrm{d} & 0 & 0 & 0 & 0 \\ \hline 0 & 0 & \mathrm{a} & \mathrm{b} & 0 & 0 \\ 0 & 0 & \mathrm{c} & \mathrm{d} & 0 & 0 \\ \hline 0 & 0 & 0 & 0 & 1 & 0 \\ \hline 0 & 0 & 0 & 0 & 0 & 1 \end{array}\right).$$

This matrix $\Gamma^{(6)}(R)$ consists of 4 separated blocks along the main diagonal, two of the blocks are two dimensional and other two are one dimensional. Therefore, $\Gamma^{(6)}(R)$ is said that to be reducible into $2\Gamma^{(1)}(R)$ and $2\Gamma^{(2)}(R)$ and it can be expressed symbolically by

$$\Gamma^{(6)}(R) = 2\Gamma^{(1)}(R) + 2\Gamma^{(2)}(R).$$

In general the reduction of Γ can be expressed by writing

$$\Gamma = \sum_i a_i \Gamma^{(i)}, \tag{4.2}$$

where a_i is a positive integer and indicates how many times the representation matrix $\Gamma^{(i)}(R)$ appears along the main diagonal of the matrix Γ. If l_i is a dimension of the ith irreducible representation, the order of the group i.e. h, can be obtained by

$$\sum_i l_i^2 = h. \tag{4.3}$$

The order of the group is the same as the number of symmetry operators belonging to that group. Let $\chi(R)$ be the character of reducible representation $\Gamma(R)$. It can be expressed by using the characters of the irreducible representation according to

$$\chi(R) = \sum_i a_i \chi^{(i)}(R). \tag{4.4}$$

The characters of the irreducible representations can be shown to be orthogonal. Using the orthogonality, the coefficient a_i can be obtained as

$$a_i = \frac{1}{h} \sum_R \chi^{(i)}(R)^* \chi(R). \tag{4.5}$$

We should also introduce the projection operator which will be used for obtaining normal mode coordinates in the next section that is the projection operator defined as

$$\rho^{(j)} = (\frac{l_j}{h}) \sum_R \chi^{(j)}(R)^* P_R. \tag{4.6}$$

The projection operator can be used to determine basis functions for the different irreducible representations of a point group. We will employ this operator to obtain the normal mode coordinates in the next section.

4.2 Application of group theory in molecules

A symmetry operator can commute with the Hamiltonian H of a molecule, $[H, P_R] = 0$. The Hamiltonian is then invariant under the operation of a symmetry operator (symmetry group). The classification of the eigenfunctions of the symmetry operator can be used to classify the eigenfunctions of the Hamiltonian. So the eigenfunction of the Hamiltonian can be classified according to the irreducible representations of a point group [46].

One example of using symmetry in the quantum chemistry is the way to form the linear configuration of the determinants to use in the MCSCF method. The symmetry adapted

D_{2h}	E	$C_2(z)$	$C_2(y)$	$C_2(x)$	i	$\sigma(xy)$	$\sigma(xz)$	$\sigma(yz)$		
A_g	1	1	1	1	1	1	1	1		x^2, y^2, z^2
B_{1g}	1	1	-1	-1	1	1	-1	-1	R_z	xy
B_{2g}	1	-1	1	-1	1	-1	1	-1	R_y	xz
B_{3g}	1	-1	-1	1	1	-1	-1	1	R_x	yz
A_u	1	1	1	1	-1	-1	-1	-1		xyz
B_{1u}	1	1	-1	-1	-1	-1	1	1	z	
B_{2u}	1	-1	1	-1	-1	1	-1	1	y	
B_{3u}	1	-1	-1	1	-1	1	1	-1	x	

D_{3h}	E	$2C_3$	$2C_2$	σ_h	$2S_3$	$3\sigma_v$		
A_1'	1	1	1	1	1	1		$x^2+y^2,\ z^2$
A_2'	1	1	-1	1	1	-1	R_z	
E'	2	-1	0	2	-1	0	(x, y)	$(x^2-y^2,\ xy)$
A_1''	1	1	1	-1	-1	-1		
A_2''	1	1	-1	-1	-1	1	z	
E''	2	-1	0	-2	1	0	$(R_z,\ R_y)$	$(xz,\ yx)$

C_{2v}	E	C_2	$\sigma_v(xz)$	$\sigma_v'(yz)$		
A_1	1	1	1	1	z	$x^2,\ y^2,\ z^2$
A_2	1	1	-1	-1	R_z	xy
B_1	1	-1	1	-1	$x,\ R_y$	xz
B_2	1	-1	- 1	1	$y,\ R_x$	yz

C_s	E	σ_h		
A'	1	1	x, y, R_z	$x^2,\ y^2$
A''	1	-1	z, R_x, R_y	$yz,\ xz$

Table 4.2 Character tables and their basis functions. Here, $x, y,\ z$ are used to denote the cartesian coordinates. Some of their combinations as well as rotation around axes, $R_x, R_y,\ R_z$ are also displayed.

linear combination is restricted to the use of Abelian point groups. The canonical Hartree-Fock spin orbitals form a basis set for an irreducible representation of the point group of the molecule. For such point groups the product of two irreducible representations gives another irreducible representation. If the MOs belonging to the irreducible representation form the configuration, the total spatial symmetry of the configuration is obtained as a simple product between the symmetries of the orbitals [20]. The common aim is to identify which spin and spatial symmetry configuration that can arise from a particular orbital occupancy.

4.3 Normal mode coordinates

In the previous chapter we have seen that the full wavefunction of a molecular system (2.6) can be expanded in terms of adiabatic electronic wavefunctions. The expansion coefficients $\chi_i(R)$ are functions of the nuclear coordinates representing the vibrational and rotational motions. For a molecule consisting of the N nuclei, $3N$ cartesian coordinates are required to specify the positions of all nuclei. From the $3N$ degrees of freedom, translational motion of the center of mass and the rotational motion of the molecule account for 6 degrees of freedom. So there are $3N-6$ vibrational degrees of freedom for a system with N nuclei[3]. It is often more convenient to use internal coordinates instead of the cartesian ones. For a non-linear molecule with N atoms there are $3N-6$ internal coordinates and the translational and rotational motions are eliminated automatically. Thus, the internal coordinates by definition are concerned only with the internal motion of the molecule. To describe the molecular structure close to the equilibrium configuration we use the symmetry of the molecule and obtain the normal mode coordinates which are special linear combinations of the displacement of the atoms from these equilibrium positions along the x, y and z direction of cartesian coordinates. For defining this coordinate system we start from the classical Hamiltonian for the vibrational motion of a nonrotating molecule with N atoms. The kinetic energy T in cartesian coordinates will be:

$$T = \frac{1}{2}\sum_{i=1}^{3N} m_i \dot{\xi}_i^{\,2}, \qquad \dot{\xi}_i \equiv \frac{d\xi_i}{dt}. \tag{4.7}$$

Let assume that the coordinate system has been fixed to the equilibrium position of each nucleus and ξ_i to be a displacement along one of the axes associated with coordinate system of

[3]Linear molecules have $3N-5$ degrees of freedom since the nuclei do not rotate about the molecular axis

the ith nucleus and $i = 1, 2, \cdots 3N$. The expression (4.7) can be rewritten using mass-scaled cartesian displacement coordinates as

$$T = \frac{1}{2}\sum_{i=1}^{3N} \dot{\mathcal{R}}_i{}^2. \tag{4.8}$$

Here, $\mathcal{R}_i$ is the mass-scaled coordinates describing displacement from the equilibrium position

$$\mathcal{R}_i = \sqrt{m_i}(\xi_i - \xi_{ie}). \tag{4.9}$$

In general, the potential energy $V(\xi_i)$ is a complicated function of the cartesian coordinates of the atoms. Expanding the potential V in a Taylor series about the equilibrium nuclear position using the mass-weighted cartesian displacement coordinates gives

$$V = V(\mathcal{R}_i = 0) + \sum_i \frac{\partial V}{\partial \mathcal{R}_i}\mathcal{R}_i + \frac{1}{2}\sum_i\sum_j \frac{\partial^2 V}{\partial \mathcal{R}_i \partial \mathcal{R}_j}\mathcal{R}_i\mathcal{R}_j + \cdots . \tag{4.10}$$

At the equilibrium position the potential energy $V(\mathcal{R}_i = 0)$ is chosen to be zero. We also have by definition $\frac{\partial V}{\partial \mathcal{R}_i}|_{\mathcal{R}_i=0} = 0$ at equilibrium . Setting

$$V_{ij} \equiv \frac{\partial^2 V}{\partial \mathcal{R}_i \partial \mathcal{R}_j},$$

we obtain the total energy based on harmonic approximation as

$$E = \frac{1}{2}\sum_i \dot{\mathcal{R}}_i{}^2 + \frac{1}{2}\sum_{ij} V_{ij}\mathcal{R}_i\mathcal{R}_j. \tag{4.11}$$

Alternatively, a matrix form of the energy is

$$E = \frac{1}{2}\dot{\boldsymbol{\mathcal{R}}}^\dagger\dot{\boldsymbol{\mathcal{R}}} + \frac{1}{2}\boldsymbol{\mathcal{R}}^\dagger\mathbf{V}\boldsymbol{\mathcal{R}}, \tag{4.12}$$

where

$$\boldsymbol{\mathcal{R}} = \begin{pmatrix} \mathcal{R}_1 \\ \mathcal{R}_2 \\ \vdots \end{pmatrix}, \quad \boldsymbol{\mathcal{R}}^\dagger = \begin{pmatrix} \mathcal{R}_1 & \mathcal{R}_2 & \cdots \end{pmatrix},$$

and

$$\mathbf{V} = \begin{pmatrix} V_{11} & V_{12} & \cdots \\ V_{21} & V_{22} & \cdots \\ \vdots & \vdots & \cdots \end{pmatrix}.$$

Since $\mathbf{V}$ is symmetric, i.e. $(V_{ij} = V_{ji})$, by defining a real orthogonal matrix A, one can diagonalize the matrix $\mathbf{V}$ according to

$$\Omega = A^{\dagger}\mathbf{V}A, \tag{4.13}$$

where Ω is a diagonal matrix whose non-vanishing elements are the eigenvalues of V. Denote them with ω_i^2. New coordinates Q_i related to the old $\mathcal{R}_i$ is introduced by the linear transformation

$$\mathbf{Q} = A^{\dagger}\boldsymbol{\mathcal{R}} \quad \Leftrightarrow \quad \boldsymbol{\mathcal{R}} = A\mathbf{Q}, \qquad\qquad AA^{\dagger} = 1. \tag{4.14}$$

From the equation (4.12) we have

$$E = \frac{1}{2}(A\dot{\mathbf{Q}})^{\dagger}(A\dot{\mathbf{Q}}) + \frac{1}{2}(A\mathbf{Q})^{\dagger}\mathbf{V}(A\mathbf{Q}) = \frac{1}{2}(\dot{\mathbf{Q}}^{\dagger}\dot{\mathbf{Q}} + \mathbf{Q}^{\dagger}\Omega\mathbf{Q}), \tag{4.15}$$

or

$$E = \frac{1}{2}\sum_i (\dot{Q_i}^2 + \omega_i^2 Q_i^2).$$

The Q_i are known as the normal mode coordinates. The canonical momentum is defined as $p_i = \frac{\partial H}{\partial \dot{Q}_i}$, then the energy expression (4.15) may be regarded as the Hamiltonian of the system and we obtain

$$H = \frac{1}{2}\sum_i^{3N} (p_i^2 + \omega_i^2 Q_i^2). \tag{4.16}$$

Therefore, the system behaves like a set of $3N-6$ independent harmonic oscillators, where each oscillator has no interaction with the others. With this classical Hamiltonian available, the quantum Hamiltonian can easily be obtained by substituting:

$$Q_i \to \hat{Q}_i, \text{ and } p_i \to \hat{p}_i = -i\frac{\partial}{\partial \hat{Q}_i},$$

which gives:

$$\hat{H} = \sum_i (-\frac{1}{2}\frac{\partial^2}{\partial \hat{Q_i}^2} + \frac{1}{2}\omega_i^2 \hat{Q_i}^2) = \sum_i \hat{H}_i \tag{4.17}$$

To summarize, using the normal mode coordinates close to the equilibrium structure, the vibrational motion can be approximated with $3N-6$ uncoupled harmonic oscillators. We will now discuss the triatomic molecule X_3 here.

4.3.1 Vibration of a triatomic molecule

To be more specific, we will consider the vibrational motion of a triatomic molecule with the shape of an equilateral triangle with three equal masses. These motions are confined to the plane of the triangle. Simultaneous displacements of the three atoms from the equilateral triangular geometry are described by three two-dimensional orthogonal coordinate systems with the unit vectors $(\xi_1 \cdots \xi_6)$ as bases. The six unit vectors $\xi_1 = (1,0,0,0,0,0)$, $\xi_2 = (0,1,0,0,0,0)$,..., $\xi_6 = (0,0,0,0,0,1)$ constitute a basis for the reducible representation Γ.

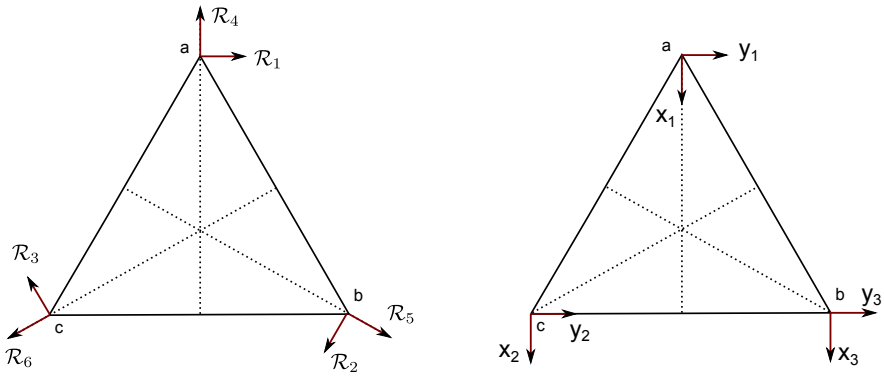

Figure 4.1 Coordinate system for an equilateral triangular molecule. The two types of space-fixed cartesian coordinates are defined.

For finding the normal mode coordinates Q_i, group theory shall be used instead of the definition of the orthogonal transformation matrix A in equation (4.14). The Hamiltonian must be invariant under all symmetry operations applied to the molecule in its equilibrium configuration. In principle, the potential energy must be invariant, i.e., it must belong to the totally symmetric representation of the symmetry group or

$$P_R \mathbf{V} = \mathbf{V},$$

where P_R is the symmetry operators. Therefore, from the invariance of the potential certain symmetry requirements on the normal mode coordinates Q_i are obtained. We know that a molecule with the shape of an equilateral triangle and equal masses belongs to the D_{3h} non-abelian point group. The abelian subgroup D_3 contains enough information about the symmetry of the molecule in order to find the normal mode coordinates. The character table of the D_3 symmetry group is shown in table 4.3.

D_3	E	$2C_3$	$3C_2$		
A_1	1	1	1		$x^2+y^2,\ z^2$
A_2	1	1	-1	z, R_z	
E	2	-1	0	$(x,y)(R_x,R_y)$	$(x^2-y^2,xy)(xz,yz)$

Table 4.3 Character table for the D_3 point group.

Instead of using cartesian coordinates introduced in equation (4.1) we will use the mass-scaled coordinates $\mathcal{R}_i$ (4.9) [See fig.4.1] and show how they transform under the various symmetry operators

$$
\begin{aligned}
&E(\mathcal{R}_1,\cdots,\mathcal{R}_6) = (\mathcal{R}_1,\cdots,\mathcal{R}_6)\\
&C_2(\mathcal{R}_1,\cdots,\mathcal{R}_6) = (-\mathcal{R}_1,-\mathcal{R}_3,-\mathcal{R}_2,\mathcal{R}_4,\mathcal{R}_6,\mathcal{R}_5)\\
&C_2'(\mathcal{R}_1,\cdots,\mathcal{R}_6) = (-\mathcal{R}_3,-\mathcal{R}_2,-\mathcal{R}_1,\mathcal{R}_6,\mathcal{R}_5,\mathcal{R}_4)\\
&C_2''(\mathcal{R}_1,\cdots,\mathcal{R}_6) = (-\mathcal{R}_2,-\mathcal{R}_1,-\mathcal{R}_3,\mathcal{R}_5,\mathcal{R}_4,\mathcal{R}_6)\\
&C_3(\mathcal{R}_1,\cdots,\mathcal{R}_6) = (\mathcal{R}_2,\mathcal{R}_3,\mathcal{R}_1,\mathcal{R}_5,\mathcal{R}_6,\mathcal{R}_4)\\
&C_3'(\mathcal{R}_1,\cdots,\mathcal{R}_6) = (\mathcal{R}_3,\mathcal{R}_1,\mathcal{R}_2,\mathcal{R}_6,\mathcal{R}_4,\mathcal{R}_5).
\end{aligned}
$$

The mass-scaled coordinates form a basis for a representation of D_3. As an example:

$$
C_2(\mathcal{R}_1,\cdots,\mathcal{R}_6) = (\mathcal{R}_1,\cdots,\mathcal{R}_6)\begin{pmatrix}
-1 & 0 & 0 & 0 & 0 & 0\\
0 & 0 & -1 & 0 & 0 & 0\\
0 & -1 & 0 & 0 & 0 & 0\\
0 & 0 & 0 & 1 & 0 & 0\\
0 & 0 & 0 & 0 & 0 & 1\\
0 & 0 & 0 & 0 & 1 & 0
\end{pmatrix}.
$$

The character of this representation matrix is zero. The other characters can be obtained in the same way:

$$
\chi(E)=6,\quad \chi(C_2)=0,\quad \chi(C_2')=0,\quad \chi(C_2'')=0,\quad \chi(C_3)=0,\quad \chi(C_3')=0.
$$

If this representation is denoted by $\Gamma(\mathcal{R})$, it is possible to reduce $\Gamma(\mathcal{R})$ using the character

table of D_3 by employing relation (4.5), where the order of the D_3 group, h is 6:

$$a_{A_1} = \frac{1}{h}\sum_R \chi(R)\chi^{A_1}(R) = \frac{1}{6}(6+0+0+0+0+0) = 1,$$

$$a_{A_2} = \frac{1}{h}\sum_R \chi(R)\chi^{A_2}(R) = \frac{1}{6}(6+0+0+0+0+0) = 1,$$

$$a_E = \frac{1}{h}\sum_R \chi(R)\chi^{E}(R) = \frac{1}{6}(6\times 2+0+0+0+0+0) = 2,$$

so

$$\Gamma(\mathcal{R}) = A_1 + A_2 + 2E.$$

The motion of the three mass points can be described in terms of four modes. Two of these are nondegenerate and two are two-fold degenerate. Nevertheless, all of them do describe the vibrational modes due to the translational and rotational motions. The translational motion here obtained must lie in the plane of the molecule (xy plane). The rotation of a molecule as a whole is only about the z axis when the nuclei are not allowed to move out of the plane of the molecule. From the character table, one can see that the rotation about the z axis belongs to the A_2 representation, and (x, y) transform according to the E representation. By eliminating A_2 and E from $\Gamma(\mathcal{R})$, the remaining modes are associated with the vibrational motion, that is

$$\Gamma^{vib}(\mathcal{R}) = A_1 + E$$

Therefore, there are three normal mode coordinates for the vibrational motions. These coordinates are associated with the symmetry stretching, bending and asymmetric stretching modes and are denoted by Q_s, Q_x and Q_y respectively. Together they are able to describe all possible vibration configurations of a triatomic molecule. To obtain the normal mode coordinates, one shall project the basis set $(\mathcal{R}_1, \cdots, \mathcal{R}_6)$ onto the irreducible representations A_1 and E using the projection operator (4.6). For A_1, the projection operator will be $\rho^{A_1} = \frac{1}{6}\{E + C_2 + C_2' + C_2'' + C_3 + C_3'\}$, and by projection onto $\mathcal{R}_1$, we have

$$\rho^{(A_1)}\mathcal{R}_1 = \frac{1}{6}(E + C_2 + C_2' + C_2'' + C_3 + C_3')\mathcal{R}_1 = \frac{1}{6}(\mathcal{R}_1 - \mathcal{R}_1 - \mathcal{R}_3 - \mathcal{R}_2 + \mathcal{R}_2 + \mathcal{R}_3) = 0$$

in the same way we obtain

$$\begin{aligned}\rho^{(A_1)}\mathcal{R}_2 &= \rho^{(A_1)}\mathcal{R}_3 = 0\\ \rho^{(A_1)}\mathcal{R}_4 &= \rho^{(A_1)}\mathcal{R}_5 = \rho^{(A_1)}\mathcal{R}_6 = \tfrac{1}{3}(\mathcal{R}_4 + \mathcal{R}_5 + \mathcal{R}_6)\end{aligned}.$$

After normalization, we obtain the totally symmetric stretching mode Q_s belonging to A_1 irreducible representation

$$Q_s = \frac{(\mathcal{R}_4 + \mathcal{R}_5 + \mathcal{R}_6)}{\sqrt{3}}. \tag{4.18}$$

For the E irreducible representation, six normalized functions are generated by the projection operator $\rho^E = \frac{1}{6}\{2E - C_3 - C_3'\}$

$$\begin{aligned} f_1 &= \tfrac{2\mathcal{R}_1 - \mathcal{R}_2 - \mathcal{R}_3}{\sqrt{6}}, \quad f_2 = \tfrac{2\mathcal{R}_2 - \mathcal{R}_1 - \mathcal{R}_3}{\sqrt{6}}, \\ f_3 &= \tfrac{2\mathcal{R}_3 - \mathcal{R}_1 - \mathcal{R}_2}{\sqrt{6}}, \quad f_4 = \tfrac{2\mathcal{R}_4 - \mathcal{R}_5 - \mathcal{R}_6}{\sqrt{6}}, \\ f_5 &= \tfrac{2\mathcal{R}_5 - \mathcal{R}_4 - \mathcal{R}_6}{\sqrt{6}}, \quad f_6 = \tfrac{2\mathcal{R}_6 - \mathcal{R}_4 - \mathcal{R}_5}{\sqrt{6}}. \end{aligned}$$

They are not independent since

$$f_1 + f_2 + f_3 = 0, \quad f_4 + f_5 + f_6 = 0 \ .$$

One choice for independent set of functions is

$$\begin{aligned} Q_x &= \tfrac{[\sqrt{3}(\mathcal{R}_2 - \mathcal{R}_3) + 2\mathcal{R}_4 - \mathcal{R}_5 - \mathcal{R}_6]}{\sqrt{12}} \\ Q_y &= \tfrac{[2\mathcal{R}_1 - \mathcal{R}_2 - \mathcal{R}_3 - \sqrt{3}(\mathcal{R}_5 - \mathcal{R}_6)]}{\sqrt{12}} \ . \end{aligned} \tag{4.19}$$

These are the coordinates describing the bending and the asymmetric stretching modes. They are illustrated in figure 4.2.

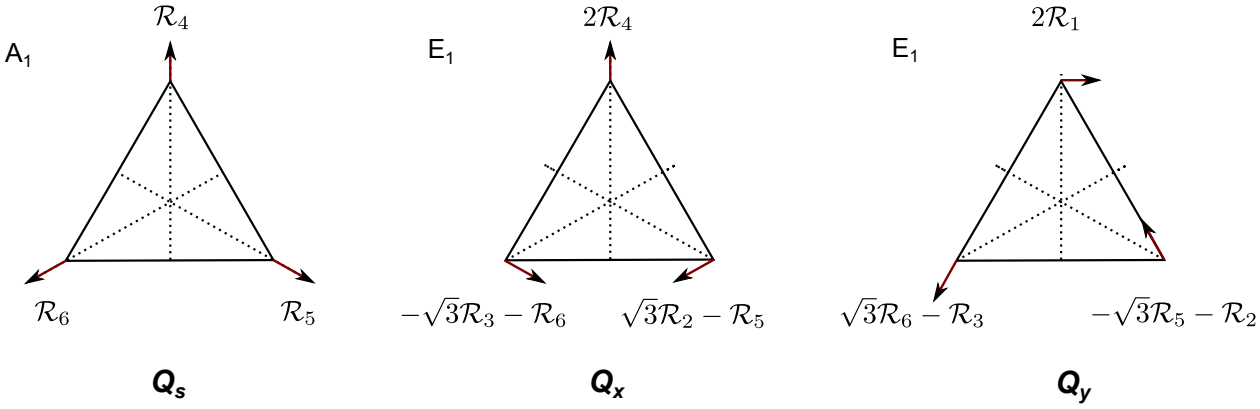

Figure 4.2 The normal modes of an X_3 molecule.

The mass-scaled coordinates $\mathcal{R}$ are related to the other type of three two-dimensional cartesian coordinates x_i, y_i, z_i located at three atoms [See fig 4.1] by the orthogonal transformation. It must not be confused with the three two-dimensional cartesian coordinates we introduced before by ξ [47]

$$\begin{aligned} \mathcal{R}_1 &= \sqrt{m}y_1, & \mathcal{R}_4 &= -\sqrt{m}x_1 \\ \mathcal{R}_2 &= \sqrt{m}(\tfrac{\sqrt{3}}{2}x_3 - \tfrac{1}{2}y_3), & \mathcal{R}_5 &= \sqrt{m}(\tfrac{1}{2}x_3 + \tfrac{\sqrt{3}}{2}y_3) \\ \mathcal{R}_3 &= -\sqrt{m}(\tfrac{\sqrt{3}}{2}x_2 - \tfrac{1}{2}y_2), & \mathcal{R}_6 &= \sqrt{m}(\tfrac{1}{2}x_2 - \tfrac{\sqrt{3}}{2}y_2). \end{aligned} \tag{4.20}$$

Substitution of the $\mathcal{R}_i$ coordinates (4.20) into equation (4.18) and (4.19) yields

$$\begin{aligned} Q_s &= \tfrac{\sqrt{m}}{\sqrt{3}}\left\{-x_1 + \left(\tfrac{1}{2}x_2 - \tfrac{\sqrt{3}}{2}y_2\right) + \left(\tfrac{1}{2}x_3 + \tfrac{\sqrt{3}}{2}y_3\right)\right\}, \\ Q_x &= \tfrac{\sqrt{m}}{\sqrt{3}}\left\{-x_1 + \left(\tfrac{1}{2}x_2 + \tfrac{\sqrt{3}}{2}y_2\right) + \left(\tfrac{1}{2}x_3 - \tfrac{\sqrt{3}}{2}y_3\right)\right\}, \\ Q_y &= \tfrac{\sqrt{m}}{\sqrt{3}}\left\{y_1 + \left(\tfrac{\sqrt{3}}{2}x_2 - \tfrac{1}{2}y_2\right) + \left(-\tfrac{\sqrt{3}}{2}x_3 - \tfrac{1}{2}y_3\right)\right\}. \end{aligned} \tag{4.21}$$

Corresponding to our calculation it is useful to employ the vibration of normal modes given in terms of internal coordinates describing interatomic distances and bond angles. The equations for Q_i in terms of internal coordinates are given by [48]

$$\begin{aligned} \delta &= (r_{ab}^2 + r_{ac}^2 + r_{bc}^2) = 9(Q_s^2 + Q_x^2 + Q_y^2), \\ \beta &= \sqrt{3}(r_{ab}^2 - r_{ac}^2) = -9Q_s(\sqrt{3}Q_x + Q_y), \\ \gamma &= (2r_{bc}^2 - r_{ab}^2 - r_{ac}^2) = 9Q_s(Q_x - \sqrt{3}Q_y). \end{aligned} \tag{4.22}$$

Chapter 5

Jahn-Teller effect

In the previous chapters we have seen how to transform from an adiabatic representation to a diabatic representation and how to find the general form of the diabatic potentials from the adiabatic potential energy surfaces and non-adiabatic couplings. Also we have seen how to employ the symmetry and point group which plays a crucial role in the description of conical intersections and how to find the normal mode coordinates. Here we will discuss a special case when the electronic states are degenerate by symmetry and leads to the Jahn-Teller effect named after the prediction by H. A. Jahn and E. Teller in 1937 [3].

"Any molecule in an orbitally degenerate[1] *electronic state is unstable unless the degeneracy is accidental*[2] *or the molecule is linear."*

Alternatively *" Any non-linear molecule undergoes distortion when its electronic state is degenerate by symmetry."*

This effect accounts for distortion of a non-linear molecule to a lower symmetry in which the energy decreases and the degeneracy is lifted. In other words, highly symmetrical configurations of molecules are very unstable due to the Jahn-Teller effect.

5.1 Formulation of the Jahn-Teller problems

The Jahn-Teller effect can be found when the adiabatic electronic potential energy surfaces of a polyatomic molecule have two or more branches that intersect in one point. Furthermore,

[1] degeneracy not arising from spin.

[2] degeneracy not caused by symmetry.

there is no extremum at this point due to a non-zero slope[3]. The electronic degeneracy in this point causes a special coupling between electronic and nuclear motions called the Jahn-Teller coupling. In the Jahn-Teller effect, vibronic coupling terms may be considered as perturbation terms to the adiabatic electronic energy which remove the degeneracy. To describe the Jahn-Teller effect let us consider the diabatic electronic potential matrix (3.40) and derive a suitable Hamiltonian. We know how the Hamiltonian for a polyatomic system can be described by three terms using a diabatic electronic basis

$$H = T_N + H_r + V(r, Q), \tag{5.1}$$

where H_r is the electronic component which includes the kinetic energy of electrons (T_e) and the interelectronic electrostatic interaction (V_{e-e}), T_N is the kinetic energy of the nuclei, and $V(r, Q)$ is the energy of the interaction of electrons with the nuclei (V_{N-e})and internuclear repulsion (V_{N-N}) [49]. The operator $V(r, Q)$ can be expanded as a series of small displacements of the nuclei around the point $Q_\alpha = Q_{\alpha\ 0} = 0$, chosen at the conical intersection:

$$V(r, Q) = V(r, 0) + \sum_{\alpha}^{N} (\frac{\partial V}{\partial Q_\alpha})_0 Q_\alpha + \frac{1}{2} \sum_{\alpha,\beta}^{N} (\frac{\partial^2 V}{\partial Q_\alpha \partial Q_\beta})_0 Q_\alpha Q_\beta + \cdots . \tag{5.2}$$

The vibronic interaction operator in the Jahn-Teller problem can be defined as

$$W(r, Q) = V(r, Q) - V(r, 0) = \sum_{\alpha} (\frac{\partial V}{\partial Q_\alpha})_0 Q_\alpha + \frac{1}{2} \sum_{\alpha,\beta} (\frac{\partial^2 V}{\partial Q_\alpha \partial Q_\beta})_0 Q_\alpha Q_\beta + \cdots . \tag{5.3}$$

The matrix element of this operator can be written

$$W_{nn'} = \textstyle\sum_\alpha F_\alpha^{nn'} Q_\alpha + \sum_{\alpha,\beta} G_{\alpha\beta}^{nn'} Q_\alpha Q_\beta + \cdots \tag{5.4}$$

where for instance

$$F_\alpha^{nn'} = \langle \tilde{\psi}_n | (\frac{\partial V}{\partial Q_\alpha}) | \tilde{\psi}_{n'} \rangle. \tag{5.5}$$

Here, $|\tilde{\psi}_n\rangle$ and $|\tilde{\psi}_{n'}\rangle$ are the diabatic wavefunctions of the two electronic states which belong to different irreducible representations of the molecular point group Γ_n and $\Gamma_{n'}$. The parameters appearing in the expression (5.4) are called the linear, the quadratic, $\cdots$ coupling constants both for diagonal $n = n'$ and off-diagonal $n \neq n'$ cases [50]. They can be directly extracted from the adiabatic potential energy surfaces in the vicinity of the intersection.

[3]This slope will be non-zero in the Renner-Teller effect that will not be considered in this work.

As we mentioned before, since we are using the normal mode coordinates associated with normal vibrational modes, the investigation of the nuclear motions is simplified due to symmetry consideration and application of group theory. At the conical intersection, Q_α, the molecule is highly symmetric and belongs to a non-abelian point group [51]. If we neglect all coupling terms and solve the Schrödinger equation for zeroth order term, i.e. $V(r,0)$, we might obtain n-fold degenerate electronic terms, $E_k = E_0$, $k = 1, 2, \cdots, n$ at this point. By including the linear terms as perturbations, the degeneracy is lifted. The deformed electronic energies are obtained as the eigenvalues of the $n \times n$ matrix containing the linear vibronic constant F_α^{nn}. The lack of extremum at the conical intersection leads to at least one nonzero linear vibronic constant. It also implies that there are no minimum at this point, so the adiabatic potential energy surfaces have the minima at another geometry, i.e. $Q_\alpha \neq 0$, where the nuclear configuration is distorted [52]. Based on group theory, Jahn and Teller proved that for any nonlinear molecule in a degenerate state there are such symmetry coordinates Q_α where $F_\alpha^{nn'} \neq 0$. They achieved this proof by checking all the point groups one by one.

In the group theoretical point of view, we can obtain the nonzero diagonal matrix element F_α^{nn} for degenerate states, only if the symmetry of the product $\Gamma_n \otimes \Gamma_n$ is the same as the symmetry of the symmetrized displacement Q_α . The physical meaning of this diagonal linear coupling constant is the force with which electrons in state Γ_n affect the nuclei in the direction of symmetrized displacements Q_α. The product of relevant electronic stats and nuclear coordinates contain the totally symmetric representation, i.e.

$$\Gamma_n \otimes \Gamma_n \otimes \Gamma_\alpha \supset \Gamma_A,$$

where Γ_n and Γ_α are the irreducible representations of the electronic states and one or more non-totally symmetric vibrational nuclear coordinates, respectively and Γ_A denotes the totally symmetric representation. Using the symmetry selection rule for $F_\alpha^{nn'}$, the matrix element will be nonzero when [53]

$$\Gamma_n \otimes \Gamma_{n'} \otimes \Gamma_\alpha \supset \Gamma_A.$$

Hence, the elements of U_{12}^d and $U_{22}^d - U_{11}^d$ in the degeneracy conditions that we mentioned before [See equation (3.41)] will be nonzero to lift degeneracy. In principle, if the off-diagonal vibronic couplings $W_{nn'}$ are neglected, we deal with the uncoupled Schrödinger

equation which describes the vibrational motion in a given electronic state. This is the Born-Oppenheimer approximation [1]. Decoupling is invalid if the electronic states is n-fold degenerate. Thus, one immediate consequence from the symmetry selection rule is that for $n = n'$ only totally symmetric modes enter the Hamiltonian in first order.

5.2 $E \otimes e$ Jahn-Teller problem

Equilateral triangular triatomic systems belonging to the non-abelian D_{3h} symmetry point group are the simplest systems that allow for two-fold degeneracy E causing $[E \otimes E] \rightarrow A + E$ which contains the totally symmetric displacement A and the non-totally symmetric representation E. The Jahn-Teller theorem predicted that the nuclear configuration is thereby distorted by the non-totally symmetric displacement. In the usual notation, D_{3h} conical intersections in planar X_3 molecular systems are a special case of $E \otimes e$ Jahn-Teller systems, where the capital symmetry designation refers to the electronic wavefunction and the lower case refers to the vibrational coordinates. The most simple and widespread $E \otimes e$ Jahn-Teller effect describes the lifting of doubly degenerate E electronic states due to intersection with doubly degenerate vibrational e modes.

If the two electronic wavefunctions of the degenerate states are denoted by $|\tilde{\psi}_x\rangle$ and $|\tilde{\psi}_y\rangle$, then the linear and quadratic vibronic coupling constants are

$$\begin{aligned} F_E &= \langle \tilde{\psi}_x | (\tfrac{\partial V}{\partial Q_x})_0 | \tilde{\psi}_x \rangle, \\ G_E &= \langle \tilde{\psi}_x | (\tfrac{\partial^2 V}{\partial Q_x \partial Q_y})_0 | \tilde{\psi}_y \rangle. \end{aligned} \tag{5.6}$$

While the so-called force constant can be defined as

$$K_E = \langle \tilde{\psi}_x | (\frac{\partial^2 V}{\partial {Q_x}^2})_0 | \tilde{\psi}_x \rangle = \langle \tilde{\psi}_y | (\frac{\partial^2 V}{\partial {Q_y}^2})_0 | \tilde{\psi}_y \rangle. \tag{5.7}$$

Considering the vibronic terms introduced in equation (5.3), a model for this Jahn-Teller conical intersection takes the form of an expansion about the point of intersection which leads to the factorized expression [54]

$$U^d = \sum_{n=1} \frac{1}{n!} \left\{ \begin{pmatrix} V^{(n)} & 0 \\ 0 & V^{(n)} \end{pmatrix} + \begin{pmatrix} 0 & W^{(n)} - iZ^{(n)} \\ W^{(n)} + iZ^{(n)} & 0 \end{pmatrix} \right\}. \tag{5.8}$$

Here, matrix elements $V^{(n)}$,$W^{(n)}$, and $Z^{(n)}$ are real functions of the real nuclear coordinates Q_x and Q_y. The first matrix contains the diagonal elements $V^{(n)}$ corresponding to the potential in the absence of the Jahn-Teller coupling, while in the second matrix, $W^{(n)}$ and $Z^{(n)}$ are the off-diagonal coupling elements for each order n.

The first few terms of these functions are given by [54]

$$
\begin{aligned}
V^{(0)} &= V_{0a} \\
V^{(1)} &= 0 \\
V^{(2)} &= V_{2a}[Q_x^2 + Q_y^2] \\
V^{(3)} &= V_{3a}[2Q_x^3 - 6Q_xQ_y^2] \\
V^{(4)} &= V_{4a}[Q_x^4 + 2Q_x^2Q_y^2 + Q_y^4] \\
&\vdots
\end{aligned}
$$

$$
\begin{aligned}
W^{(0)} &= 0 \\
W^{(1)} &= V_{1e}Q_x \\
W^{(2)} &= V_{2e}[Q_x^2 - Q_y^2] \\
W^{(3)} &= V_{3e}[Q_x^3 + Q_xQ_y^2] \\
W^{(4)} &= V_{4e}[Q_x^4 - 6Q_x^2Q_y^2 + Q_y^4] + V'_{4e}[Q_x^4 - Q_y^4] \\
&\vdots
\end{aligned}
$$

$$
\begin{aligned}
Z^{(0)} &= 0 \\
Z^{(1)} &= V_{1e}Q_y \\
Z^{(2)} &= -2V_{2e}Q_xQ_y \\
Z^{(3)} &= V_{3e}[Q_x^2Q_y + Q_y^3] \\
Z^{(4)} &= V_{4e}[4Q_x^3Q_y - 4Q_xQ_y^3] + V'_{4e}[-2Q_x^3Q_y - 2Q_xQ_y^3]
\end{aligned}
$$

Let us identify V_{2a}, V_{1e} and V_{2e} by K_E, F_E and G_E, as force constant, linear and quadratic Jahn-Teller coupling respectively. The general truncated form up to the quadratic term of the diabatic Hamiltonian can be written as

$$
H^d = -(\frac{1}{2M})\nabla^2 + \frac{1}{2}K_E(Q_x^2 + Q_y^2) + F_E \begin{pmatrix} 0 & Q_x - iQ_y \\ Q_x + iQ_y & 0 \end{pmatrix} \tag{5.9}
$$

$$+\frac{G_E}{2}\begin{pmatrix} 0 & Q_x^2 - Q_y^2 + i2Q_xQ_y \\ Q_x^2 - Q_y^2 - i2Q_xQ_y & 0 \end{pmatrix}.$$

By scaling the coordinates with $\alpha = (K_E M)^{\frac{1}{4}}$, $X = \alpha Q_x$, and $Y = \alpha Q_y$, equation (5.9) is transformed into [47]

$$H = \omega_e \left[\frac{1}{2} \begin{pmatrix} -\frac{\partial^2}{\partial X^2} - \frac{\partial^2}{\partial Y^2} + X^2 + Y^2 & 0 \\ 0 & -\frac{\partial^2}{\partial X^2} - \frac{\partial^2}{\partial Y^2} + X^2 + Y^2 \end{pmatrix} + \right.$$
$$\left. k \begin{pmatrix} 0 & X - iY \\ X + iY & 0 \end{pmatrix} + \frac{1}{2} g \begin{pmatrix} 0 & X^2 - Y^2 + i2XY \\ X^2 - Y^2 - i2XY & 0 \end{pmatrix} \right],$$

where $\omega_e = (\frac{K_E}{M})^{\frac{1}{2}}$, $k = \frac{F_E}{\alpha \omega_e}$ and $g = \frac{G_E}{K_E}$. Since only X and Y coordinates are involved, it is sensible to introduce polar coordinates for the X/Y plane

$$\rho = X^2 + Y^2, \quad \tan(\phi) = \tfrac{Y}{X}. \tag{5.10}$$

The matrix notation in the polar coordinates yields the following well-known Hamiltonian [55, 56]

$$H_{JT}^d = T_N \mathbf{1} + \frac{\omega_e}{2}\rho^2 \mathbf{1} + \begin{pmatrix} 0 & k\rho e^{-i\phi} + \frac{g}{2}\rho^2 e^{2i\phi} \\ k\rho e^{i\phi} + \frac{g}{2}\rho^2 e^{-2i\phi} & 0 \end{pmatrix}. \tag{5.11}$$

Here, T_N denotes the kinetic energy

$$T_N = -\frac{\omega_e}{2}\left[\frac{\partial^2}{\partial \rho^2} + \frac{1}{\rho}\frac{\partial}{\partial_\rho} + \frac{1}{\rho^2}\frac{\partial^2}{\partial \phi^2}\right].$$

The diagonalization of the potential energy part $H_{JT}^d - T_N$ yields the adiabatic potential energy surface as eigenvalues

$$S^\dagger [H_{JT}^d - T_N] S = S^\dagger U^d S = \begin{pmatrix} U_1^{JT} & 0 \\ 0 & U_2^{JT} \end{pmatrix}.$$

For better understanding of the problem we will consider the potential part of equation (5.11) and show how the adiabatic potential energy surface is obtained:

$$\det \begin{pmatrix} -\lambda & x \\ x^* & \lambda \end{pmatrix} = 0, \quad x = k\rho e^{i\phi} + \frac{1}{2} g \rho^2 e^{-2i\phi},$$

and

$$\lambda^2 - |x|^2 = 0 \rightarrow \lambda_{1,2} = \pm|x|,$$

then,

$$U^{JT}_{1,2} = \frac{\omega_e}{2}\rho^2 \pm \lambda_{1,2} = \frac{\omega_e}{2}\rho^2 \pm |k\rho e^{i\phi} + \frac{1}{2}g\rho^2 e^{-2i\phi}|,$$
$$U^{JT}_{1,2} = \frac{\omega_e}{2}\rho^2 \pm |k\rho + \frac{1}{2}g\rho^2 e^{-3i\phi}|.$$

Finally it is obtained

$$U^{JT}_{1,2} = \frac{\omega_e}{2}\rho^2 \pm k\rho\sqrt{1 + \frac{g}{k}\rho\cos(3\phi) + \frac{g^2}{4k^2}\rho^2}. \tag{5.12}$$

Here, degeneracy occurs at $\rho = 0$. We can directly obtain the eigenvectors as follow up to the linear coupling terms for convenience

- - λ_1,

$$\begin{pmatrix} -k\rho & k\rho e^{i\phi} \\ k\rho e^{-i\phi} & -k\rho \end{pmatrix} \begin{pmatrix} S_{11} \\ S_{21} \end{pmatrix} = 0,$$
$$-S_{11} + e^{i\phi}S_{21} = 0 \rightarrow S_{11} = e^{i\phi}A_{21},$$
$$S_{11} = \frac{1}{\sqrt{2}}e^{-i\frac{\phi}{2}},\ S_{21} = \frac{1}{\sqrt{2}}e^{i\frac{\phi}{2}}.$$

- - λ_2,

$$\begin{pmatrix} k\rho & k\rho e^{i\phi} \\ k\rho e^{-i\phi} & k\rho \end{pmatrix} \begin{pmatrix} S_{22} \\ S_{12} \end{pmatrix} = 0,$$
$$S_{22} + e^{i\phi}S_{12} = 0 \rightarrow S_{22} = -e^{i\phi}S_{12},$$
$$S_{22} = -\frac{1}{\sqrt{2}}e^{i\frac{\phi}{2}},\ S_{21} = \frac{1}{\sqrt{2}}e^{-i\frac{\phi}{2}}.$$

So that we obtain

$$S = \frac{1}{\sqrt{2}} \begin{pmatrix} e^{-\frac{i\phi}{2}} & e^{-\frac{i\phi}{2}} \\ e^{\frac{i\phi}{2}} & -e^{\frac{i\phi}{2}} \end{pmatrix}. \tag{5.13}$$

The transformation matrix S from diabatic to the adiabatic representation including the quadratic coupling has in general the following form:

$$S = \frac{e^{-is\gamma}}{\sqrt{2}} \begin{pmatrix} 1 & 1 \\ e^{i\gamma} & -e^{i\gamma} \end{pmatrix}, \tag{5.14}$$

with

$$\gamma = \arctan\left(\frac{\sin\phi - \frac{g\rho}{2k}\sin(2\phi)}{\cos\phi + \frac{g\rho}{2k}\cos(2\phi)}\right). \tag{5.15}$$

Here, the constant s is deeply related to the underlying gauge structure of the system which will be discussed in the next section. It can be seen as a gauge choice and we will pick $s = \frac{1}{2}$ [6,57]. Considering the transformation matrix (5.13) as an simple case we can calculate adiabatic basis set from the diabatic basis $\tilde{\psi}_+$ and $\tilde{\psi}_-$ according to [See chapter 2]:

$$\begin{pmatrix} \psi_1^{ad} \\ \psi_2^{ad} \end{pmatrix} = S^\dagger \begin{pmatrix} \tilde{\psi}_+ \\ \tilde{\psi}_- \end{pmatrix},$$

$$\psi_1^{ad} = \tfrac{1}{\sqrt{2}}\left(e^{i\frac{\phi}{2}}\tilde{\psi}_+ + e^{-i\frac{\phi}{2}}\tilde{\psi}_-\right)$$

$$\psi_2^{ad} = \tfrac{1}{\sqrt{2}}\left(e^{i\frac{\phi}{2}}\tilde{\psi}_+ - e^{-i\frac{\phi}{2}}\tilde{\psi}_-\right)$$

Using $\tilde{\psi}_+ = \frac{1}{\sqrt{2}}(\tilde{\psi}_x + i\tilde{\psi}_y)$ and $\tilde{\psi}_- = \frac{1}{\sqrt{2}}(\tilde{\psi}_x - i\tilde{\psi}_y)$ gives

$$\psi_1^{ad} = (\cos\tfrac{\phi}{2}\tilde{\psi}_x - \sin\tfrac{\phi}{2}\tilde{\psi}_y)$$

$$\psi_2^{ad} = i(\sin\tfrac{\phi}{2}\tilde{\psi}_x + \cos\tfrac{\phi}{2}\tilde{\psi}_y)$$

We can see that the adiabatic wavefunctions depend on $\frac{\phi}{2}$ when encircling a 2π loop around the $\rho = 0$, i.e. the wavefunctions do not transform into themselves

$$\psi_1^{ad}(2\pi) = -\psi_1^{ad}(0),$$
$$\psi_2^{ad}(2\pi) = -\psi_2^{ad}(0).$$

This is the general behavior for two-dimensional conical intersections. For integer values of s in the transformation matrix the electronic wavefunction i.e. the column vector of S, are single-valued functions of ϕ, but for half-integer values of s the electronic wavefunction are double valued. Because of the single valuedness of total wavefunction, which is a product of the electronic and the nuclear part, the single or double values of the electronic part imply the single or double valuedness of the nuclear part. This sign change in the adiabatic wavefunction is a special case of the so-called geometric or Berry phase which we discuss in the next section.

To obtain the scaled potential parameters for a molecular system, we use data from *ab initio* calculations. For the smaller rang of the normal mode coordinates, the truncated

expression at the quadratic term is valid to a good approximation. However, when going further away from conical intersection, higher order terms are needed. Hence, over large extension of the normal mode coordinates generally the cubic term in the Jahn-Teller coupling and anharmonicity V_{3a} are necessary to match the analytic expression to the *ab initio* data [58]. We have here used the potential energy surfaces up to the third order. First, the Jahn-Teller potential energy matrix from equation (5.8) will be[4]

$$\begin{aligned} U^d = \quad & \sigma_I[V_{2a}(Q_x^2+Q_y^2)+V_3a(Q_x^3-3Q_xQ_y^2)]+ \\ & \sigma_x[V_{1e}Q_x+V_{2e}(Q_x^2-Q_y^2)+V_{3e}(Q_x^3+Q_xQ_y^2)]+ \\ & \sigma_y[V_{1e}Q_y-2V_{2e}Q_xQ_y+V_{3e}(Q_y^3+Q_x^2Q_y)]. \end{aligned}$$

In the polar coordinates it will be

$$U^d = \begin{pmatrix} V_{2a}r^2+V_{3a}r^3\cos 3\phi & 0 \\ 0 & V_{2a}r^2+V_{3a}r^3\cos 3\phi \end{pmatrix} + \begin{pmatrix} 0 & V_{1e}r^2e^{-i\phi}+V_{2e}r^2e^{2i\phi}+V_{3e}r^3e^{-i\phi} \\ V_{1e}r^2e^{i\phi}+V_{2e}r^2e^{-2i\phi}+V_{3e}r^3e^{i\phi} & 0 \end{pmatrix}.$$

So the eigenvalues are given by

$$\begin{aligned} & U_{1,2}^{JT}(r,\phi) = V_{2a}r^2+V_{3a}\cos(3\phi)r^3 \\ & \pm r\left[V_{1e}^2+(2V_{1e}V_{2e}\cos(3\phi))r+(2V_{1e}V_{3e}+V_{2e}^2)r^2+(2V_{2e}V_{3e}\cos(3\phi))r^3+V_{3e}^2r^4\right]^{\frac{1}{2}}, \end{aligned} \tag{5.16}$$

where V_{2a} is elastic force constant for e mode and V_{3a} describes cubic force constant or anharmonicity of this mode. V_{ie}, $i=1,2,3$ are the linear, quadratic and cubic coupling parameters. The equation (5.16) is obtained from the diagonalization of the potential part

[4] In general for matrix $M = a\sigma_I + b\sigma_x + c\sigma_y + d\sigma_z$, eigenvalues can be obtained from

$$\lambda_\pm = a \pm \sqrt{b^2+c^2+d^2},$$

where

$$\sigma_I = \begin{pmatrix} 1 & 0 \\ 0 & 1 \end{pmatrix}, \quad \sigma_x = \begin{pmatrix} 0 & 1 \\ 1 & 0 \end{pmatrix}, \quad \sigma_y = \begin{pmatrix} 0 & -i \\ i & 0 \end{pmatrix}, \quad \sigma_z = \begin{pmatrix} 1 & 0 \\ 0 & -1 \end{pmatrix}.$$

of the Jahn-Teller Hamiltonian, including all couplings up to the third order in the polar coordinates [58]. For the realistic models, the parameters of the potential energy matrix are determined by a least-squares fitting of its eigenvalue (5.16) to the adiabatic potential energy surfaces which are calculated by the standard *ab initio* electronic structure methods. We fit both components of the surfaces simultaneously along both coordinates. The quality of fitting can be checked for either diagonal or off diagonal terms of potential matrix from the lower order Jahn-Teller coupling i.e. linear coupling, to the higher order for instance third order. Calculations show that the anharmonicity of the e vibrational mode plays an important role and also the contribution of the cubic terms in the topography of the potential energy surface in the $E \otimes e$ Jahn-Teller problem is essential [See ref [49]]. Here, the transformation angle in the polar coordinates is defined by

$$\gamma = \arctan \frac{V_{1e} r \sin\phi - 2V_{2e} 2r^2 \sin 2\phi + V_{3e} r^3 \sin\phi}{V_{1e} r \cos\phi + V_{2e} r^2 \cos 2\phi + V_{3e} r^3 \cos\phi}.$$

In the diabatic potential energy matrix of the Hamiltonian (5.11), the off-diagonal terms which contain the first and second order terms are responsible for the mixing of diabatic electronic states. Typical adiabatic Jahn-Teller potential energy surfaces are shown in figure 5.1 and 5.2. The symmetry of the system and the molecular dynamics become especially transparent from these potential energy surfaces. As we mention above, both surfaces are degenerate at $\rho = 0$ where they form a conical intersection. The lower state has a " Mexican hat " shape. For $g = 0$, the potential energy surface does not depend on the ϕ coordinate thus there is a cylindrical symmetry on the lower surface so the nuclear wavepacket can freely move around the conical intersection, called pseudorotation, i.e. the molecule can move from one obtuse isosceles geometry to another one without going through the equilateral configuration by passing through an acute isosceles geometry. This corresponds to the motion along a near-circular path around the origin. For $g \neq 0$ this pseudorotation, is hindered by energy barrier, now there are three equivalent minima and saddle points on the lower surface. At each of these minima the equilateral triangle is distorted to an isosceles one.

The extremal points of the lower surface are at geometries (ρ and ϕ) given by [59]:

$$\rho = \frac{\pm k}{\omega \mp (-1)^n g}, \ \phi = \frac{n\pi}{3}, \ n = 0, 1, \cdots, 5,$$

where upper and lower signs correspond to the case $k > 0$ and $k < 0$, respectively. If k and g are of the opposite sign the points with $n = 0$, 2 and 4 are saddle points and the points with

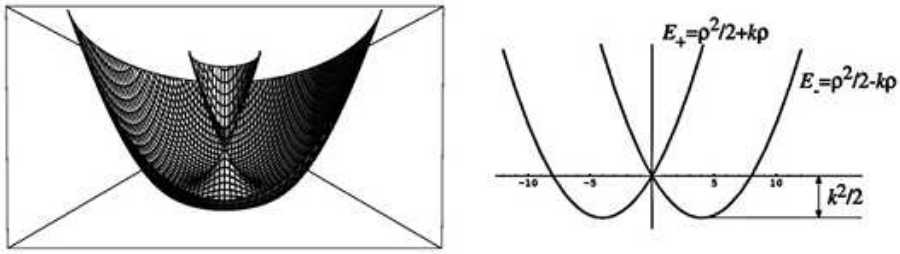

Figure 5.1 Adiabatic potential energy surface in the case of linear Jahn-Teller effect, i.e. the quadratic and higher couplings are zero. The potential is cylindrically symmetric and nuclear configuration can freely move along the through of surface [60].

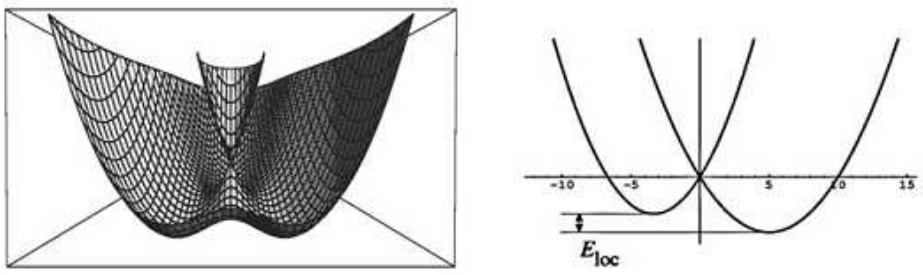

Figure 5.2 Adiabatic potential energy surfaces in the case of linear and quadratic Jahn-Teller couplings. The potential has no longer cylindrical symmetry and there are three distinct minima such that pseudorotational motion of the nuclei are slowed down by potential barriers [60].

$n = 1$, 3 and 5 are the minima. The Jahn-Teller stabilization energy, E_{JT}, is defined as the difference between the conical intersection energy and the minimum in the lower electronic state

$$E_{JT} = \frac{k^2}{2(\omega - g)}. \tag{5.17}$$

E_s is referred to the energy difference between conical intersection and the saddle point. For the alkali trimers like Li_3, E_{JT} are obtained from the $^2B_2$ (C_{2v}) minimum on the ground electronic state surface and E_s obtain from the lowest energy on $^2A_1$ geometry on this state. The global minima of the B_2 symmetry are reached at negative Q_x values, corresponding to obtuse distortions. Saddle points A_1 states at positive Q_x values are similar to global minima in the one-dimensional scan. The localization energy is defined as a barrier height between the minima

$$E_{loc} = E_{min} - E_{sadd} = \frac{k^2|g|}{\omega^2 - g^2}. \tag{5.18}$$

When g is large then E_{loc} is also large and pseudorotation becomes impossible, i.e. the atomic positions become localized in the minimum of the energy surface [See fig 5.6].

5.2.1 Li_3 molecule

When the Jahn-Teller theorem is applied to Li_3 at equilateral geometry, a doubly degenerate E electronic state splits into states with lower symmetry due to vibronic coupling between two degenerate modes, so-called symmetric and asymmetric bending. Figure 5.3 illustrates possible point groups for Li_3 at equilateral configuration. The adiabatic potential energy surface of Li_3 as a function of the normal mode coordinates was presented by Schumacher *et al* [61] for the first time and a numerical solution for the corresponding $E \otimes e$ Jahn-Teller system was given [See figs 5.4, 5.5 and 5.6]. Figure 5.4 shows two potential energy curves of the Li_3 by one dimensional scan, when the symmetric stretching normal coordinates fixed at $Q_s = 0.07$ and the asymmetric stretching normal mode coordinates is zero. Figure 5.5 shows one possible channel of the reaction $Li_3 \longrightarrow Li_2$+Li. Figure 5.6 shows the strongly anharmonic Mexican hat type potential as a function of degenerate normal coordinates Q_x and Q_y with three minima.

Schumacher *et al* used the normal mode coordinates which are shown in figure 5.7. Q_x corresponds to the normal coordinates of the bending mode, and Q_y to that of the asymmetric stretching mode. So there exist two symmetry-breaking vibrational modes for Li_3, while here

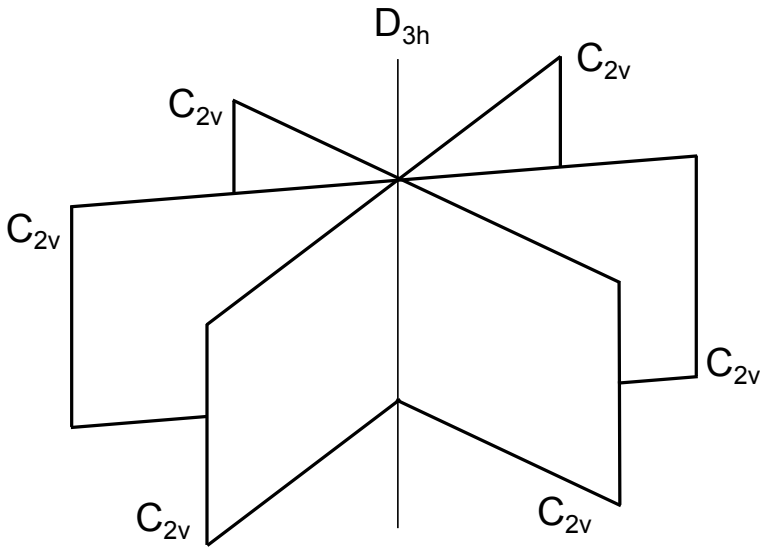

Figure 5.3 possible symmetry point groups in the D_{3h} symmetry configuration of the Li_3. Notice that there are three mirror symmetry planes.

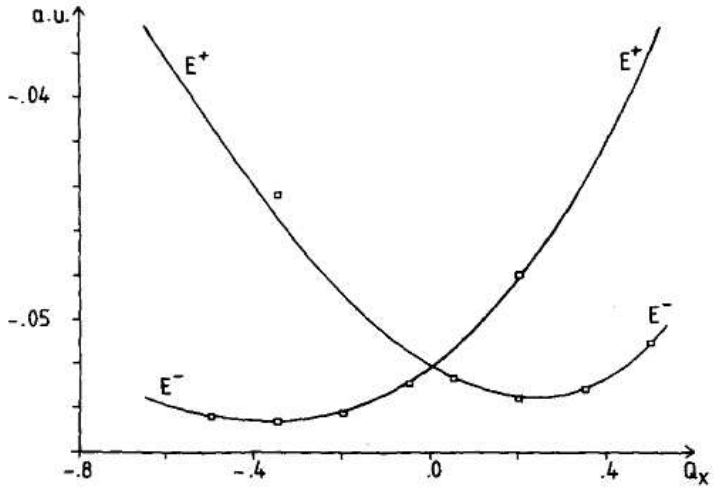

Figure 5.4 Potential energy curves at $Q_s = 0.07$ and $Q_y = 0$ a.u. taken from ref [61].

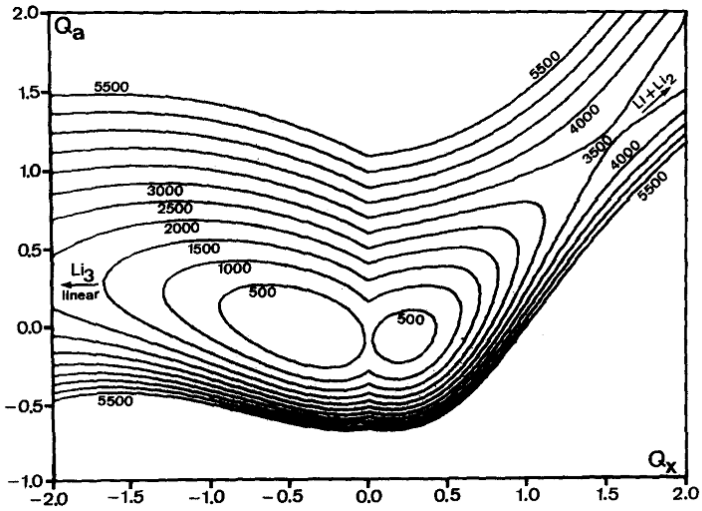

Figure 5.5 Survey of the adiabatic potential of Li_3 at $Q_y = 0$ a.u. corresponding to ref [61].

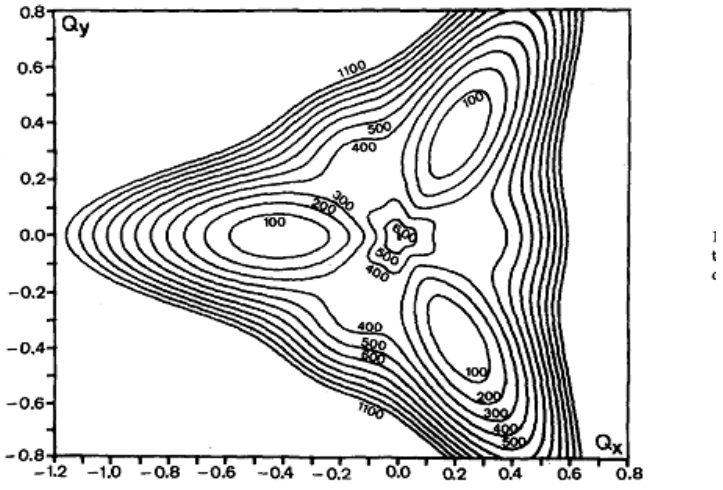

Figure 5.6 Adiabatic potential energy surface at $Q_s = 0$ a.u. obtained from ref [61]

by the symmetric stretching vibration Q_a, D_{3h} symmetry is preserved. Hence, the Q_x and Q_y are referred as the Jahn-Teller active normal coordinates.

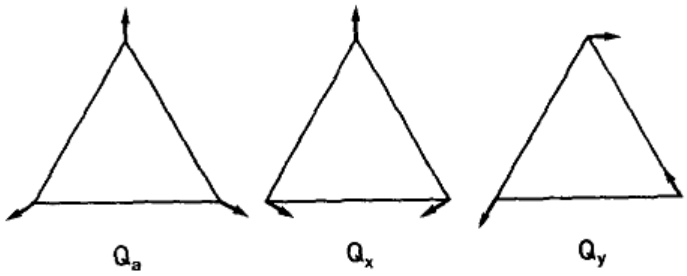

Figure 5.7 Normal mode coordinates used in ref [61].

5.3 Molecular gauge theory

Dynamical studies of the Jahn-Teller effect were first derived by Moffitt and Liehr [62] and simultaneously by Longuet-Higgins *et al* [63] in 1956. As we have discussed before, Herzberg and Longuet-Higgins in 1963 [64] proved theoretically that the adiabatic electronic wavefunction of the ground state changes sign when it completes a path in the nuclear configuration space which encircles a line of conical intersection. In other words, in the $E \otimes e$ Jahn-Teller situation the adiabatic electronic wavefunctions depend on the pseudorotation angles. The sign change around a degeneracy of the eigenstates of system whose Hamiltonian is real and Hermitian has been discussed also by Longuet-Higgins in 1975 [45], Mead 1979 [65], Mead and Truhlar in 1979 [66], Mead in 1980 [67, 68], Berry and Wilkinson 1984 [4]. This sign change of the wavefunction in the vicinity of the conical intersection is a special case of Berry's geometric phase [4]. The geometric phases have found application in several areas of physics and chemistry. It is also the earliest example of a singular gauge transformation that transform a single valued wavefunction to a multi-valued wavefunction that later, was taken into account by introducing the gauge potential and referred to as the Molecular Aharnove-Bohm effect [69]. It has been shown how the presence of an intrinsic vector potential can affect the free electron interference pattern. The change in interference pattern occurs due to Aharonove-Bohm phases, i.e. a special case of the geometric phase.

The adiabatic electronic wavefunctions change sign when encircling the conical intersection in the nuclear configuration space. Since the total wavefunction of the system must

remain single valued, the nuclear wavefunction must as well change its sign upon circling the point of degeneracy. As a consequence of this sign change, the internal rotation quantum number can only take half-integer values. It is possible to eliminate the sign change from the nuclear wavefunctions, but it leads to a vector potential term entering into the vibrational Hamiltonian. The Berry approach of the Abelian geometric phase is restricted to cyclic and adiabatic evolution of non-degenerate pure state. Wilkzek and Zee [70] pointed out that adiabatic transport of degenerate quantum states is associated with a non-Abelian geometric phase. Later Aharonove and Anandan [71] generalized the geometric phase to non-adiabatic evolution. The non-integrable, i.e. path dependent, phase factor is gauge invariant. Here, we will show that it is possible to introduce a non-abelian gauge field in the linear $E \otimes e$ Jahn-Teller Hamiltonian model in contrast to the standard abelian gauge field.

5.3.1 Introducing the gauge formalism

As we have seen. in the Born-Oppenheimer approximation the total wavefunction of a molecular system (2.6) is obtained as a product of the electronic and the nuclear wavefunction. It is always possible to define a new set of wavefunctions by performing the phase transformation

$$|\psi(r;R)\rangle \longrightarrow |\tilde{\psi}(r;R)\rangle = e^{i\gamma(R)}|\psi(r;R)\rangle, \tag{5.19}$$

$$\chi(R) \longrightarrow \tilde{\chi}(R) = e^{i\gamma(R)}\chi(R),$$

where $\gamma(R)$ is arbitrary real phase angle. If we restricted ourselves to phase transformations in which the phase factors $e^{i\gamma(R)}$ are single valued functions, these transformations are also called gauge transformations [72]. In principle, the total wavefunction of the system must not be affected by the gauge transformation.

$$\Psi(r,R) = \sum_i \psi_i(r;R)\chi_i(R) = \sum_i \tilde{\psi}_i(r;R)\tilde{\chi}_i(R).$$

For a system evolving in the closed path C in parameter space, γ depends only on the path of the loop traced by R and is referred to a geometric phase or the Berry phase. We shall in general use the term Berry phase for the geometrical phase obtained in a cyclic and adiabatic evolution of non-degenerate states. The geometrical phase can be calculated according to [4]

$$\gamma(C) = i \oint_C \langle\psi(r;R)|\nabla_R\psi(r;R)\rangle \cdot d\mathbf{R}, \tag{5.20}$$

where ∇_R denotes the gradient in parameter space. We can see that it is defined in terms of an integral over a vector-valued function

$$A(R) = i\langle\psi(r;R)|\nabla_R|\psi(r;R)\rangle. \tag{5.21}$$

This vector-valued function is called the Mead-Berry vector potential [4, 65, 67]. The Mead-Berry vector potential is well defined only with the use of the single-valued basis functions and we assume that the path C is a single path for which a complete set of smooth and single-valued basis function exists. Under a gauge transformation (5.19), $A(R)$ is transformed accordingly

$$\begin{aligned}
&A(R) \longrightarrow \tilde{A}(R) = i\langle\tilde{\psi}(r;R)|\left(\nabla_R|\tilde{\psi}(r;R)\rangle\right)\\
&= i\langle\psi(r;R)|e^{-i\gamma(R)}\left(\nabla_R e^{i\gamma(R)}|\psi(r;R)\rangle\right)\\
&= i\langle\psi(r;R)|\nabla_R|\psi(r;R)\rangle + ie^{-i\gamma(R)}\left(\nabla_R e^{i\gamma(R)}\right)\\
&= A(R) - \nabla_R\gamma(R).
\end{aligned}$$

Then the Mead-Berry vector potential satisfies the gauge transformation rule, as a vector potential in electromagnetism. The set of phase factors $e^{-i\gamma(R)}$ form the symmetry group $\mathcal{U}(1)$. This is analogous to electromagnetic gauge theory which is called an abelian gauge theory. Here, we have a gauge theory with potential $A(R)$ which is not invariant with respect to a gauge transformation. The gauge potential (5.21) is defined in terms of the eigenfunctions of the electronic Hamiltonian and for a M-dimensional parameter space we again have a gauge theory, but now the gauge transformations and gauge potentials depend on M parameters $R = R_1, \cdots, R_M$ and $A(R)$ consists of M components $A_i(R)$, where $i = 1, \cdots, M$. If the parameter space has three dimensions, i.e. $M \subseteq \mathbb{R}^3$, then one can define

$$B_i = \frac{1}{2}\varepsilon_{ijk}F_{jk},$$

where ε_{ijk} are the components of the totally antisymmetric Levi-Civita symbol. From the Lorentz force notation, in terms of a vector potential one can define

$$B = \nabla_R \times A(R).$$

We can use the gauge-invariant Berry phase angle to see what happens when two energy states become degenerate for some values of the parameter. From the definition of the strength field curvature F and using the completeness of the basis functions $|\psi_i(r;R)\rangle$, then

after substituting equation (3.11) into F we obtain the expression of F

$$F = i \sum_{i \neq j} \frac{\langle \psi_i(r;R) | \nabla_R H_{el} | \psi_j(r;R) \rangle \times \langle \psi_j(r;R) | \nabla_R H_{el} | \psi_i(r;R) \rangle}{|U_i(R) - U_j(R)|^2}. \tag{5.22}$$

This form does not depend on the phase factor of the basis functions. Therefore, one can calculate the Berry phase angle even for cases where the curve C lies in a region in parameter space where smooth and single-valued basis functions do not exist. The formula (5.22) shows also that the singularities of F happen at those parameter values where the eigenvalues are degenerate $U_i(R) = U_j(R)$.

In order to generalize the above abelian gauge theory we introduce the following notation as an N dimensional unitary representation of the symmetry group G

$$\mathcal{U}^g(\gamma(R)) \in \mathcal{U}(N).$$

Then the transformation (5.19) is written as

$$\psi(r;R) \longrightarrow \tilde{\psi}(r;R) = \mathcal{U}^g(\gamma(R))\psi(r;R), \tag{5.23}$$

$$\chi(R) \longrightarrow \tilde{\chi}(R) = \mathcal{U}^g(\gamma(R))\chi(R).$$

Here, the components of the gauge field or the potential are $N \times N$ matrices, with N being the dimension of the representation space. Transformation of the gauge potential under the transformation (5.23) reads

$$\tilde{A}_i^g(R) = \mathcal{U}^g(\gamma(R)) A_i^g(R) \mathcal{U}^{g^{-1}}(\gamma(R)) + i[\partial \mathcal{U}^g(\gamma(R)) \mathcal{U}^{g^{-1}}(\gamma(R))]. \tag{5.24}$$

The gauge potential defines the gauge-covariant derivatives as [72]

$$D_i(A^g) = \partial_i + i A_i^g(R).$$

The transformation properties of the gauge-covariate derivative can be shown using (5.23) and (5.24)

$$D_i(\tilde{A}^g) = \partial_i + i\tilde{A}_i^g(R) = \mathcal{U}^g(\gamma(R)) D_i(A^g) \mathcal{U}^{g^{-1}}(\gamma(R)),$$

and

$$D_i(A^g)\psi \longrightarrow D_i(\tilde{A}^g)\tilde{\psi} = \mathcal{U}^g(\gamma(R)) D_i(A^g)\psi.$$

This means that the covariant derivatives of ψ, $D_i(A^g)\psi$, transform in the same way as ψ does. One can define the non-abelian gauge field strength tensor according to

$$F^g_{ij} = \frac{1}{i}[D_i, D_j] = \partial_i A^g_j - \partial_j A^g_i + i[A^g_i, A^g_j]. \tag{5.25}$$

Here, the brackets mean the commutator of $N \times N$ matrices with components

$$[A^g_i, A^g_j]^{nm} = \sum_l^N (A^{nl}_i A^{lm}_j - A^{nl}_j A^{lm}_j).$$

Now we will discuss the molecular gauge theory as an example of gauge theories with the unitary symmetry group $G = \mathcal{U}(N)$.

5.3.2 Molecular Schrödinger equation using gauge theory

As we have shown before, to obtain the total Schrödinger equation we need to express the nuclear momentum operator $\mathbf{P}$ operating on the total wavefunction $|\Psi(R)\rangle$, [See chapter 2]. This is done as follows:

$$\langle\psi_j(r;R)|\mathbf{P}|\Psi(R)\rangle = \sum_i \langle\psi_j(r;R)|\frac{1}{i}\nabla_R|\psi_i(r;R)\rangle\langle\psi_i(r;R)|\Psi(R)\rangle = \tag{5.26}$$

$$\sum_i \left(\langle\psi_j(r;R)|\psi_i(r;R)\rangle \frac{1}{i}\nabla_R \langle\psi_i(r;R)|\Psi(R)\rangle - i\langle\psi_j(r;R)|\nabla_R|\psi_i(r;R)\rangle\langle\psi_i(r;R)|\Psi(R)\rangle \right).$$

Using the orthogonality, we write this as

$$\langle\psi_j(r;R)|\mathbf{P}|\Psi(R)\rangle = \sum_i \left(\frac{1}{i}\nabla_R \delta_{ij} - A_{ji}(R) \right) \langle\psi_i(r;R)|\Psi(R)\rangle, \tag{5.27}$$

$$\equiv \sum_i \frac{1}{i} D_{ji} \langle\psi_i(r;R)|\Psi\rangle,$$

where ∇_R is with respect to the nuclear coordinates R. The vector-potential like term $A_{ij}(R)$ is defined by

$$A_{ij}(R) = \frac{1}{i}\langle\psi_i(r;R)|\nabla_R|\psi_j(r;R)\rangle, \tag{5.28}$$

i.e. D_{ij} is introduced as

$$\frac{1}{i}D_{ij} = \frac{1}{i}\nabla_R - A_{ij}(R). \tag{5.29}$$

A_{ij} and D_{ij} define the $N \times N$ matrix A and the $N \times N$ matrix-valued differential operator D respectively, where N is the dimension of the electronic Hamiltonian H_{el}. A is an example of a gauge potential, whereas D is the corresponding gauge-covarient derivative. The case $N = 1$, which was originally introduced in [65, 67], has the same form as the Mead-Berry vector potential defined in equation (5.21), but in the case $N \neq 1$ we deal with a general non-abelian gauge potential. Following the same approach for nuclear momentum operator, we can find the matrix elements of the operator $\mathbf{P}^2$ by pursuing the derivative of the relation (5.26)

$$\langle \psi_j(r;R)|\mathbf{P}^2|\Psi(R)\rangle = -\sum_i \langle \psi_j(r;R)|\nabla_R^2|\psi_i(r;R)\rangle\langle\psi_i(r;R)|\Psi(R)\rangle \tag{5.30}$$

$$= \sum_{i,k}\left(\frac{1}{i}\nabla_R\delta_{jk} - A_{jk}\right)\cdot\left(\frac{1}{i}\nabla_R\delta_{ki} - A_{ki}\right)\langle\psi_i(r;R)|\Psi(R)\rangle.$$

By using the molecular Hamiltonian (3.1) and the definition of $\mathbf{P}^2$ and substituting into equation (2.7) we obtain the matrix elements of total molecular Schrödinger equation as

$$\sum_l \left[\langle\psi_j|\frac{\mathbf{P}^2}{2M}\chi_l(R)|\psi_l(r;R)\rangle + \langle\psi_j(r;R)|H_{el}\chi_l(R)|\psi_l(r;R)\rangle\right] = \tag{5.31}$$

$$\sum_l \langle\psi_j(r;R)|E\chi_l(R)|\psi_l(r;R)\rangle,$$

giving

$$\sum_l\left[\sum_k \frac{1}{2M}\left(\frac{1}{i}\nabla_R\delta_{jk} - A_{jk}\right)\cdot\left(\frac{1}{i}\nabla_R\delta_{kl} - A_{kl}\right) + U_l(R)\delta_{jl}\right]\chi_l(R) = E_j\chi_j(R).$$

Let us look at a simple example that is related to our study, the $E \otimes e$ Jahn-Teller system that includes a conical intersection in the potential energy surfaces. We recall the Jahn-Teller Hamiltonian and we consider only the potential part with linear coupling for convenience, i.e.

$$U^{dJT} = \begin{pmatrix} 0 & Q_x - iQ_y \\ Q_x + iQ_y & 0 \end{pmatrix} = \begin{pmatrix} 0 & re^{-i\phi} \\ re^{i\phi} & 0 \end{pmatrix},$$

Using the transformation matrix S we can diagonalize this potential and find the adiabatic potential energy surfaces

$$S^\dagger U^{dJT} S = \begin{pmatrix} H_{el,u} & 0 \\ 0 & H_{el,l} \end{pmatrix}.$$

The cost of this diagonalization is the using of the $|\tilde{\psi}(r;R)\rangle = S|\psi(r;R)\rangle$ instead of $|\psi(r;R)\rangle$. Let us consider the transformation matrix (5.14). We discussed in the previous section that we can pick $s = \frac{1}{2}$ and in the zero value of the quadratic coupling we obtain the transformation matrix (5.13) with $\gamma = \phi$ and

$$S = \frac{1}{\sqrt{2}} \begin{pmatrix} e^{-i\frac{\phi}{2}} & e^{-i\frac{\phi}{2}} \\ e^{i\frac{\phi}{2}} & -e^{i\frac{\phi}{2}} \end{pmatrix}.$$

Using the definition of the vector potential (5.21) and the transformed basis function (5.23), we can obtain the Q_x and Q_y components of the vector potential

$$A_{Q_x} = -iS\nabla_{Q_x}S^\dagger = -iS\nabla_\phi S^\dagger \frac{\partial\phi}{\partial Q_x}, \tag{5.32}$$

where

$$\begin{aligned} S\nabla_\phi S^\dagger &= \frac{i}{4} \begin{pmatrix} e^{\frac{-i\phi}{2}} & e^{\frac{-i\phi}{2}} \\ e^{\frac{i\phi}{2}} & -e^{\frac{i\phi}{2}} \end{pmatrix} \begin{pmatrix} e^{\frac{i\phi}{2}} & -e^{\frac{-i\phi}{2}} \\ e^{\frac{i\phi}{2}} & e^{\frac{-i\phi}{2}} \end{pmatrix} \\ &= \frac{i}{2}\sigma_z, \end{aligned} \tag{5.33}$$

and

$$\frac{\partial\phi}{\partial Q_x} = \frac{1}{Q_y} \cdot \frac{1}{1 + (\frac{Q_x}{Q_y})^2}. \tag{5.34}$$

Substituting equations (5.33) and (5.34) into equation (5.32) gives

$$A_{Qx} = \frac{1}{2}\frac{Q_y}{Q_x^2 + Q_y^2}\sigma_z.$$

In the same way we can obtain A_{Q_y}, where $\frac{\partial\phi}{\partial Q_y} = \frac{-Q_x}{Q_x^2+Q_y^2}$, as

$$A_{Qy} = -iS\nabla_{Q_y}S^\dagger = \frac{-1}{2}\frac{Q_x}{Q_x^2 + Q_y^2}\sigma_z.$$

It implies that the gauge field is abelian, i.e.

$$[A_{Q_x}, A_{Q_y}] = 0.$$

So for abelian gauge field we can obtain the magnetic field as

$$B_z = \partial_{Q_x}A_{Q_y} - \partial_{Q_y}A_{Q_x} = \frac{\sigma_z}{2}\left\{\partial_x(\frac{-Q_x}{Q_x^2+Q_y^2}) - \partial_{Q_y}(\frac{Q_y}{Q_x^2+Q_y^2})\right\}.$$

By carrying out the derivative it can be derived

$$B_z = \frac{\sigma_z}{2}\{(\frac{Q_x^2 - Q_y^2}{(Q_x^2+Q_y^2)^2}) - (\frac{Q_x^2 - Q_y^2}{(Q_x^2+Q_y^2)^2})\} = 0.$$

We see that the magnetic field is strictly zero everywhere expect at the origin (Q_x, Q_y)=(0,0) where, it is illdefined. Nevertheless, we know that integrating the vector potential along a line encircling the conical intersection we obtain a non-zero Berry phase which means that there is a non-zero magnetic flux through the conical intersection. This is a example of the well-known Ahronove-Bohm effect [72].

Lets us instead, rewrite the linear $E \otimes e$ Jahn-Teller Hamiltonian as in the form

$$H^{dJT} = \frac{P_{Q_x}^2}{2} + \frac{P_{Q_y}^2}{2} + \omega_e \left(\frac{Q_x^2 + Q_y^2}{2}\right) + k(Q_x\sigma_x + Q_y\sigma_y).$$

According to the Rashba spin-coupling form [5] we will have

$$H^{JT} = \frac{\omega_e(Q_x + \frac{k\sigma_x}{\omega_e})^2}{2} + \frac{\omega_e(Q_y + \frac{k\sigma_y}{\omega_e})^2}{2} + \frac{P_{Q_x}^2 + P_{Q_y}^2}{2} - \frac{k^2}{\omega_e}$$

$$= \frac{\omega_e(Q_x - \tilde{A}_{Q_x})^2}{2} + \frac{\omega_e(Q_y - \tilde{A}_{Q_y})^2}{2} + V(P_{Q_x}, P_{Q_y}) - \frac{k^2}{\omega_e}.$$

Given in this form, the Hamiltonian can be interpreted as a charged particle moving in a harmonic potential and under the influence of the gauge potential $\tilde{A} = \frac{k}{\omega_e}(\sigma_x, \sigma_y)$. That is,

[5] Free spin-orbital coupled electrons in a plane can be described by [73, 74]

$$H = \frac{P_x^2}{2m} + \frac{P_y^2}{2m} + g(P_x\sigma_x + P_y\sigma_y) \Leftrightarrow \frac{(p_x + mg\sigma_x)^2}{2m} + \frac{(p_y + mg\sigma_y)^2}{2m} - mg^2,$$

where, σ-matrices are the Pauli ones obeying the commutation relation

$$[\sigma_i, \sigma_j] = i2\varepsilon_{ijk}\sigma_k.$$

Written in the second form, the Roshba spin-orbit coupling can be viewed as effective gauge field. The field is non-abelian and the corresponding magnetic field becomes state dependents

$$B_j = \frac{1}{2}\varepsilon_{jkl}F_{kl}.$$

By definition of F_{kl}, we obtain

$$B_z = mg^2 * 2\sigma_z.$$

In condensed matter theory, such state dependent magnetic fields gives rise to phenomena such as spin and anomalous Hall effects.

in this picture the meaning of position and momentum has been reversed. The interesting aspect is that the corresponding magnetic field, now is non-abelian. The field curvature becomes

$$\tilde{F}_{xy} = (\nabla_{P_{Q_x}, P_{Q_y}} \times \tilde{A})_z - i[\tilde{A}_{Q_x}, \tilde{A}_{Q_y}] = \frac{2k^2}{\omega_e}\sigma_z.$$

Thus, the corresponding magnetic field will be proportional to $\frac{2k^2}{\omega_e^2}\sigma_z$. Note that the first part, the abelian contribution is zero and the magnetic field stems solely from the non-abelian part.

We may point out that when include higher order terms in the $E \otimes e$ Jahn-Teller model, i.e. quadratic, cubic, $\cdots$ finding these generalized gauge field is non-trivial.

Chapter 6

Results

We have seen before that the dynamical Jahn-Teller effect can not be treated if not the motions of electrons and nuclei are coupled together. The couplings between adiabatic potential energy surfaces cause a conical intersection. Metal cluster X_3 systems with a conical intersections at the geometric D_{3h} symmetries are special cases of the $E \otimes e$ Jahn-Teller systems. Furthermore, alkali metal trimers are convenient systems for experimental studies due to their possibility of vibrational excitation in the visible or near infrared regions [75]. Since, the molecular theory predicts that the Li_3 molecule in the high symmetry configuration is degenerate in its electronic ground states and according to the Jahn-Teller theorem it tends to distort into a more stable nondegenerate configuration with lower symmetry, it has been a well studies system in terms of the dynamical Jahn-Teller effect. The adiabatic potential energy surface of the ground state for this system shows that there are several minima separated by low potential barriers and the potential energy surface is quite flat in the region close to these minima corresponding to the isosceles configurations. Tunneling from one minima to another minima causes pseudorotation of the trimer. In this chapter our aim is to report the results from the quantum chemistry computations and to determine the potential energy surfaces of the Li_3 molecule. Optimizing the eigenvalues of the Jahn-Teller Hamiltonian to the adiabatic potential energy surfaces gives the Jahn-Teller parameters. Using these parameters we can construct the unitary matrix that transforms the matrix from adiabatic to diabatic representations and set up the diabatic Jahn-Teller potential. The nuclear dynamics is explored using wavepacket propagation on the diabatic potentials. To confirm the accuracy of the quantum chemistry calculations on Li_3, we start by performing

calculation on the diatomic Li_2 system.

6.1 Li_2 Molecule

We start our calculations on the diatomic molecule, Li_2. The Lithium dimer is after the hydrogen molecule the smallest stable homonuclear diatomic molecule. Two Li atoms attract each other when their electronic spins are antiparallel and repel each other when their spins are parallel. Each Li atom has 3 electrons that occupy the 1s and 2s atomic orbitals with the electronic configuration $1s^2 2s^1$.

6.1.1 Potential energy curves of Li_2

The first *ab initio* calculation on Li_2 were performed by Konowalow *et al* [76, 77] in 1976, where they computed and analyzed the potential energy curves in the long range region of the the 26 lowest lying states [78]. We calculate the potential energy curves for the ground and several low-lying excited states of Li_2 at the Hartree-Fock, MCSCF levels and MRCI calculations, respectively. All our calculations reported in the present work were performed using the MOLPRO program package [19]. The calculated adiabatic potential energy curves correlate to Li(^2S)+Li(^2S) ground electronic asymptote and Li(^2S)+Li(^2P) excited atomic asymptote. We here use the aug-cc-PVTZ basis set by Dunning *et al* [24] which is composed by $(12s, 6p, 3d, 2f)$ primitive basis functions contracted into $(5s, 4p, 3d, 2f)$. A homonuclear molecule like Li_2 belongs to the $D_{\infty h}$ point group, but for practical performance the symmetry is reduced to D_{2h}. The CI calculation can only treat abelain point groups and the $D_{\infty h}$ is a nonabelian point group. However, there is a one to one correspondence between symmetries in $D_{\infty h}$ and D_{2h}. Then, we used the abelian subgroup D_{2h} in our quantum chemistry computations. In this program package, the symmetry of the molecular orbitals σ_g, $\pi_{u,x}$, $\pi_{u,y}$, δ_g, σ_u, $\pi_{g,x}$, $\pi_{g,y}$, and δ_u in the $D_{\infty h}$ point group fall into the $A_g, B_{3u}, B_{2u}, B_{1g}, B_{1u}, B_{2g}, B_{3g}$ and A_u respectively. This is summarized in table 6.1.

We have introduced the character table of the D_{2h} before in the chapter 4 [See the table 4.2]. The table 6.2 shows the direct product for the D_{2h} point group. Using these tables we can determine the symmetry of wavefunctions for different configurations of molecular states. We have obtained the MOs for the Li_2 molecule by using the Hartree-Fock level of theory. The results are shown in table 6.3. By using this table, the lowest molecular orbitals

Orbitals in D_{2h}	orbitals in $D_{\infty h}$	No.
a_g	$\sigma_g,\ \delta_g$	1
b_{3u}	π_u	2
b_{2u}	π_u	3
b_{1g}	δ_g	4
b_{1u}	$\sigma_u,\ \delta_u$	5
b_{2g}	π_g	6
b_{3g}	π_g	7
a_u	δ_u	8

Table 6.1 Classification of $D_{\infty h}$ orbitals in the D_{2h} with the symmetry number.

	A_g	B_{1g}	B_{2g}	B_{3g}	A_u	B_{1u}	B_{2u}	B_{3u}
A_g	A_g	B_{1g}	B_{2g}	B_{3g}	A_u	B_{1u}	B_{2u}	B_{3u}
B_{1g}	B_{1g}	A_g	B_{3g}	B_{2g}	B_{1u}	A_u	B_{3u}	B_{2u}
B_{2g}	B_{2g}	B_{3g}	A_g	B_{1g}	B_{2u}	B_{3u}	A_u	B_{1u}
B_{3g}	B_{3g}	B_{2g}	B_{1g}	A_g	B_{3u}	B_{2u}	B_{1u}	A_u
A_u	A_u	B_{1u}	B_{2u}	B_{3u}	A_g	B_{1g}	B_{2g}	B_{3g}
B_{1u}	B_{1u}	A_u	B_{3u}	B_{2u}	B_{1g}	A_g	B_{3g}	B_{2g}
B_{2u}	B_{2u}	B_{3u}	A_u	B_{1u}	B_{2g}	B_{3g}	A_g	B_{1g}
B_{3u}	B_{3u}	B_{2u}	B_{1u}	A_u	B_{3g}	B_{2g}	B_{1g}	A_g

Table 6.2 Product table for D_{2h} point group.

orbital number.symm	occupation	symbol	energy
1.1	2	$1\sigma_g$	-2.4569
1.5	2	$1\sigma_u$	-2.4537
2.1	2	$2\sigma_g$	-0.1927
2.5	0	$2\sigma_u$	0.0111
1.2	0	$1\pi_{ux}$	0.0243
1.3	0	$1\pi_{uy}$	0.0243
3.1	0	$3\sigma_g$	0.0412
1.6	0	$1\pi_{gx}$	0.0577
1.7	0	$1\pi_{gy}$	0.0577
3.5	0	$3\sigma_u$	0.0667
⋮	⋮	⋮	⋮

Table 6.3 Orbitals of Li_2 molecule in order to their energies in the D_{2h} symmetry point group.

according to their energies will be:

$$(1\sigma_g)(1\sigma_u)(2\sigma_g)(2\sigma_u)(1\pi_{u,x})(1\pi_{u,y})(3\sigma_g)(1\pi_{g,x})(1\pi_{g,y})(3\sigma_u)(2\pi_{u,x})(2\pi_{u,y})(4\sigma_g)\cdots .$$

The configuration of the ground electronic state, $^1\Sigma_g^+$, for the Li_2 molecule is

$$(1\sigma_g)^2(1\sigma_u)^2(2\sigma_g)^2.$$

Table 6.4 shows the main configurations of the molecular excited states of the Li_2 molecule using in our computation. Figure 6.1 illustrates a molecular orbital diagram for the first excited state, $^3\Sigma_u^+$, of the Li_2 as an example.

6.1.2 MRCI computation method of electronic-states

To obtain a good description of the molecular orbitals, state-averaged MCSCF calculations are performed. The active space of the MCSCF calculations involves 10 molecular orbitals ($3\sigma_g$, $3\sigma_u$, $1\pi_{u,x/y}$, $1\pi_{g,x/y}$) composed of $2s, 2p$ atomic orbitals from each Li atom. The state-averaged calculations includes all the excited states. The MRCI calculations were carried out using the same active space for the MCSCF calculation. Furthermore, excitation from

State	main configuration	total symmetry of wavefunction
$^3\Sigma_u^+$	$(1\sigma_g)^2(1\sigma_u)^2(2\sigma_g)^1(2\sigma_u)^1(1\pi_u)^0(3\sigma_g)^0(1\pi_g)^0(3\sigma_u)^0$	$\sigma_g \otimes \sigma_u = 5$
$^3\Pi_u$	$(1\sigma_g)^2(1\sigma_u)^2(2\sigma_g)^1(2\sigma_u)^0(1\pi_u)^1(3\sigma_g)^0(1\pi_g)^0(3\sigma_u)^0$	$\sigma_g \otimes \pi_u = 2$
$^1\Pi_u$	$(1\sigma_g)^2(1\sigma_u)^2(2\sigma_g)^1(2\sigma_u)^0(1\pi_u)^1(3\sigma_g)^0(1\pi_g)^0(3\sigma_u)^0$	$\sigma_g \otimes \pi_u = 2$
$^3\Sigma_g^+$	$(1\sigma_g)^2(1\sigma_u)^2(2\sigma_g)^1(2\sigma_u)^0(1\pi_u)^0(3\sigma_g)^1(1\pi_g)^0(3\sigma_u)^0$	$\sigma_g \otimes \sigma_g = 1$
$^3\Pi_g$	$(1\sigma_g)^2(1\sigma_u)^2(2\sigma_g)^1(2\sigma_u)^0(1\pi_u)^0(3\sigma_g)^0(1\pi_g)^1(3\sigma_u)^0$	$\sigma_g \otimes \pi_g = 6$
$^1\Pi_g$	$(1\sigma_g)^2(1\sigma_u)^2(2\sigma_g)^1(2\sigma_u)^0(1\pi_u)^0(3\sigma_g)^0(1\pi_g)^1(3\sigma_u)^0$	$\sigma_g \otimes \pi_g = 6$
$^1\Sigma_u^+$	$(1\sigma_g)^2(1\sigma_u)^2(2\sigma_g)^1(2\sigma_u)^0(1\pi_u)^0(3\sigma_g)^0(1\pi_g)^(3\sigma_u)^1$	$\sigma_g \otimes \sigma_u = 5$

Table 6.4 The electronic configurations of the excited states for the Li_2 molecule.

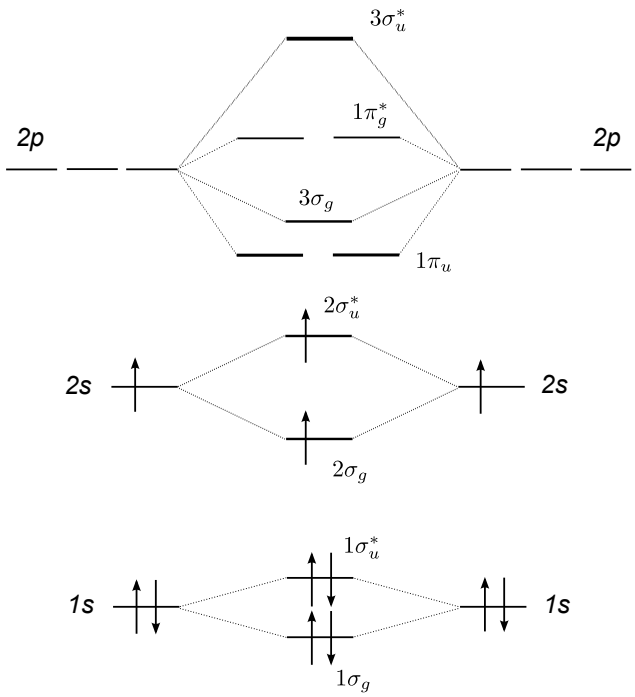

Figure 6.1 Molecular orbital correlation diagram in the $^3\Sigma_u^+$ state of the Li_2 molecule.

the core orbitals ($1\sigma_g$ and $1\sigma_u$) and single and double external excitation were considered. The potential energy curves are computed for 20 values of the internuclear distance ranging from 4-14 a_0. Potential energy curves for ground electronic and low-lying excited states computed using the MRCI method are depicted in figure 6.2. From the figure we can see that the $^1\Sigma_g^+$ ground electronic state has a potential curve with a deep minimum and that is a stable state. On the other hand, the $^3\Sigma_u^+$ state is unstable. We have examined the accuracy of the calculation by varying the basis set and the active space. By increasing the basis set to aug-cc-PCVTZ $(14s, 8p, 4d, 2f)$ more accurate dissociation energies are obtained [79]. Figure 6.3 shows the calculated potential energy curves for larger active space. The basis set has been augmented with a f function which is obtained by minimizing the energy for Li_2 to better describe the correlation effects and diffused functions to improve excited states description [See fig. 6.4]. The agreement between the aug-cc-PVTZ with the mentioned active space and the other theoretical reported data is good. Our calculated potential curves are in excellent agreement with the calculations reported by Hotta *et al* [80] and also by Jasik *et al* [78]. Figure 6.5 shows the comparison between our reported data and the data reported by ref [78].

6.2 Li_3 trimer

We will now peresent results on our theoretical study of the Li_3 system. First the relevant potential energy surfaces are computed and fitted to a Jahn-Teller Hamiltonian. Then wavepacket are propagated on diabatic potentials.

6.2.1 Computational investigation of potential energy surfaces of Li_3

The ground and three low-lying excited states were investigated by the MRCI method with orbitals obtained from the MCSCF calculation. The MCSCF calculation was performed by distributing three valence electrons into fifteen orbitals, which correspond to all the Li $2s$ and $2p$ valence orbitals. The MCSCF active space consists of seven a_1, four b_1, three b_2 and one a_2 molecular orbitals, while two a_1 and one b_1 molecular orbitals were chosen as core orbitals. We started the numerical calculation by computing of the Li_3 ion at the Hartree-

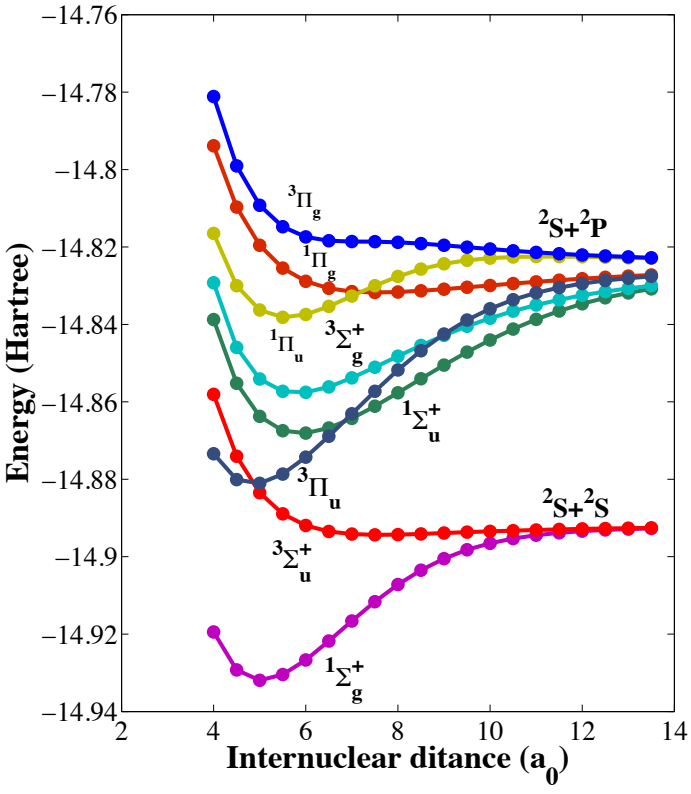

Figure 6.2 Potential energy curves for electronic states of the Li_2 molecule at the MRCI level. The MCSCF active space composed of ten MOs.

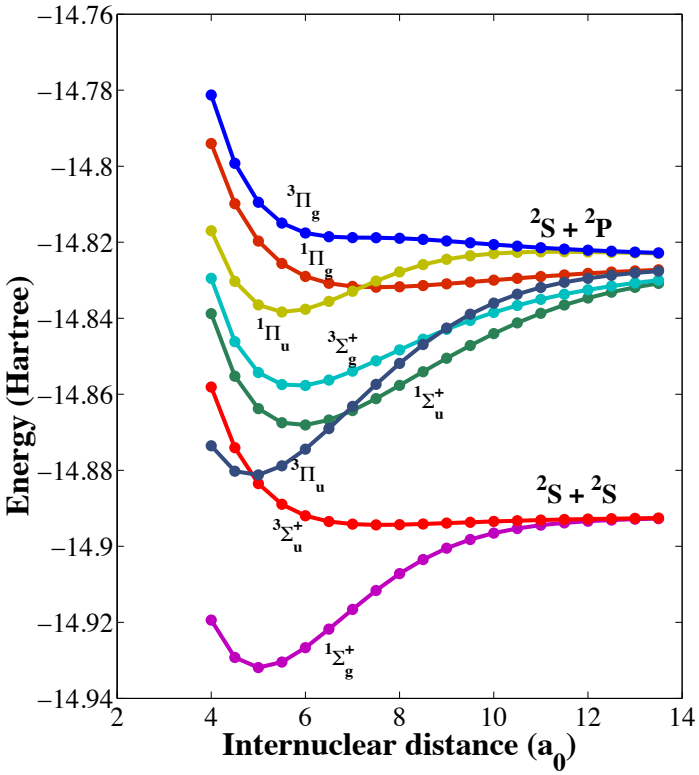

Figure 6.3 Potential energy curves for electronic states of the Li_2 molecule at the MRCI level. The MCSCF active space composed of 16 MOs.

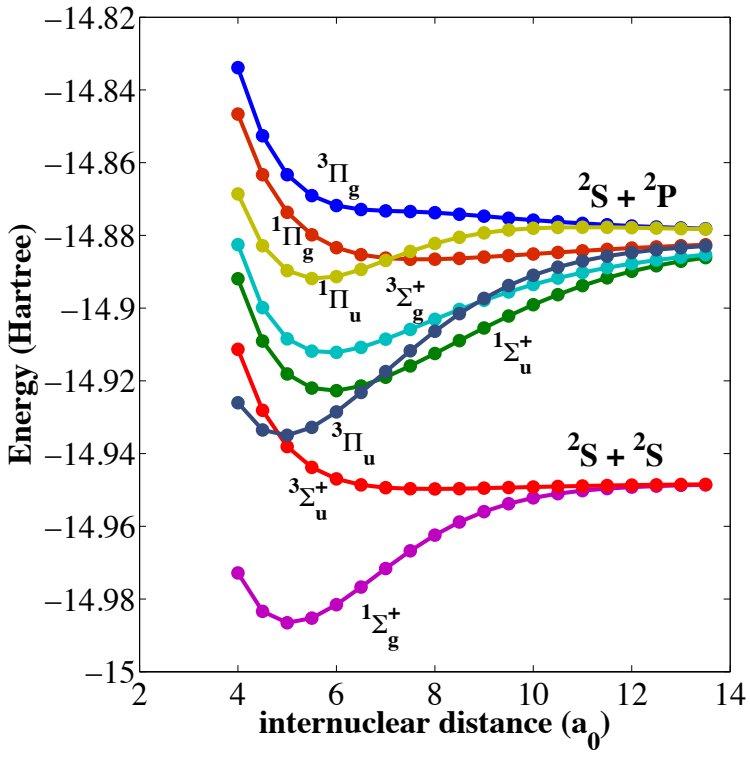

Figure 6.4 Potential energy curves for each electronic state of the Li_2 molecule at the MRCI level by using larger basis set $(14s, 8p, 4d, 2f)$.

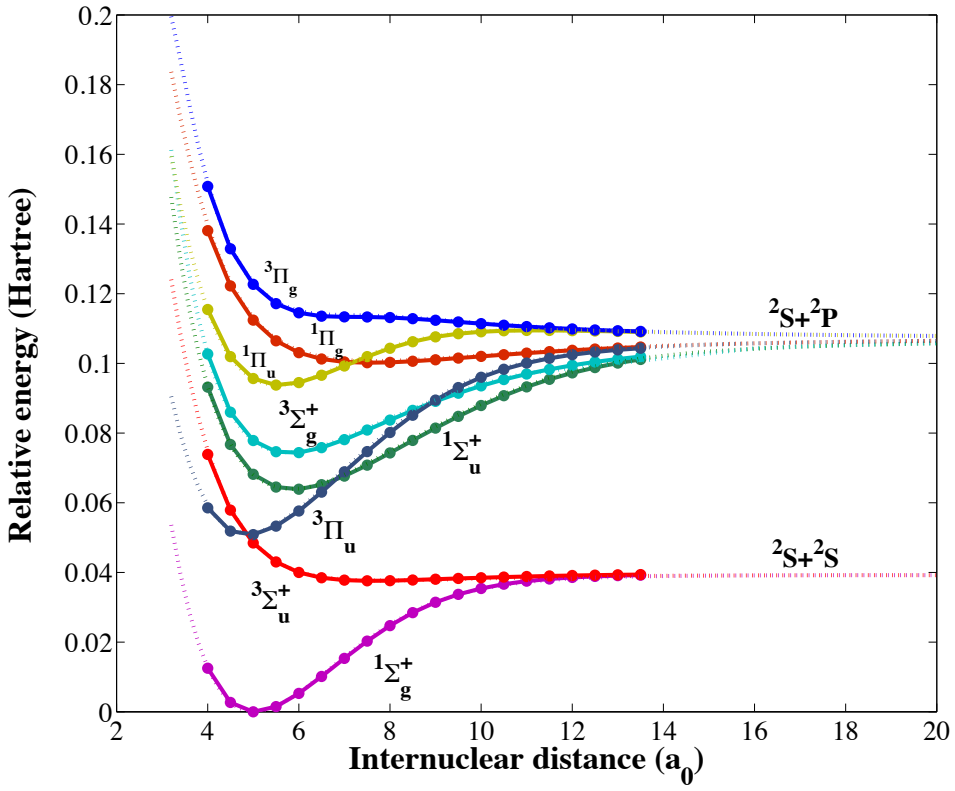

Figure 6.5 Comparison of the reported ground molecular state and excited molecular states corresponding to $^2S + {}^2S$ and $^2S + {}^2P$ asymptotes and the theoretical results of Jasik *et al* [78]. Solid lines with symbols show the present work results for ten MOS in active space and doted lines show the potential energy curves reported by Jasik *et al* [78].

orbital number.symm	occupation	symbol	energy
1.1	2	$1a_1$	-2.6258
2.1	2	$2a_1$	-2.6253
1.3	2	$1b_1$	-2.6251
3.1	2	$3a_1$	-0.3683
4.1	1	$4a_1$	-0.1254
2.3	0	$2b_1$	-0.1251
1.2	0	$1b_2$	-0.1062
5.1	0	$5a_1$	-0.0927
6.1	0	$6a_1$	-0.0718
3.3	0	$3b_1$	-0.0717
2.2	0	$2b_2$	-0.0558
1.4	0	$1a_2$	-0.0556
7.1	0	$7a_1$	-0.0501
⋮	⋮	⋮	⋮

Table 6.5 Orbitals of Li_3 molecule in order to their energies in the C_{2v} point group.

Fock level of theory. The energy of these orbitals are given in table 6.5. In the C_{2v} point group, the symmetries of the irreducible representation a_1, b_2, b_1, a_2 are 1, 2, 3, 4 respectively. The ground electronic state configuration is given by

$$(1a_1)^2(2a_1)^2(1b_1)^2(3a_1)^2(4a_1)^1.$$

The MRCI calculation is performed using the same active space as for the MSCSF method. Excitation from the core orbitals $1a_1, 2a_1$ and $1b_1$ and single and double external excitations were considered as well. The potential energy curves of the ground electronic and several excited states of Li_3 are represented in figure 6.6 as a function of the normal mode coordinates Q_x at fixed $Q_s = 3.2\ a_0$ and $Q_y = 0\ a_0$. These curves are obtained by symmetrically bending the triangular Li_3 molecule. Here we can see the agreement between our reported calculation and theoretical calculations were performed by Ehara *et al* [48] which are displayed by doted lines. Potential energy curves for the $1^2E'$ ground state of Li_3 are doubly degenerate at D_{3h} symmetry which occurs only at the symmetric bending normal mode coordinate $Q_x = 0.0\ a_0$.

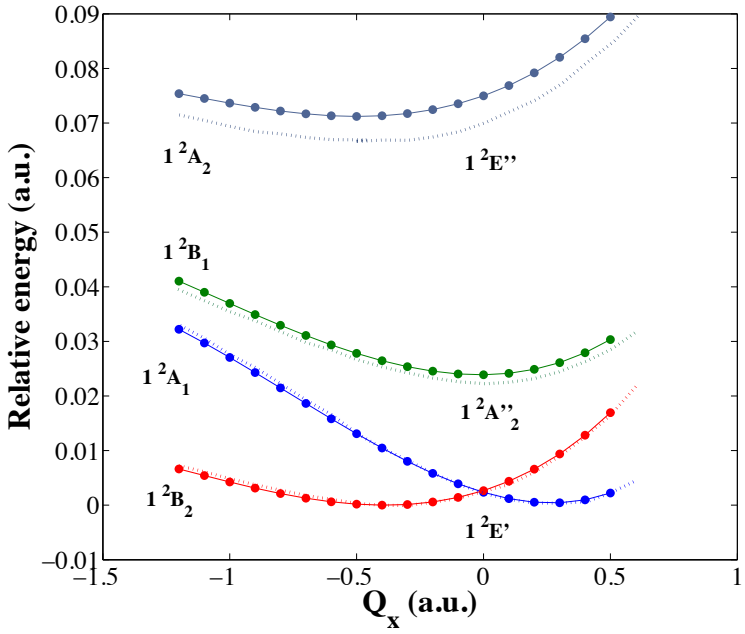

Figure 6.6 Potential energy curves of the ground state and low-lying excited states of the Li_3 molecule in the C_{2v} structure for the fixed normal mode coordinate $Q_s = 3.2a_0$ and $Q_y = 0.0a_0$. Solid lines with symbols show our calculated results and doted lines show the potential energy curves reported by Ehara *et al* [48].

D_{3h}	$C_{2V}(\sigma_h \rightarrow \sigma_v(xy))$	$C_s(\sigma_h)$	$C_s(\sigma_v)$
A_1'	A_1	A'	A'
A_2'	B_1	A'	A''
E'	$A_1 + B_2$	$2A'$	$A' + A''$
A_1''	A_2	A''	A''
A_2''	B_1	A''	A'
E''	$A_2 + B_1$	$2A''$	$A' + A''$

Table 6.6 The D_{3h} correlation table

For nonzero values of Q_x the degeneracy is symmetrically lifted by lowering the symmetry to C_{2v} while a clear conical intersection point exists for all values of the symmetric stretching normal mode coordinates Q_s, i.e. each degenerate state separates into an upper and a lower states at nonzero Q_x, fixed Q_s and zero Q_y. The conical intersection point exists for all values of Q_s and discontinuity appears at these point of intersection. The degenerate pair of the $1^2E'$ state consists of the 1^2B_2 and 1^2A_1 states [See table 6.6]. There is a global minimum on the electronic state 1^2B_2 at the obtuse geometry $Q_s = 3.2\ a_0$ and $Q_x = -0.4\ a_0$ and a local minimum on the state 1^2A_1 at the acute geometry $Q_s = 3.2\ a_0$ and $Q_x = 0.3\ a_0$. The double minima of the electronic state is quite shallow. The geometry values (bond length and bond angle) and adiabatic energies under the C_{2v} and the D_{3h} symmetries are summarized in the table 6.7. These parameters are also in good agreement with the results reported in ref [81]. Figure 6.7 shows potentials of the two lowest electronic states of Li_3 with the equal side of the isosceles triangle length ranging from 4.85-6.02 a_0 and as a function of the bond angle. It is obvious that the conical intersection occurs at equilateral triangle geometry.

Electronic configurations for the D_{3h} structure of Li_3 are displayed in figure 6.8 for high spin and low spin states. In the D_{3h} structure, the degenerate molecular orbitals can be observed. The occupation on each one of the degenerate molecular orbitals e' is identical with that on the other in the high spin case so the Jahn-Teller distortion can not occur in the $^4A_2$ state with D_{3h} symmetry to remove degeneracy in the high spin case. Furthermore, as we see from the potential energy curves in figure 6.6, the Li_3 molecule is stable in the C_{2v} symmetry but not in the D_{3h} symmetry for the low spin states where the degeneracy is lifted. It can be concluded that the molecular orbital degeneracy has been removed by

D_{3h}	C_{2v}	bond length [Å]	bond angle $[deg]$	Q_s a_0	Q_x a_0.	Relative Energy cm^{-1}	ref
$1^2E'$		2.93	60	3.2	0.0	0.0	present work
	1^2B_2	2.77	73	3.2	-0.4	515.76	
	1^2A_1	3.08	51	3.2	0.3	419.20	
$1^2E'$		2.89	60	3.2	0.0	0.0	[48]
	1^2B_2	2.79	71.8	3.2	-0.362	506	
	1^2A_1	3.08	52	3.2	0.269	432	
$1^2E'$		2.87	60	-	-	0.0	[82]
	1^2B_2	2.76	71.6	-	-	501.8	
	1^2A_1	3.02	52.2	-	-	429.7	

Table 6.7 Parameters of the two lowest states of the Li_3 calculated by *ab initio* method.

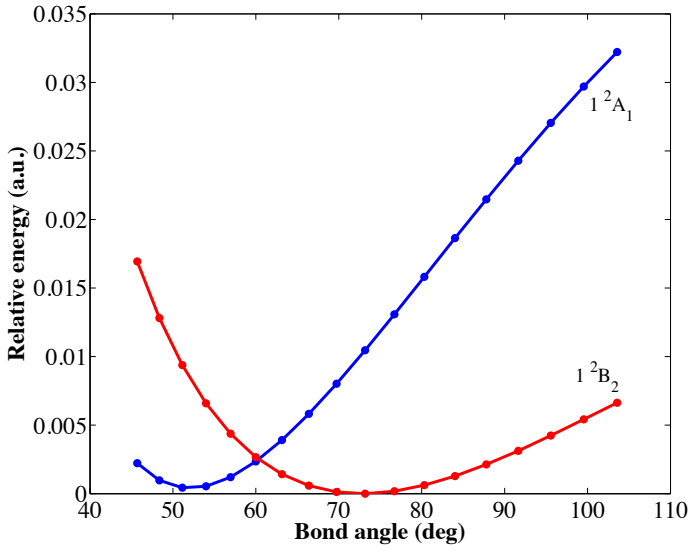

Figure 6.7 Two lowest potential energy curves printed as a function of bond angle.

occupation of the doublet state and the Jahn-Teller distortion is effective in the low spin electronic state [80].

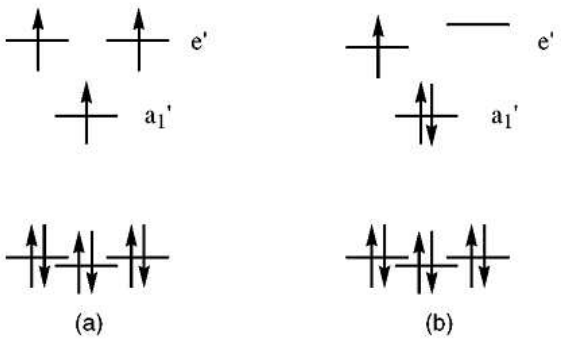

Figure 6.8 Electronic configurations for the D_{3h} geometry of the Li_3 molecule in (a) the high spin (b) the low-spin states.

In a two dimensional scan, the two lowest adiabatic potential energy surfaces were calculated which correlated with 1^2A_1 and 1^2B_2 states in the C_{2v} structure and the degenerate state in the D_{3h} structure. We keep the asymmetric stretching normal mode coordinate Q_y value fixed at zero, restricting the geometry to the C_{2v} symmetry, and scan the energy as a function of the symmetric stretching Q_s and the bending Q_x normal mode coordinates. The calculations were performed for different isosceles triangle geometries over a grid of 180 points with the stretching coordinates Q_s ranging from 2.8 to 4.6 a_0 and the bending coordinate Q_x from -1.2 to 0.6 a_0. The discrete *ab initio* results are interpolated with cubic splines to provide a smooth surface. The contour plot of the ground electronic surface is shown in figure 6.9. Two minima can be found on the surface, separated by a sharp cusp at the conical intersection between the two electronic states.

When Q_y is nonzero, the molecule has a C_s symmetry. Figure 6.10 displays the three-dimension plots of the lower and upper surfaces at fixed $Q_s = 3.2\ a_0$ as a function of Q_x and Q_y. The calculations were performed for different C_s geometries using the polar coordinate r and ϕ over 73 points for ϕ ranging from 0 to 360° and 23 points in r ranging from 0 to 2 a_0. The discrete *ab initio* results are interpolated with cubic splines to provide smooth surfaces on a product grids in the bending Q_x and the asymmetric stretching Q_y normal mode coordinates ranging from -1.5 to 1.5 a_0. The calculated lower surface represents all the characteristics which have been discussed before. The shallow three-fold wells at the

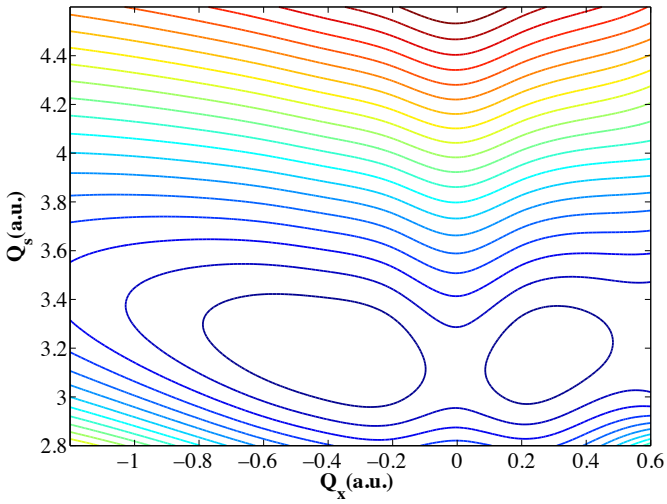

Figure 6.9 Contour plot of the lowest potential energy surface of Li_3 at the fixed asymmetric normal mode coordinates, $Q_y = 0.0a_0$.

C_{2v} obtuse configuration, barriers to pseudorotation at the C_{2v} configurations and conical intersection of the D_{3h} symmetry are shown in figure 6.11.

We did all these calculations for three-dimensional potential energy surfaces for the different fixed symmetric stretching normal mode coordinates Q_s ranging from 2.7 to 4.2 a_0. Therefore, by using these *ab initio* calculations, all the adiabatic potential energy surfaces can be found.

6.2.2 Fitting and diabatization of the potential energy surfaces

The next step is to perform the diabatiztion of the computed adiabatic potential energy surfaces. For this purpose we need an unitary transformation matrix. This matrix can be obtained by diagonalizing of the diabatic Jahn-Teller Hamiltonian and finding its eigenvectors as we have discussed in the previous chapters. By obtaining the parameters of the Jahn-Teller Hamiltonian, we can calculate the transformation angles needed to construct this transformation matrix. We can determine the Jahn-Teller parameters by optimizing the eigenvalues of the diabatic Jahn-Teller Hamiltonian to the computed adiabatic potential energy surfaces. This optimization was performed in the vicinity of the conical intersection where the Jahn-Teller Hamiltonian is valid. This process was done for each value of the

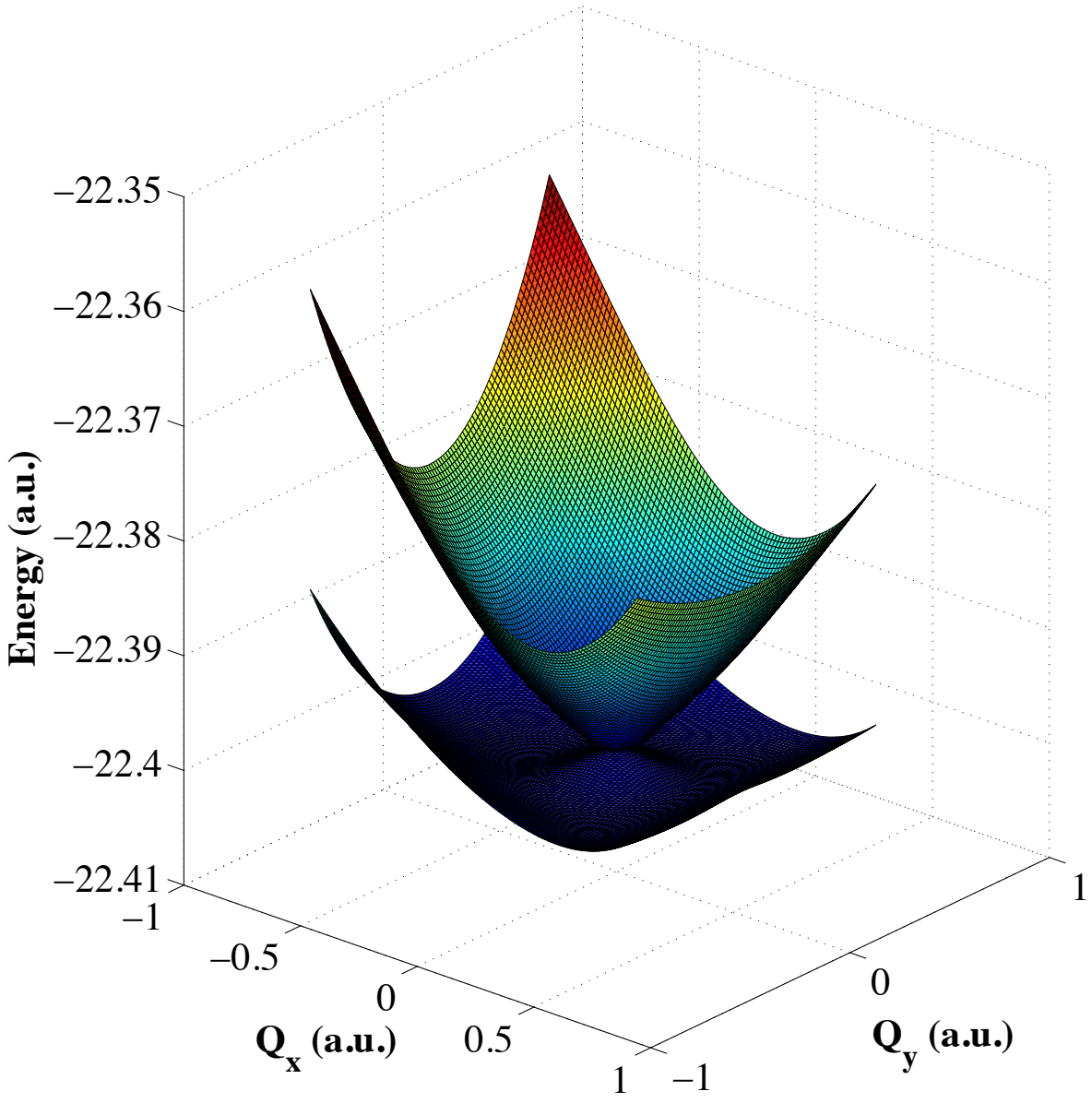

Figure 6.10 Three dimensional plot of the lowest two potential energy surfaces at the fixed symmetry normal mode coordinates, $Q_s = 3.2a_0$.

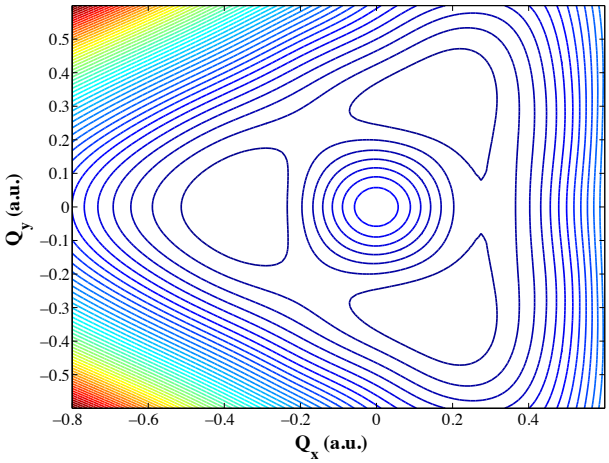

(a)

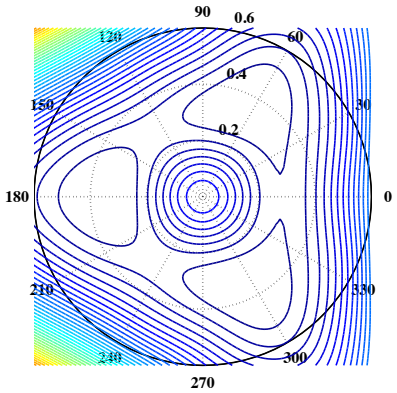

(b)

Figure 6.11 Contour plot of the lowest adiabatic potential energy surface of the Li_3 at the fixed $Q_s = 3.2\ a_0$ using (a) normal mode coordinates and (b) polar coordinates.

symmetric stretch normal mode coordinate and the Jahn-Teller parameters are then given as functions of the coordinate Q_s.

The results from the fitting procedure for the lower components of the E' state of Li_3 are shown graphically in figures 6.12, 6.13, and 6.14 where in all figures the symmetric stretch coordinate is fixed at $Q_s = 3.2\ a_0$. In these figures, the computed lower adiabatic potential energy surface is shown with the symbols connected with a solid line. The different types of lines show the results from the fitting from the different Jahn-Teller models. We considered different terms of the Jahn-Teller Hamiltonian up to third order and call them the linear, quadratic and cubic Jahn-Teller Hamiltonian by $JT1 + harm$, $JT2 + harm$ and $JT3 + harm$. When the anharmonicity term is added to the linear, quadratic and cubic Jahn-Teller Hamiltonian, we used the notations of $JT1 + anharm$, $JT2 + anharm$ and $JT3 + anharm$ respectively. The figures 6.12 and 6.13 show the potential as a function of the polar coordinate r for fixed values of ϕ (0°,60°) and figure 6.14 shows the potential as a function of the polar coordinate ϕ at the distance from the conical intersection to the minimum of the potential energy surface.

In the fitting procedure, numerical data were fitted to the analytical potential energy surfaces of both the lower and upper states by using a least square method. We summarize all the analytical expressions for the adiabatic potentials in the table 6.8.

From the figures 6.12 and 6.13 we can examine the quality of different models. It is clear that the Jahn-Teller Hamiltonian model $JT2 + harm$ gives a poor representation of the adiabatic potential surfaces. In contrast, the Jahn-Teller Hamiltonian model $JT3 + anharm$ is in well agreement with the computed data. Figure 6.14 presents the cut along the ϕ when r is equal to distance from the conical intersection to the minimum of the lower state. From this figure it becomes apparent that the third order terms (either diagonal or non-diagonal) are needed to obtain the correct ϕ-dependence of the potential. For larger range of r we need even higher order terms added to the Jahn-Teller Hamiltonian. Our fitting was performed up to $r = 1\ a_0$. All the fitting results are collected and summarized in the table 6.9. Finally, the parameters used come from fitting the data with the $JT3 + anharm$ model.

From the Jahn-Teller parameters we can set up the diabatic Jahn-Teller potentials. It is then possible to construct the unitary transformation matrix that transforms from the adiabatic to the diabatic representations by using the eigen-vectors of the Jahn-Teller potential. The transformation matrix is used to transform the coupled computed adiabatic potential

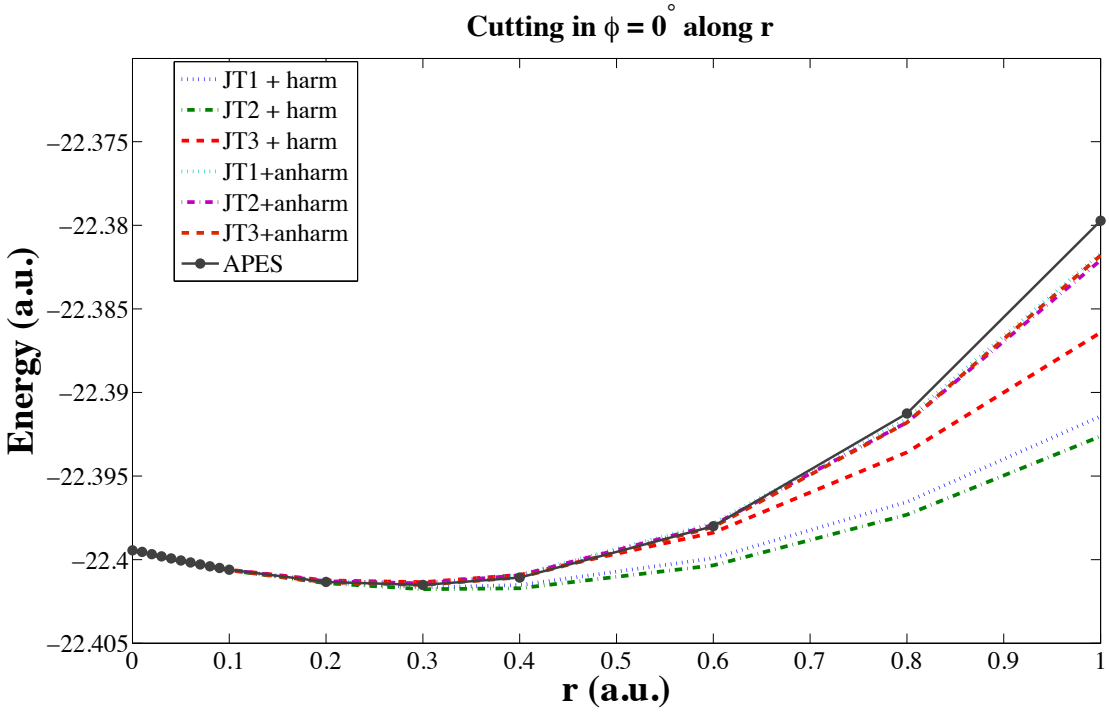

Figure 6.12 The lower adiabatic potential energy surface along the r polar coordinate for fixed $\phi = 0°$ and $Q_s = 3.2\ a_0$.

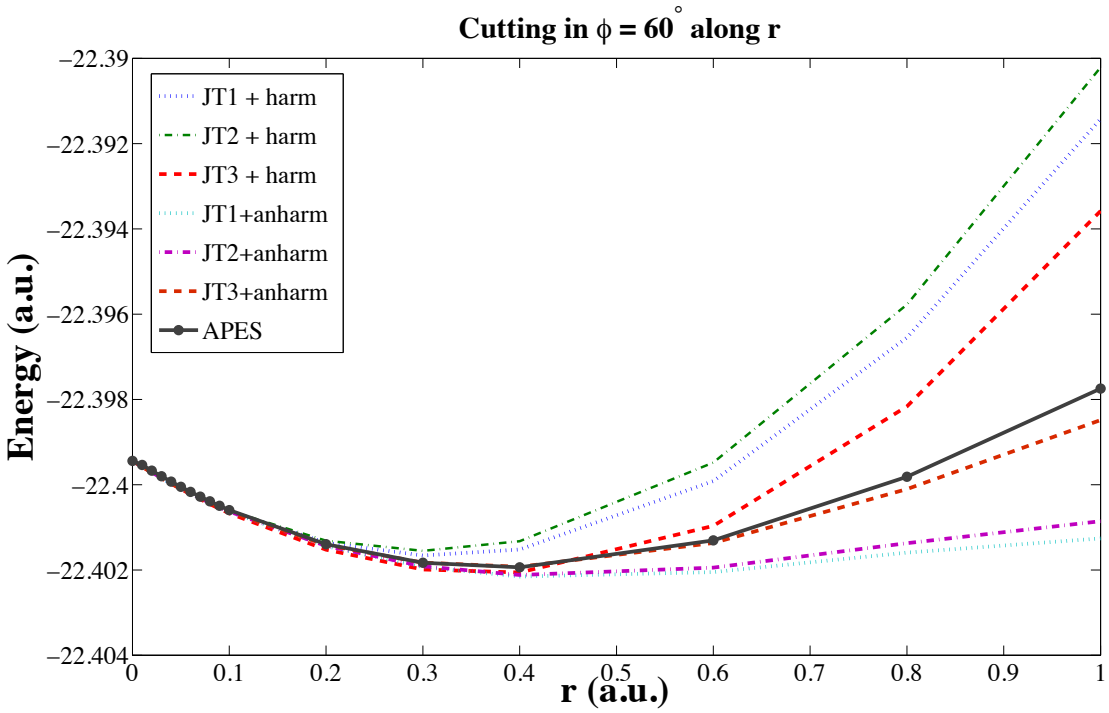

Figure 6.13 The lower adiabatic potential energy surfaces along the r polar coordinate for fixed $\phi = 60°$ and $Q_s = 3.2\ a_0$.

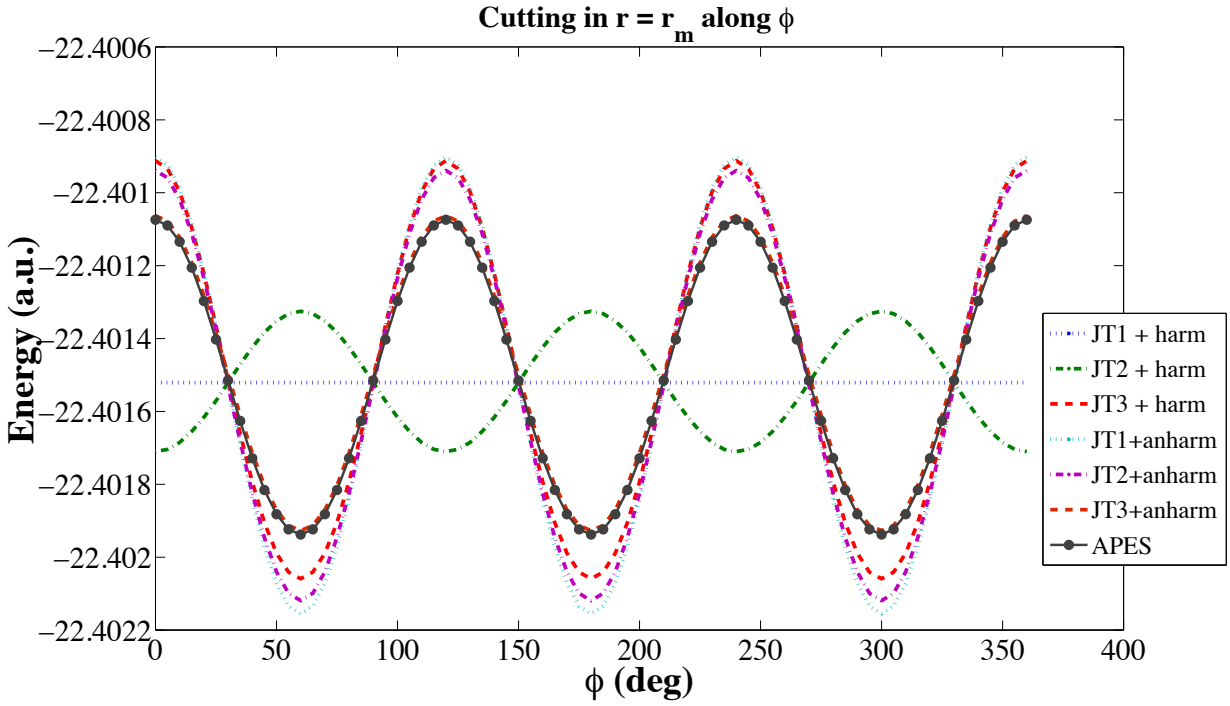

Figure 6.14 The lower adiabatic potential energy surfaces along the ϕ polar coordinate for fixed $r = r_m$, where r_m is the distance from the conical intersection to the minimum of the potential energy surface.

Fitting model	Eigenvalues of the Jahn-Teller Hamiltonian
$JT1 + harm$	$V_{2a}r^2 \pm V_{1e}r$
$JT2 + harm$	$V_{2a}r^2 \pm r[V_{1e}^2 + 2V_{1e}V_{2e}r\cos 3\phi + V_{2e}^2r^2]^{\frac{1}{2}}$
$JT3 + harm$	$V_{2a}r^2 \pm r\left[V_{1e}^2 + 2V_{1e}V_{2e}r\cos 3\phi + V_{2e}^2r^2 + 2V_{1e}V_{3e}r^2 + 2V_{2e}V_{3e}\cos 3\phi r^3 + V_{3e}^2r^4\right]^{\frac{1}{2}}$
$JT1 + anharm$	$V_{2a}r^2 + V_{3a}\cos 3\phi r^3 \pm V_{1e}r$
$JT2 + anharm$	$V_{2a}r^2 + V_{3a}\cos 3\phi r^3 \pm r\left[V_{1e}^2 + 2V_{1e}V_{2e}r\cos 3\phi + V_{2e}^2r^2\right]^{\frac{1}{2}}$
$JT3 + anharm$	$V_{2a}r^2 + V_{3a}\cos 3\phi r^3 \pm r\left[V_{1e}^2 + 2V_{1e}V_{2e}r\cos 3\phi + V_{2e}^2r^2 + 2V_{1e}V_{3e}r^2 + 2V_{2e}V_{3e}\cos 3\phi r^3 + V_{3e}^2r^4\right]^{\frac{1}{2}}$

Table 6.8 Models for fitting

expansion	V_{0a} $[a.u.]$	V_{2a} $[a.u.]$	V_{3a} $[a.u.]$	V_{1e} $[a.u.]$	V_{2e} $[a.u.]$	V_{3e} $[a.u.]$
harm.+JT_1	-22.3994415	0.022	-	0.0140	-	-
harm.+JT_2	-22.3994415	0.022	-	0.0140	0.0012	-
harm.+JT_3	-22.3994415	0.022	-	0.0140	0.0036	-0.0016
anharm.+JT_1	-22.3994415	0.022	0.0098	0.0140	-	-
anharm.+JT_2	-22.3994415	0.022	0.0095	0.0140	0.001	-
anharm.+JT_3	-22.3994415	0.0229	0.0098	0.0142	-0.0013	-0.0014

Table 6.9 Parameters obtained from fitting the adiabatic potential energy surfaces to the different Jahn-Teller models at $Q_s = 3.2\ a_0$.

energy surfaces to a diabatic representation, i.e.

$$U^{dJT} = S \begin{pmatrix} U_u^{ad} & 0 \\ 0 & U_l^{ad} \end{pmatrix} S^{\dagger}.$$

The advantage of this approach is that the diabatic Hamiltonian U^{dJT} describes the states of the system over a much larger region than the Jahn-Teller Hamiltonian.

All the Jahn-Teller parameters were extracted for each value of the symmetric stretch normal mode coordinate Q_s. Figures 6.15, 6.16 and 6.17 show the obtained linear, quadratic and cubic parameters respectively as a function of Q_s. The two other Jahn-Teller parameters, V_{2a} and V_{3a}, are also reported and displayed in figure 6.18 as a function Q_s.

Figure 6.19 shows the energy of the point of degeneracy for different values of Q_s. The harmonic shape of the potential can be clearly observed. We use the harmonic oscillator approximation to find the frequency of the totally symmetric a_1-mode. the parameters of the Jahn-Teller Hamiltonian as well as the frequency ω_a of the totally symmetric a_1-mode and comparison with other theoretical results. The previous reported theoretical results of ω_a are 349 cm^{-1} in the ref [83, 84] and 327 cm^{-1} in the [81, 84].

The Jahn-Teller stabilization energy and the barrier height between the minima are obtained in this present study as

$$E_{JT} = 515.76\ cm^{-1},\ E_{loc} = 96.57\ cm^{-1},$$

and the relevant geometry of the system is shown in Figure 6.20.

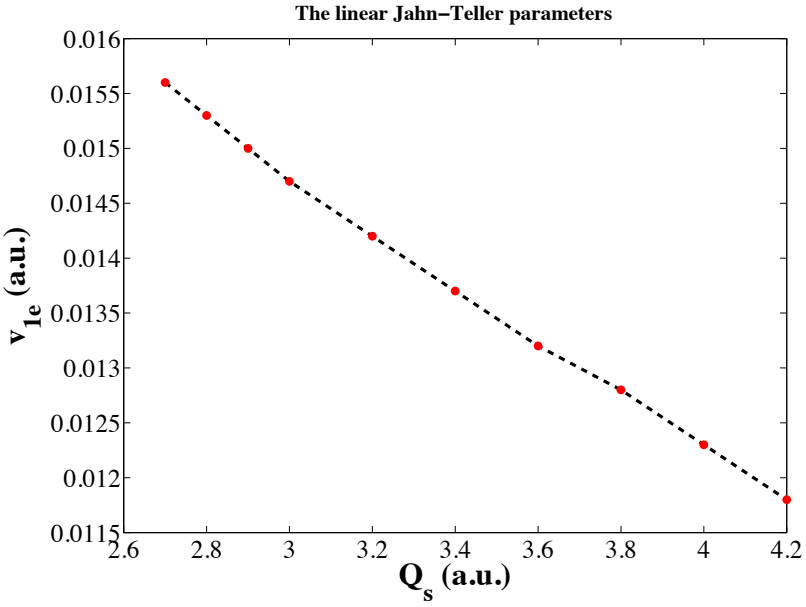

Figure 6.15 The coupling constant $V_{1e}(a_0)$ as a function of Q_s.

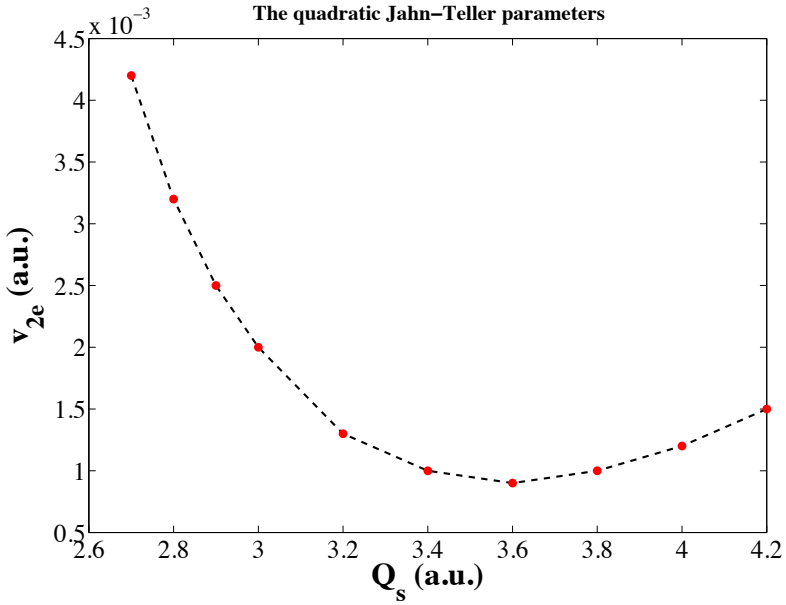

Figure 6.16 The quadratic coupling constants $V_{2e}(a_0)$ as a function of Q_s.

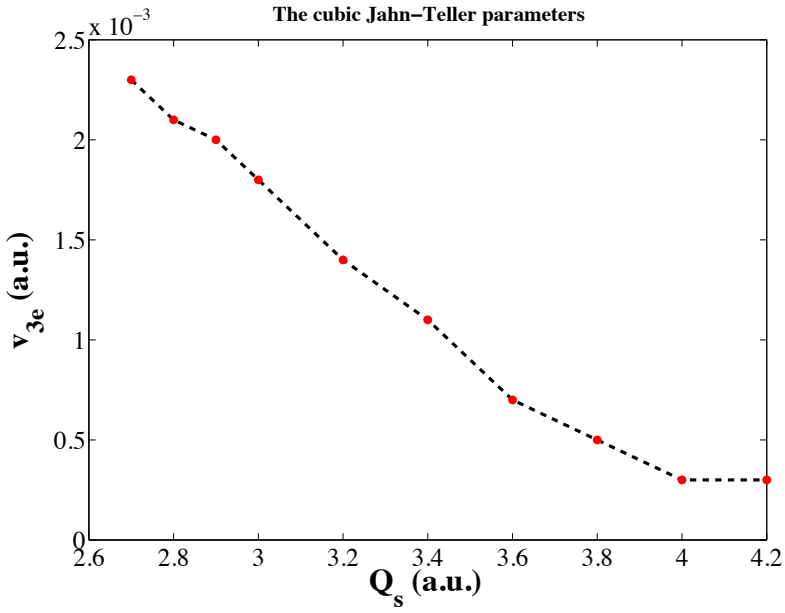

Figure 6.17 The cubic coupling constants $V_{3e}(a_0)$ as a function of Q_s.

system	k	g	ω_e $[cm^{-1}]$	ω_a $[cm^{-1}]$	ref
Li_3	2.007	0.227	245.06	368.21	present work
	1.96±0.33	0.22±0.07	278±61		[51, 85]
	2.25±0.24	0.14±0.06	250±41		[51, 81]

Table 6.10 Scaled parameters of the Jahn-Teller Hamiltonian.

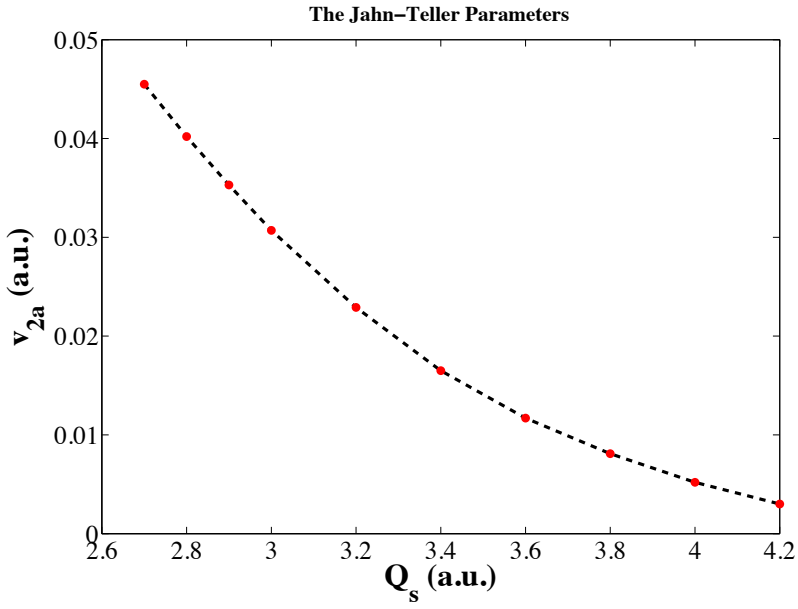

(a)

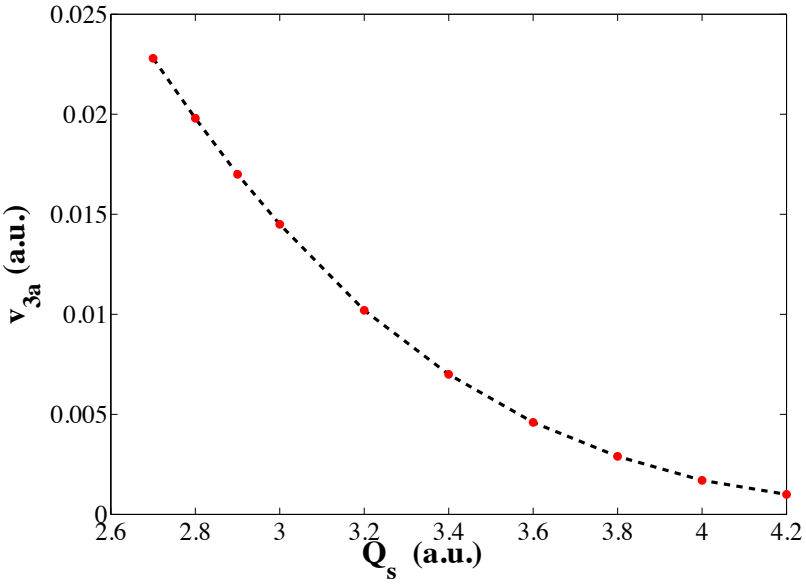

(b)

Figure 6.18 (a)The harmonic force constant $V_{2e}(a_0)$ and (b) anharmonicity constant $V_{3a}(a_0)$ as a function of Q_s.

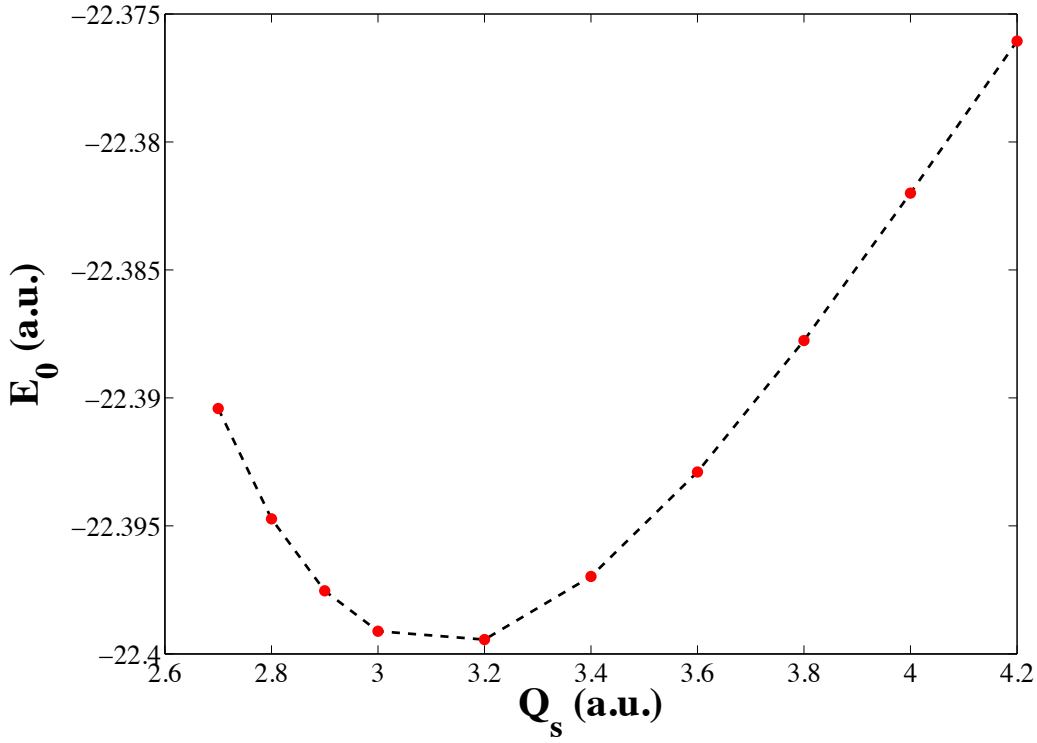

Figure 6.19 Energy of the degenerate point as a function of Q_s.

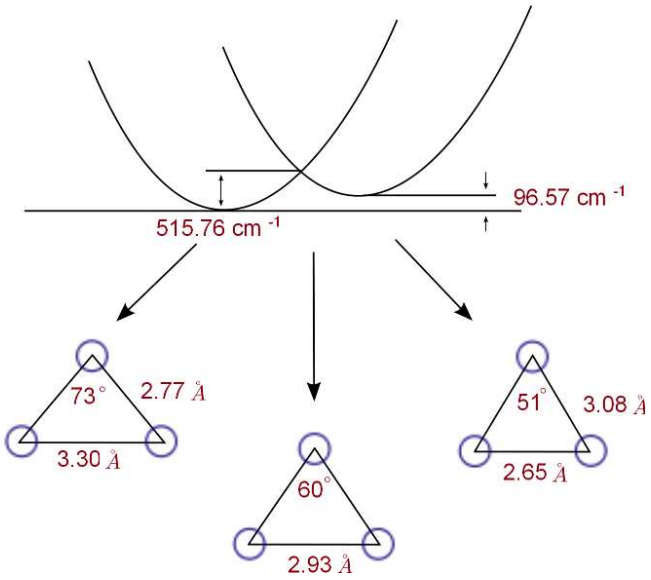

Figure 6.20 The Jahn-Teller stabilization energy, the height of barrier and geometric characteristics of Li_3 in D_{3h} configuration.

Wöste et al [86] reported the first observation of an excited state of the Li_3 molecule. Analysis based on the dynamical Jahn-Teller model reversed very weak distortion and localization characteristic. In this work the best fit for the $2^2E'$ state was obtained $\omega_e = 191cm^{-1}$ and for the linear and the quadratic Jahn-Teller parameters $k = 0.77$ and $g = 0.15$, respectively. The totally symmetric mode of this state is also observed at 326 cm^{-1} [See fig 6.21]. The later measurement on the gas phase Li_3 trimer were performed in the group of

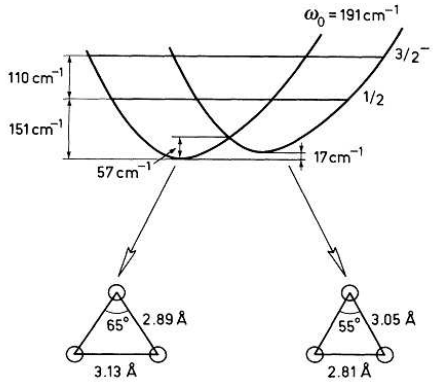

Figure 6.21 Vibronic and geometric characteristics of the $2^2E'$ excited state [86].

Wöste and Broyer in 1990 [87]. The results reported for the parameters of the Jahn-Teller Hamiltonian and the totally symmetric a_1-mode frequency are

$$k = 1.84,\ g = 0.050,\ \omega_e = 150cm^{-1}\ \ \omega_a = 301cm^{-1}$$

They also found the potential energy surface of Li_3 from their observation where the bond angle and bond length were obtained as 72°and 2.73 Å for obtuse geometry, and 50 ° and 3.05 Å for the acute geometry.

6.2.3 Wave-packet propagation

Quantum dynamic simulations of the system are performed using wave packet propagation. To examine the time evolution of the system we need to solve the time-dependent Schrödinger equation. The wave packet dynamics is an initial value problem, i.e., the wave packet is given at $t = 0$ and then propagated forward in time by integrating the corresponding Schrödinger equations. One powerful wave packet dynamics solver is the Multi-Configuration Time-Dependent Hartree (MCTDH) method. This method was for the first time introduced in 1990 by Meyer *et al* [9] and it is very powerful for propagating multidimensional wave packets. Its basic theory has been discussed in detail in two review articles [88, 89] and in the book of ref [90]. The MCTDH method can in particular be used to propagate wave packets on coupled states. We here use it to propagate wave packets on the two coupled states of Li_3 in a diabatic representation. Our system Hamiltonian including all three normal modes will be

$$H^d = \frac{1}{2M}[\frac{\partial^2}{\partial Q_x^2} + \frac{\partial^2}{\partial Q_y^2} + \frac{\partial^2}{\partial Q_s^2}] + \begin{pmatrix} U_{11}^{JTd} & U_{12}^{JTd} \\ U_{12}^{JTd} & U_{22}^{JTd} \end{pmatrix}, \tag{6.1}$$

where the diagonal and off-diagonal elements of the Hamiltonian depends on all three coordinates. We can use the Hamiltonian (6.1) in the time-dependent Schödinger equation and obtain

$$i\frac{\partial}{\partial t}\bar{\Psi} = H^d\bar{\Psi}. \tag{6.2}$$

The standard approach to propagate a multi-dimensional wave packet is to expand the wave packet in a time-independent product basis set. Different basis functions can be used for the different dimensions. By inserting the ansatz into the time-dependent Schrödinger equation, coupled equations for the expansion coefficients are obtained that are solved numerically.

The basic idea in the MCTDH method is to expand the wave packet in time-dependent basis functions. In our case, we obtain:

$$\Psi(t, Q_s, Q_x, Q_y) = \sum_{i=1}^{n_s} \sum_{j=1}^{n_x} \sum_{k=1}^{n_y} A_{ijk}(t) \Phi_i^{(s)}(t, Q_s) \Phi_j^{(x)}(t, Q_x) \Phi_k^{(y)}(t, Q_y),$$

where $A_{ijk}(t)$ are the expansion coefficients. In the present study we included $n_s = n_x = n_y = 10$ single particle functions for the three modes. By inserting this wave packet into the Schrödinger equation, the MCTDH equations of motions for the coefficients and the single-particle functions are obtained. The single particle functions are expanded using a primitive basis functions. Here, 300 sine-functions are used for the three modes.

As an initial condition for the wave packet, we start with a Gaussian wave packet. This wave packet can be written as

$$\Psi(t = 0, Q_x, Q_y, Q_z) = \Phi_s(Q_s) \Phi_x(Q_x) \Phi_y(Q_y),$$

where the one-dimensional gaussian functions are

$$\Phi_R(R) = (2\pi\Delta_R)^{\frac{-1}{4}} \exp\{\frac{-(R - R_0)^2}{4\Delta_R^2}\} e^{iP_0(R-R_0)}.$$

The initial wave packet is normalized and R_0 and P_0 are the center of the gaussian function as well as the initial momentum. The width of the gaussian function is chosen such that the gaussian wave packet is the lowest eigenstate of the harmonic oscillators with frequencies ω_a or ω_e. This is done in order to minimize the spreading of the wave packet.

Wave packet demonstration of inherent asymmetry

We have seen that in the lower adiabatic potential energy surface there are three minima separated by saddle points. There are three mirror reflection planes around the conical intersection [see fig. 5.3]. We here put the initial wave packet on the lower potential energy surface at $Q_x = -0.7a_0$, $Q_y = 0\ a_0$ for the symmetric stretch coordinate at $Q_s = 3.2\ a_0$. The wave packet is thus placed on one of the mirror planes. It has no initial momentum. We let the wave packet propagate. In the lower surface we can observe splitting an asymmetry of the wave packet for motion in the Q_y direction. Monitoring the wave packet propagation shows that the the inherent symmetry is broken. Snapshots of the wave packet on the lower adiabatic state for different propagation times are shown in figure 6.22. By following the evolution of the wave packet we can see that the symmetrical Gaussian shape wave packet

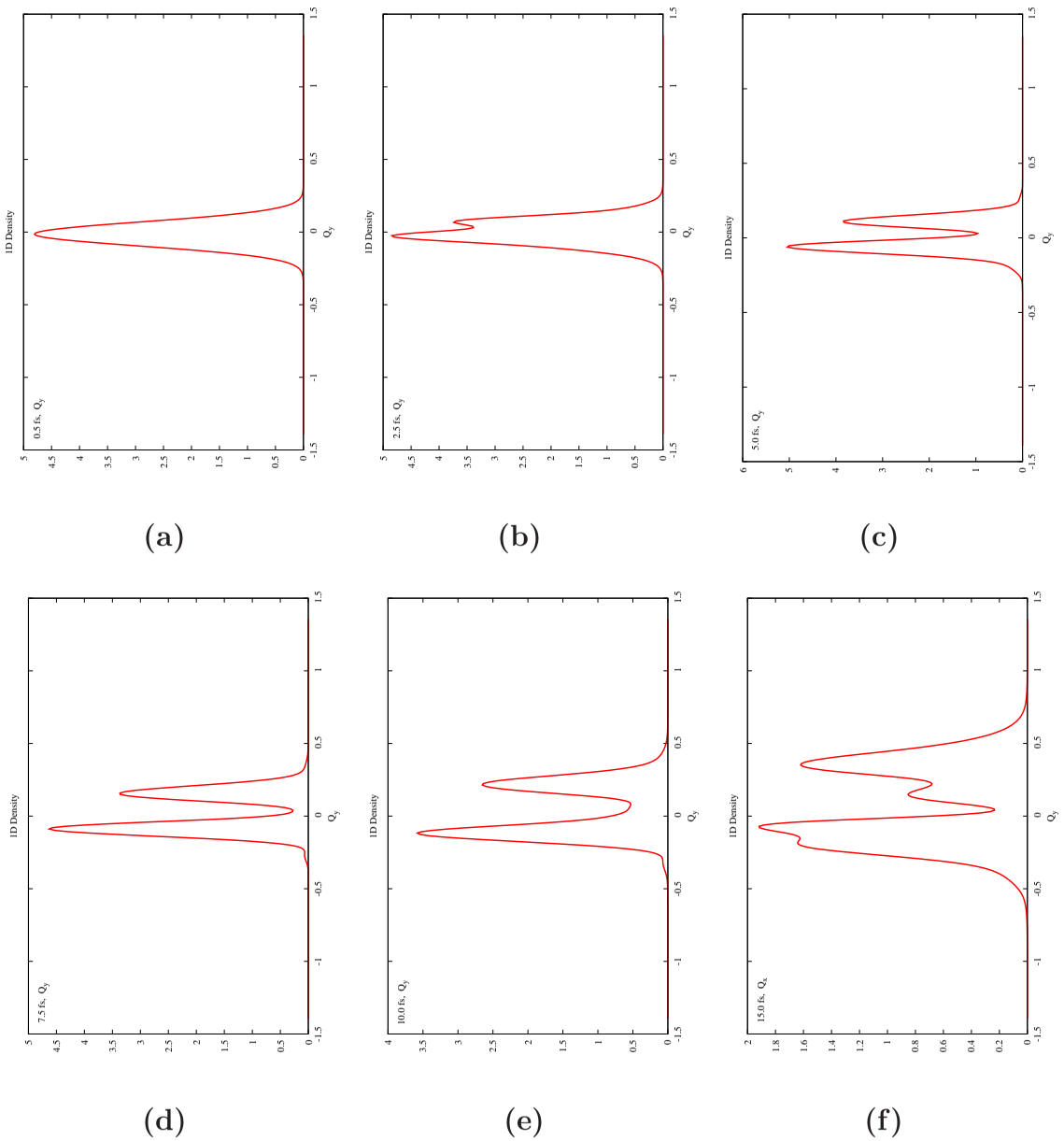

Figure 6.22 Wave packet at different propagation times. The wave packet demonstrates the inherent asymmetry.

starts dividing into two asymmetric branches that go around the conical intersection. Most part of the wave packet tends to move to the left hand side.

It should be noted that a considerable amount of the flux is transferred from one state to the other. Furthermore, the wave packet is spreading to a large amount. This can be explained by the strong anharmonic terms in the Hamiltonian.

Wave packet study of the chirality

If we just consider the linear $E \otimes e$ Jahn-Teller system, it is similar to systems with Rashba spin-orbital coupling appearing in condensed matter systems and these systems in return are known to be chiral [91]. This implies that the time-reversal symmetry is broken in the presence of the spin-orbital coupling. One way to investigate the chirality is to propagate the wave packet around the conical intersection. A chiral system will not give the same result whether the wave packet is propagated to the right or the left around the conical intersection. This is the idea of our investigation. We start the wave packet close the one of the minima and we give it a kick (momentum). The system is then chiral if we do not get the same result when the wave packet propagates to the left and the right. We will then observe time-reversal symmetry breaking. For taking a closer look at this phenomena we consider the expectation values of Q_x, P_x and Q_y, P_y. The expectation values of these operators will describe how the center of the wave packet moves in phase space. Time-dependent expectation values, i.e., $\langle\Psi(t)|\hat{O}|\Psi(t)\rangle$, can be calculated using the MCTDH program. Figure 6.23 and 6.24 display time evolution of the expectation values of the position and momentum operators in the cases where the wave packet propagates to the left or to the right of the conical intersection. We can see the spiral shape of the dynamics in phase spaces. This spiral shape derives from the anharmonically indeed spreading of the wavepacket. After sufficient long times, the wavepacket has spread out more or less symmetrically around the conical intersection.

The strong non-adiabatic coupling between the adiabatic states leads to a femtosecond population decay of the upper electronic state to the lower one. We use the MCTDH analysis to obtain the diabatic population. We consider both cases when the initial value of the momentum is positive and then negative. By subtracting the population of the two states, figure 6.25, we observe a difference when the wave packet is propagated to the left and to the right. In this figure the red line belongs to the population difference for the wave packet propagating to the right with a positive initial momentum and the blue line is for the population difference for the wave packet propagating to the left with a negative initial

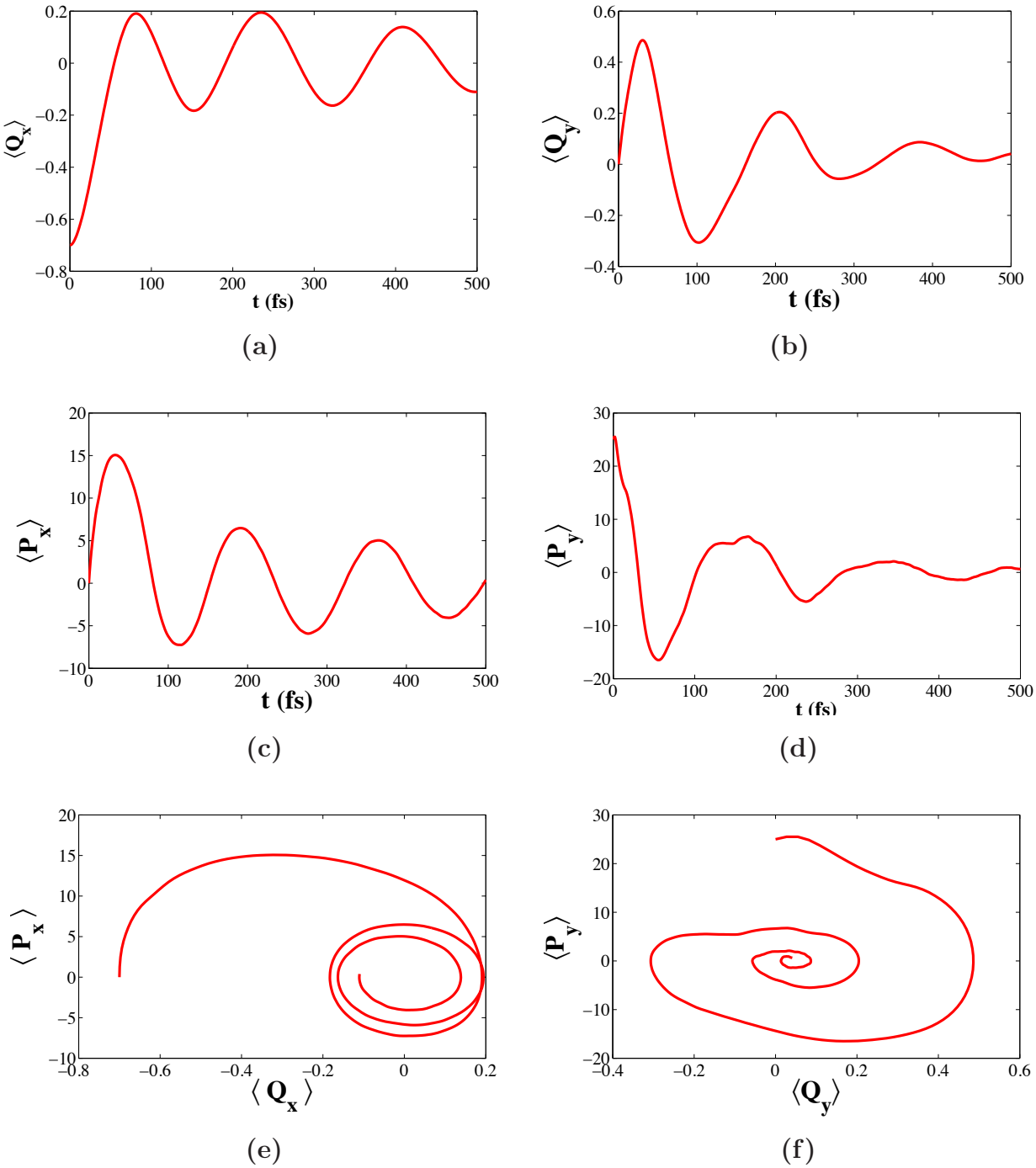

Figure 6.23 Wave packet propagation where the initial wave packet has a positive momentum in Q_y direction. (a) and (b) show the expectation values of Q_x and Q_y as a function of propagation time, (c) and (d) display the evolution of the expectation values of momentum P_x and P_y, and (e) and (f) show the trajectory in the phase spaces of the two e normal mode coordinates.

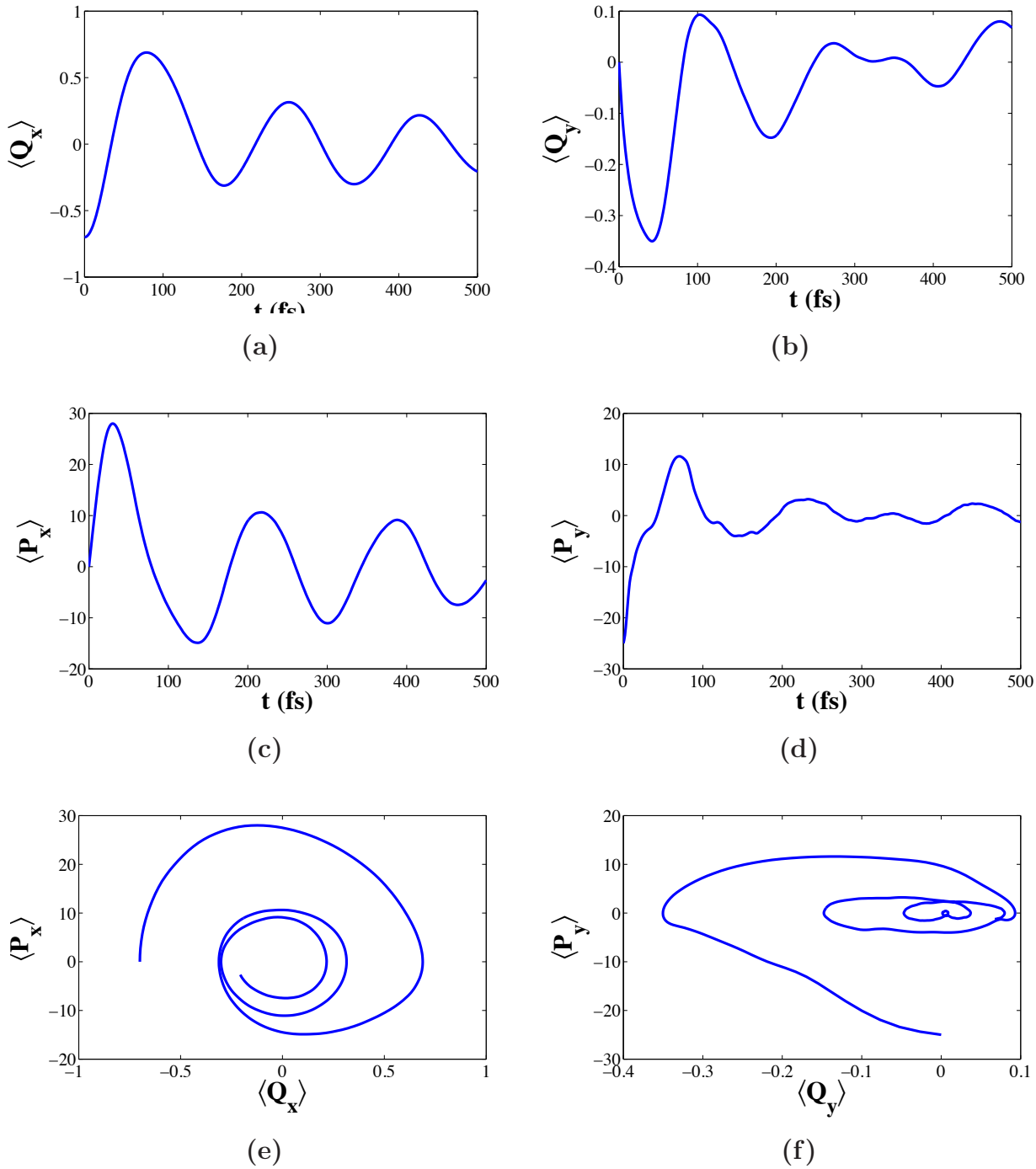

Figure 6.24 Wave packet propagation where the initial wave packet has a negative momentum in the Q_y direction. (a) and (b) show the expectation values of Q_x and Q_y as a function of propagation time, (c) and (d) display the evolution of the expectation values of momentum P_x and P_y, and (e) and (f) show the trajectory in the phase spaces of the two e normal mode coordinates.

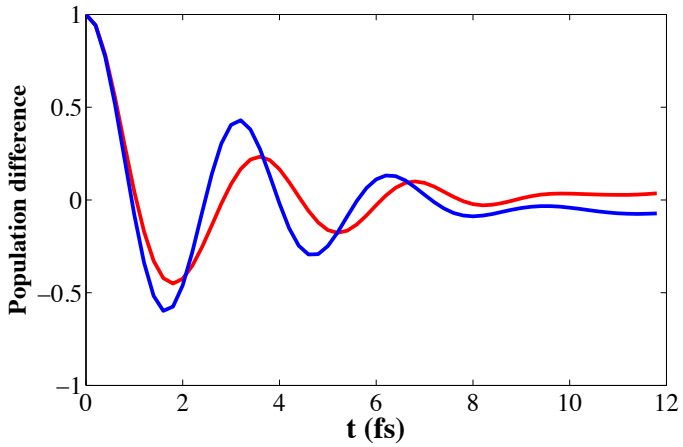

Figure 6.25 Difference of the population of the two diabatic states. The blue curve shows the population difference for a wave packet with the negative initial momentum and the red curve is the same for a wave packet with positive initial momentum.

momentum. The difference between the two curves seen in the figure 6.25 is an effect of chirality, thus clockwise and anti-clockwise propagation give different results.

6.3 Conclusion

In this thesis we considered the $E \otimes e$ Jahn-Teller conical intersection in the Li_3 molecule. We have investigated the molecular dynamics in the vicinity of the conical intersection.

- We used the *ab initio* MCSCF/MRCI method to calculate the adiabatic potential energy surfaces of Li_3. The accuracy of our method was checked by applying the same method to calculate potential curves of the ground electronic and several low-lying excited states of the Li_2 molecule. We also compared our obtained results with the previous theoretically as well as experimentally reported results. Then potential energy surfaces of ground electronic and first excited states of the Li_3 molecule were calculated. Three minima separated by three saddle points and a conical intersection were found in the lower adiabatic potential energy surface.

- The Jahn-Teller effect, particularly the $E \otimes e$ Jahn-Teller effect was discussed and models of the Hamiltonian for this type of system were introduced.

- To obtain a simpler description of the Jahn-Teller effect, the normal mode coordinates were computed by exploiting the symmetry properties of the molecular system using group theory. We found that the conical intersection of Li_3 is in the D_{3h} symmetry and adiabatic states of the system are symmetric under reflections in three symmetry planes separated by the angles 60°.

- To transform the computed adiabatic potential energy surface to a diabatic picture, eigenvalues and eigen-vectors of the Jahn-Teller Hamiltonian were obtained. All adiabatic potential energy surfaces were fitted to the eigen-values of the Jahn-Teller Hamiltonian and the Jahn-Teller parameters were optimized. By means of these parameters we could construct the unitary transformation matrix and set up diabatic potential energy surfaces from the computed data. Using this approach allowed us to create the diabatic potential energy surfaces much further away from the conical intersection where the Jahn-Teller Hamiltonian is no longer valid.

- Dynamics of the system was explored utilizing the wave packet propagation. The Multi-Configuration Time-Dependent Hartree method was used for propagating the three-dimensional wave packets on the coupled states. The inherent asymmetry of the wave packet was illustrated and the chirality of the present $E \otimes e$ Jahn-Teller system was investigated.

Bibliography

[1] M. Born, J. R. Oppenhiemer, *Ann. Physik.*, **84**, 457 (1927).

[2] M. Baer, *Chem. Phys. Lett*, **35**, 112 (1975).

[3] H. A. Jahn and E. Teller , *Proc. Royal Soc. London*, **161**, 220 (1937).

[4] M. V. Berry, *Proc. R. Soc. A London Ser.*, **392**, 45 (1984).

[5] A. Mead, *R. Mol. Phys.*, **64**, 51 (1992).

[6] T. Pacher, C. A. Mead, L. S. Cederbaum and H. Köppel , *J. Chem. Phys.*, **91**, 7057 (1989).

[7] T. C. Thompson, D. G. Truhlar, and C. A. Maed, *J. Chem. Phys.*, **82**, 2392-2407 (1985).

[8] T. C. Thompson, G. Izmirlian, S. J. Lemon, D. G. Truhlar, and C. A. Maed, *J. Chem. Phys.*, **82**, 5597-5603 (1985).

[9] G.A Worth, M.H. Beck, A. Jäckle and H.-D. Meyer. The MCTDH package, University of Heidelberg,Heidelberg, Germany. H-D .Meyer , Version 8.4, 2002.

[10] U. Burkert and N.L Allinger, "*Molecular Mechanics*", ACS Monograph 177, (ACS,Washington,1982).

[11] V. Fock, *Z. Phys.*, **61**, 126-148 (1930).

[12] W. Pauli, Z. Physik., **31**, 765ff (1925).

[13] A. Szabo and N. S. Ostlund, "*Modern Quantum Chemistry*", Dover, 1996.

[14] F. Jensen, "*Introduction to computational chemistry* " , Willy, 2007.

[15] H. J. Silverstone and O. Sinanoglu, *J. Chem. Phys.*, **44**, 3608 (1966).

[16] D. K. W. Mok, R. Neumann and N. C. Handy, *J. Phys. Chem.*, **100**, 6225 (1996).

[17] B. O. Roos, P. R. Taylor, P. E. M. Seigbahn, *Chem. Phys.*, **48**, 157 (1980).

[18] M. Lewin,J. Math. Chem., **44**, 967-980 (2008).

[19] MOLPRO is a package of *ab initio* program written by H. J. Werner and P. J. Knowles, with contributions from J. Almolf, R. D. Amos, M. J. O. Deegan, S. T. Elbert, C. Hampel, W. Meyer, K. Peterson, R. Pitzer, A. J. Stone, P. R. Taylor.

[20] B. O. Roos, "*Lecture Notes in Quantum Chemistry* ", Springer- Verlag, 1992.

[21] H. J. Werner and P. Knowles, *J. Chem. Phys.*, **89**, 5803 (1988).

[22] M. W. Schmidt and M. S. Gordon, *Annu. Rev. Phys. Chem.*, **46**, 233 (1998).

[23] F. Brouwer, "Chapter 5. Quantum chemistry in molecular modeling", *Lab. of Organic Chemistry*, University of Amsterdam, 1995.

[24] T. H. Dunning, *J. Chem. Phys.*, **90**, 1007 (1989).

[25] A. K. Wilson, T. V. Mourik, and T. H. Dunning, Jr., *J. Mol. Struct.*, **388**, 339 (1996).

[26] F. Jensen, *J. Chem. Phys.*, **115**, 9113 (2001).

[27] E. Papajak, H. R. Leverentz, J. Zhang and D. G. Truhlar, *J. Chem. Theory Comput.*, **5**, 1197 (2006).

[28] C. A. Mead, D. G. Truhlar, *J. Chem. Phys.*, **77**, 6090 (1982).

[29] M. Baer, "Beyond Born-Oppenheimer", Willy, 2005.

[30] F. Hund, *Phys. Z*, **40**, 742-64 (1927).

[31] J. V. Neumann and E. Wigner, *Phys. Z.*, **30**, 467 (1929).

[32] E. Teller, *J. Chem. Phys.*, **41**, 109-116 (1937).

[33] C. Zenner, *Proc. R. Soc. Lond. A*, **137**, 696-702 (1932).

[34] G. A. Worth, L. S. Cederbaum, *Annu. Rev. Phys. Chem.*, **55**, 127-58 (2004).

[35] H. Hellmann, J. K. Syrkin, *Acta. Physicochim.URSS.*, **2**, 433-466 (1935).

[36] F. T. Smith, *Phys. Rev.*, **179**, 111-123 (1969).

[37] M. Baer, *Chem. Phys.*, **259**, 123-47 (2000).

[38] M. Stenrup, Å. Larson, N. Elander, *Phys. Rev. A*, **79**, 012713 (2009).

[39] M. Baer, P*hys. Rep.*, **358**, 75 (2002).

[40] M. Baer, A. Alijah, *Chem. Phys. Lett.*, **319**, 489-93 (2000).

[41] M. Baer, *J. Phys. Chem. A*, **104**, 3181-84 (2000).

[42] G. Herzberg and H. Longuet-Higgins, *Discuss Faradey Soc.*, **35**, 77-82 (1963).

[43] Razi Naqvi and W. Bayer Brown, *Int. J. Quantum Chem.*, **6**, 271 (1972).

[44] K. Razi Naqvi, *Chem. Phys. Lett*, **15**, 634 (1972).

[45] H. C. Longuet-Higgins, *Proc. R. Soc. Lond. A*, **344**, 147-156 (1975).

[46] M. Weissbluth, "*Atoms and Molecules*", Academic press, 1978.

[47] T. C. Thompson, D. G. Truhlar, and C. A. Mead, *J. Chem. Phys.*, **82**, 2392 (1985).

[48] M. Ehara, K. Yamashita, *Theor. Chem. Acc.*, **102**, 226-236 (1998).

[49] P. G. Fernandez, I. B. Bersuker, J. A. Aramburu, M. T. Barriuso, and M. Moreno, *Phys. Rev. B*, **71**, 184117 (2005).

[50] G. A. Worth, H. D. Meyer, H. Köppel and L. S. Cederbaum, *Int. Rev. Phys. Chem*, **27**, 569-606 (2008).

[51] I. Bersuker, "*The Jhan-Teller effect*", Cambridge, 2006.

[52] I. B. Bersuker, *Chem. Rev.*, **101**, 1067-1114 (2002).

[53] G. A. Worth, H. D. Meyer, H. Köppel, L. S. Cederbaum, and I. Burghardt, *Int. Rev. Phys. Chem.*, **27**, 596-606 (2008).

[54] A. Viel and W. Eisfeld, *J. Chem. Phys.*, **120**, 4603 (2004).

[55] J. Schön and H. Köppel, *J. Chem. Phys.*, **103**, 9292 (1995).

[56] J. Schön and H. Köppel, *J. Chem. Phys.*, **108**, 1503 (1998).

[57] A. Thiel and H. Köppel , *J. Chem. Phys.*, **110**, 9371 (1999).

[58] A. W. Hauser, G. Auböck, C. Callegari, and W. E. Ernst, *J. Chem. Phys.*, **132**, 164310 (2010).

[59] A. J. Dobbyn and J. M. Huston, *J. Chem. Phys.*, **98**, 11428-11438 (1994).

[60] W. E. Ernst and O. Golonzka, *Phys. Scripta*, **T112**, 27-32 (2004).

[61] W. H. Gerber and E. Schumacher, *J. Chem. Phys.*, **69**, 1692- 1703 (1977).

[62] W. Moffitt and A. D. Liehr, *Phys. Rev.*, **106**, 1195 (1958).

[63] H. C. Longuet-Higgins, U. Opik, M. H. L. Pryce and R. A. Sack, *Proc. R. Soc. Lond. A.*, **244**, 1-16 (1958).

[64] G. Herzberg and H. C. Longuet-Higgins, *Discuss Faraday Soc.*, **35**, 77 (1963).

[65] A. C. Mead, *J. Chem. Phys.*, **70**, 2276 (1979).

[66] A. C. Mead and D. G. Truhlar, *J. Chem. Phys*, **70**, 2284 (1979).

[67] A. C. Mead, *Chem. Phys.*, **49**, 23 (1980a), *Chem. Phys.*, **49**, 33 (1980b), *J. Chem. Phys*, **72**, 3839 (1980c).

[68] C. A. Mead, *Chem. Phys.*, **49**, 23 (1980).

[69] A. Aharonov, D. Bohm, *Phys. Rev.*, **115**, 485 (1959).

[70] F. Wilczek and A. Zee, *Phys. Rev. Lett.*, **52**, 2111 (1984).

[71] Y. Aharonove and J. S. Anandan, *Phys, Rev, Lett.*, **58**, 1593 (1987).

[72] A. Bohm, A. Mostafazadeh, H. Koizumi, Q. Niu, J. Zwanziger, " *The Geometry Phase in Quantum Systems: Foundations, Mathematical Concepts and Applications in Molecular and Condensed Matter Physics*", Springer, 2003.

[73] J. Larson, *Phys. Rev. A.*, **81**, 051803-1 (2010).

[74] J.Larson and S. Levin, *Phys. Rev. Let.*, **103**, 013602-1 (2009).

[75] A. I. Voronin, J. M. Marques, and A. J. C. Varandas, *J. Phys. Chem. A*, **102**, 6057 (1998).

[76] M. L. Olson, D. D Konowalow, *Chem. Phys. Lett.*, **39**, 281 (1976).

[77] M. L. Olson, D. D Konowalow, *Chem. Phys.*, **21**, 392 (1977).

[78] P. Jasik and J. E. Sienkiewicz, *Chem. Phys.*, **323**, 563 (2006).

[79] L. Dekock Roger, B.Harry, "*Chemical structure and bonding* ", Gray University science book 1989.

[80] S. Hotta, K. Doi, K. Nakamura and A. Tachibana, *J. Chem. Phys.*, **117**, 142 2002.

[81] J. L. Martins, R. Car and J. Buttet, *J. Chem. Phys.*, **78**, 5646 (1983).

[82] M. Keil, H. G. Kramer, A. Kudell, M. A. Baig, J. Zhu and W. Demtröder, *J. Chem. Phys.*, **113**, 7414 (2000).

[83] W. H. Gerber and E. Schumacher, *J. Chem. Phys.*, **69**, 1962 (1978).

[84] T. C. Thompson, G. Izmirlian, S. J. Lemon, D. G. Truhlar and C. A. Mead, *J. Chem. Phys.*, **82**, 5597 (1985).

[85] M. Peric, R. J. Buenker and S. D. Peyerimhoff, *Astrophys. Lett.*, **24**, 69 (1984).

[86] J. P. Wolf, G. Delacretaz and L. Wöste, *Phys. Rev. Lett*, **63**, 1946-49 (1989).

[87] Ph. Dugourd, J. Chevaleyre, M. Broyer, J. P. Wolf, L. Wöste, *Chem. Phys. Lett*, **175**, 555-60 (1990).

[88] M.H. Beck et al., *Phys. Rep.*, **324**, 1- 105 (2000).

[89] H.D. Meyer and G.A. Worth, *Theor. Chem. Acc.*, **109**, 251-267 (2003).

[90] H.D. Meyer, F. Gatti, and G.A. Worth (eds.) "*High dimensional quantum dynamics: Basic Theory, Extensions, and Applications of the MCTDH method*", VCH, Weinheim, Germany, 2008.

[91] Y. A. Bychkov and E. I. Rashba, *J. Phys. C*, **17**, 6034 (1984).